ORNL/SPR-2024/3414

# Oak Ridge National Laboratory Final Report on Characterization of Irradiated Sensors and Coupling Adhesive Bonds

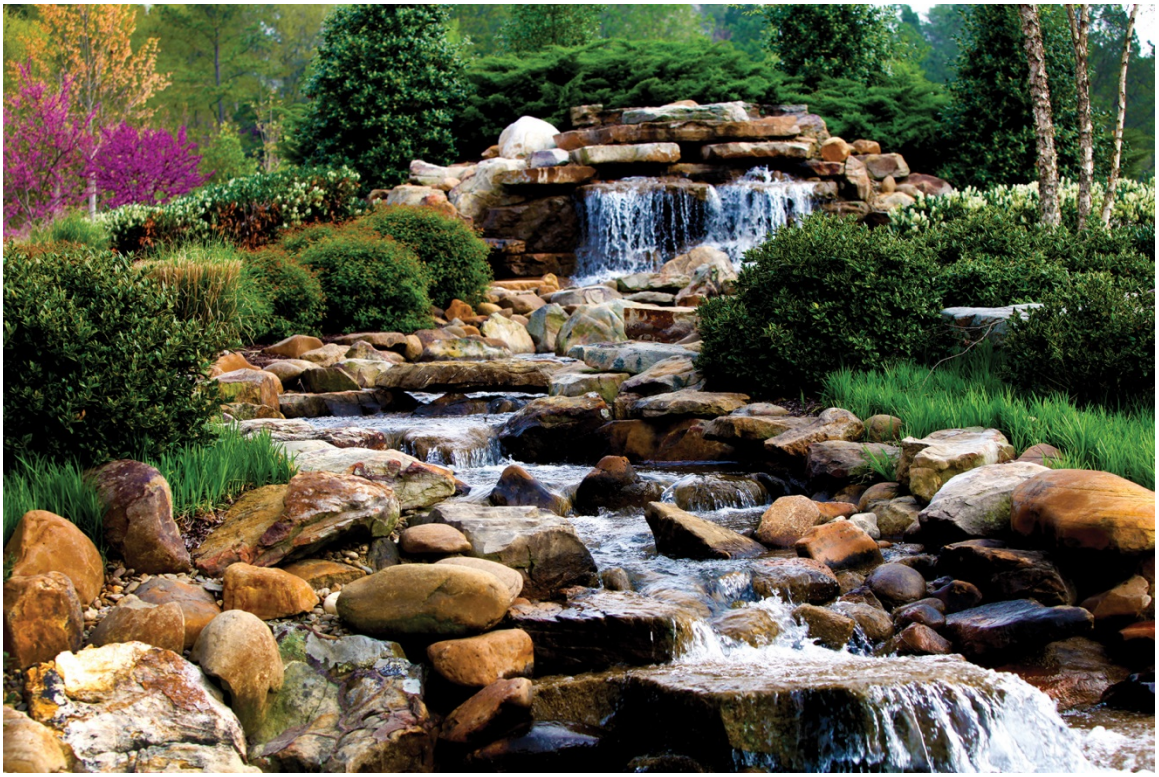

Chad M. Parish (ORNL)

Sabrina Calzada (ORNL)

James Wall (EPRI)

**June 2024**

OAK RIDGE National Laboratory

ORNL IS MANAGED BY UT-BATTELLE LLC FOR THE US DEPARTMENT OF ENERGY

**ORNL/SPR-2024/3414**

Materials Science and Technology Division

# FINAL REPORT ON CHARACTERIZATION OF IRRADIATED SENSORS AND COUPLING ADHESIVE BONDS

NSUF Milestone: M3UA-22OR0803013

Chad M. Parish

Sabrina Calzada

James Wall

June 2024

Prepared by

OAK RIDGE NATIONAL LABORATORY

Oak Ridge, TN 37831

managed by

UT-BATTELLE LLC

for the

US DEPARTMENT OF ENERGY

under contract DE-AC05-00OR22725

**CONTENTS**

# Contents

## FIGURES

## ABSTRACT

This report summarizes characterization via scanning/transmission electron microscopy of the microstructures of the unirradiated and irradiated piezoelectric ultrasonic sensor/aluminum substrate assemblies using four commercially available inorganic coupling adhesives to bond two types of piezoelectric crystals to the substrates. The sample assemblies were irradiated in the PULSTAR reactor at NC State University and ultrasonic data was collected in-situ. ORNL LAMDA Laboratory capabilities were utilized to perform pre- and post-irradiation examination of the sensor assemblies. This document summarizes the PIE performed at the ORNL LAMDA laboratory. The results of the PIE described in this report are consistent with the ultrasonic data collected during irradiation – in particular, high temperature epoxy adhesive seemed to provide the best coupling as compared to the refractory ceramic adhesives. It was determined that the quality of the sensor-adhesive-substrates governed the ultrasonic performance of the sensors. It was also apparent that irradiation did not significantly affect bond quality, which is also supported by the ultrasonic data collected during irradiation. A more comprehensive DOE NSUF Final Report including details of materials selection, sample fabrication, initial ultrasonic testing, irradiation and in-situ ultrasonic testing, positron annihilation lifetime spectroscopy and doppler broadening spectroscopy performed at EPRI and NC State University will be published at the conclusion of the project.


# 1. INTRODUCTION

## 1.1 RECAP OF PAST WORK

This project was initiated by the Electric Power Research Institute (EPRI) in conjunction with Nuclear Science User Facility (NSUF) partners to study the effects of in-pile irradiation on the coupling bonds between ultrasonic transducers and substrates to better determine materials choices for online monitoring of crack growth in stainless steels in light water reactor (LWR) primary loop piping and components.

In a prior milestone report [1], samples consisting of ≈13 mm diameter, <1 mm thick piezoelectric ultrasonic sensors were bound to 25 mm diameter, 10 mm thick aluminum substrates. The ultrasonic sensors were approximately $(PbTiO_3)_{0.64}(BiScO_3)_{0.36}$ (morphotropic lead titanate-bismuth scandate: PTO-BSO, referred to as simply "bismuth titanate" in the Final Report) or of $LiNbO_3$ (lithium niobate). The ultrasonic sensors were bound to the substrates with different bonding layers, and the bonding layers were the materials of interest for the irradiation experiments. These layers were examined via scanning electron microscopy (SEM) with energy dispersive X-ray spectroscopy (EDS) and electron backscatter diffraction (EBSD). These were examined in both as-fabricated and post-irradiated states; samples were prepared by sectioning with a low-speed diamond saw, mounting in conductive (graphite-doped) epoxy, and grinding and polishing to an EBSD finish. Samples of aluminosilicate, alumina, zirconia, and epoxy-based bonding layers were tested.

In a prior journal publication [2], the effects of irradiation on the transducer / couplant combinations were examined. Lithium niobate-on-epoxy and PTO-BSO-on-aluminosilicate samples gave the best results at the end of the irradiation experiment.

## 1.2 THIS WORK

In this work, a subset of the samples—irradiated and unirradiated—were repolished for focused ion beam (FIB) preparation of thin lamellas for scanning-transmission electron microscopy (STEM) to analyze the microstructures of the adhesive couplants. Samples were examined via STEM, with an emphasis on STEM-EDS, to determine any gross structural or chemical changes before to after irradiation. Because

epoxies are not amenable to examination via STEM, the subset of samples chosen were the ceramic-based bond layers specimens, four unirradiated and three irradiated. The samples analyzed using STEM are summarized in Table 1.

**Table 1. List of samples examined in this report.**

| Status | ID | Piezoelectric | Bonding (elements) | Bonding (interpretation) |
|---|---|---|---|---|
| Unirradiated | 1 | (Pb,Bi)(Sc,Ti)-O | Si-Al-K-Na-O | Alkali slurry |
| | 5 | (Pb,Bi)(Sc,Ti)-O | Al-Si-O | Aluminosilicate |
| | 11 | (Pb,Bi)(Sc,Ti)-O | Al-O | Alumina |
| | 12 | (Pb,Bi)(Sc,Ti)-O | Zr-(Si-Ca-Al-Na-)O | Zirconia |
| Irradiated | 1 | (Pb,Bi)(Sc,Ti)-O | Si-Al-K-Na-O | Alkali slurry |
| | 4 | (Pb,Bi)(Sc,Ti)-O | Al-(Si-Na)-O | Alumina |
| | 5 | (Pb,Bi)(Sc,Ti)-O | Zr-(Si-Ca-Al-Na-)O | Zirconia |

## 2. PROCEDURES

The samples were as described in the previous ORNL/SPR report [1] and journal publication [2]. Briefly, they were lead titanate-bismuth scandate piezoelectrics or lithium niobate piezoelectrics in the form of thin 13 mm diameter disks, attached to 25 mm diameter, 10 mm thick aluminum substrates by different ceramic slurries or epoxy. The epoxy-embedded samples were cut down slightly to ~10 mm in height to be accommodated by the FIB tool, and the foils were prepared from the ceramic bonding layers via FIB liftout procedures using $Ga^+$-beam FIB. FIB tools used were DualBeam™ FIB-SEMs, either the FEI Quanta3D 200i or FEI Versa3D tool at ORNL LAMDA laboratory.

As was observed in the previous work [1], the aluminosilicate samples suffered growth of sodium-oxide based structures between polishing and examination; this was attributed to high humidity and a delay (~weeks) between polishing and SEM examination. This time, samples were repolished and immediately (~minutes) loaded into the FIB tool to avoid the growth of sodium oxides; this was successful.

STEM was performed in the FEI Talos F200X tool, operated at 200 kV. Imaging in high-angle annular dark field (HAADF) and bright field (BF) modes were emphasized to see details in the microstructures. This tool has the four-detector EDS system resulting in very high throughput of analysis. All X-ray maps below are presented as the estimated atom percentage, as determined by the ThermoFisher Scientific Velox software. Due to inherent approximations and inaccuracies in EDS data, these ratios will never match perfectly with exact stoichiometries. Further, *regions of vacuum show "speckle" due to random spurious X-rays in the regions of low count rate*; this is essentially a "small number divided by small number"-type artifact and should be ignored. Maps are averaged 3×3 pixels in pre-processing prior to quantification. It was decided to use Python to render the maps instead of the native Velox software maps, other than for color-composite comparison overlays, because the human eye can be misled when maps are given in different colors: i.e., the human eye is more sensitive to green, so an element presented in a green map will appear stronger than a blue- or red-color mapped element, even if it is a quantitatively weaker signal. A scientifically designed colormap is used to present the data [3].

# 3. RESULTS

## 3.1 UNIRRADIATED

### 3.1.1 Sample 1: Alkali Slurry

Unirradiated Sample 1 showed an alkali/slurry class bonding layer, and the microscopy (Figure 1) shows a mixture of pores and micron-sized, blocky grains in a space-filling matrix. At higher magnification (Figure 2) the details are easier to see. Specifically, the matrix around the blocky ceramic grains is seen to contain a large fraction of open space or very light pockets. This indicates intimate contact between the different phases of the slurry used to produce the bonding layer. Small (<50 nm) pores are present in the ceramic grains, Figure 3, as well as at grain triple points. The larger cavities show hexagonal shapes, probably due to surface energy effects.

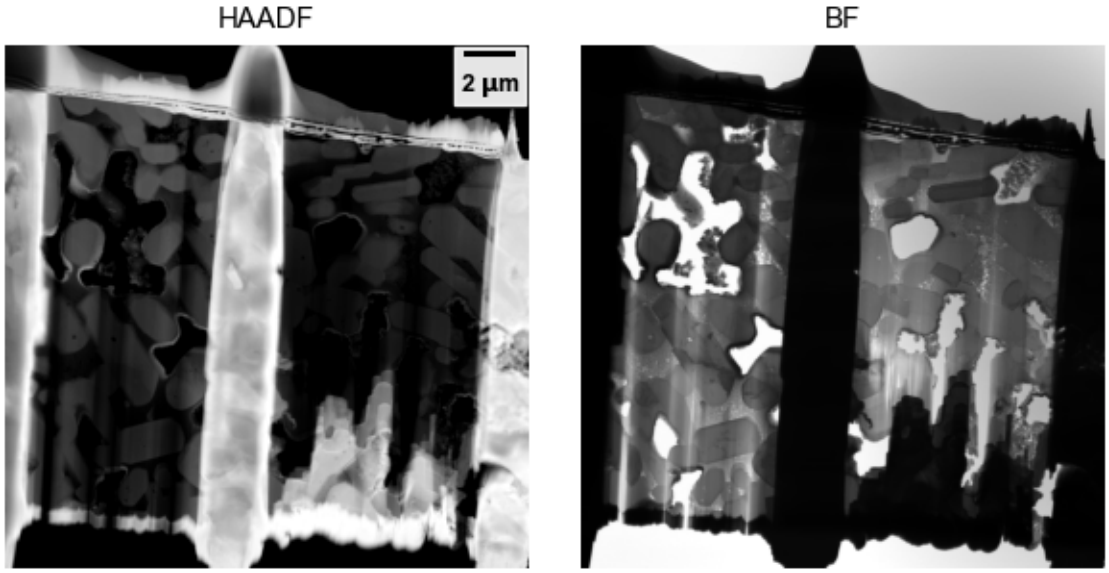


**Figure 1. Low-magnification STEM images of a FIB liftout from Unirradiated Sample 1.**

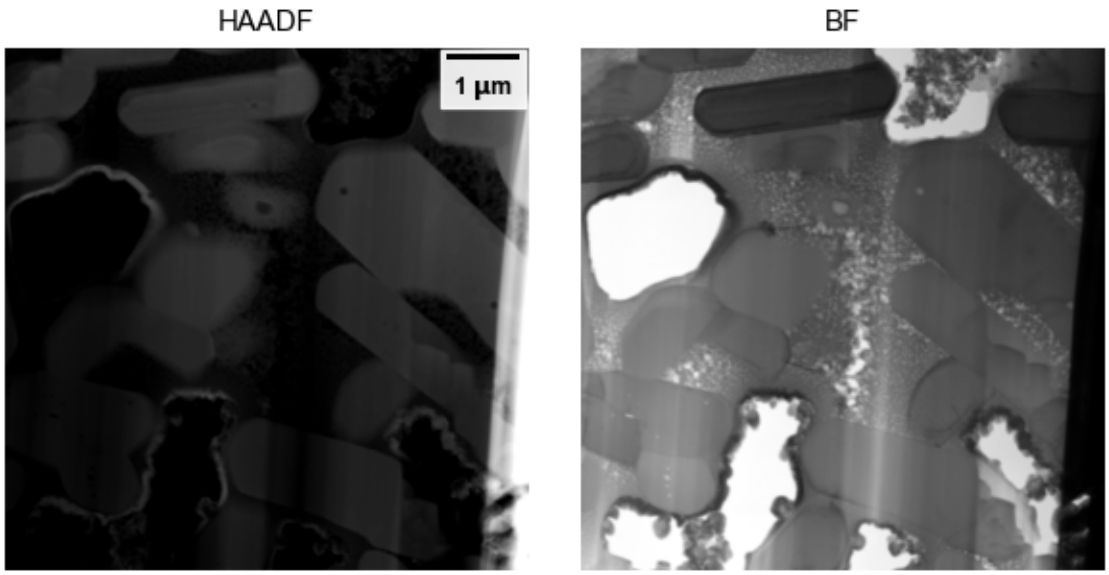


**Figure 2. A more details view of the alkali-slurry sample showing cavities, grains, and a semi-porous matrix around the grains.**

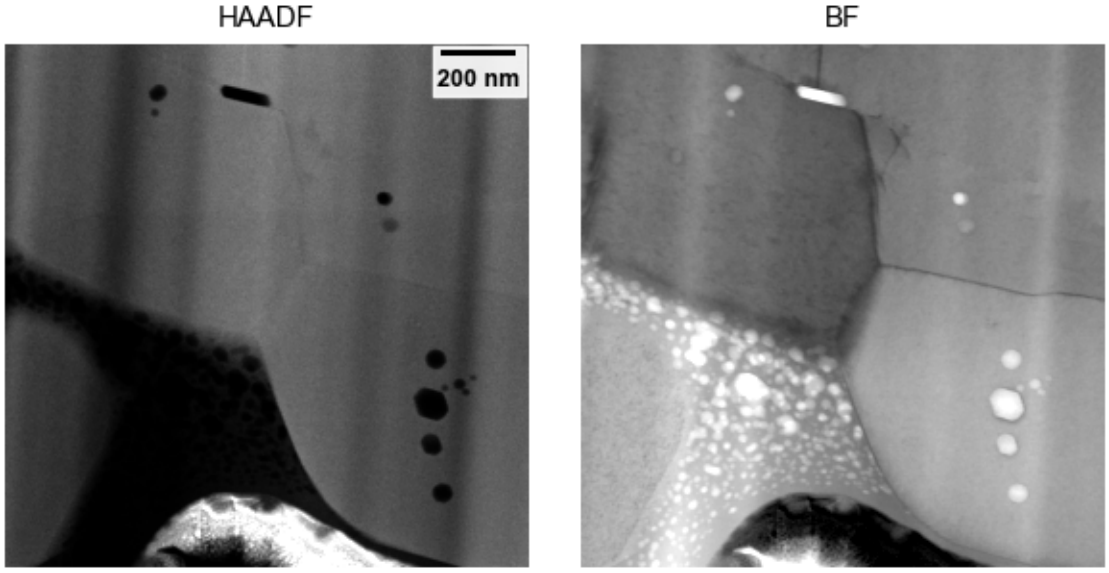


**Figure 3. A more detailed view, showing cavities with roughly hexagonal shape are present in the grains.**

In Figure 4, the X-ray mapped data, presented at estimated atom%, of the region seen in Figure 2 is shown. The major elements O, Na, Al, Si, K, and Ca are found, consistent with an soda- or alkali-lime type specimen. As mentioned in Section 2, aggressive "speckle" in the cavities are observed due to the nearly-zero count rate on the vacuum and should be ignored. The aluminum-oxygen particles are easily seen in the X-ray data; these are $Al_2O_3$ grains, as seen in the EBSD data of the prior milestone report [1]. The large blocky grains are Al-O rich by EDS and the matrix surrounding the grains is Si-O rich, showing an amorphous silica phase that also contains a small amount of Na. Regions rich in K and Ca are seen in Figure 4, in addition to the low levels of K and Ca dispersed in the Si-O phase, but not in the Al-O phase. In Figure 5, left, a color composite image is given, with three areas marked. Summed spectra from these

two areas are shown in the right side, and one K-rich and one Ca-rich, confirming the mapping results. It's worth noting that the α and β peaks from both K-K and Ca-K are seen, indicating that the peaks are real and not sum or escape peaks. (Si-K + Si-K sum peaks would be at 3.48 keV, in between K-Kα and K-Kβ/Ca-Kα; Si-K + O-K sum would be at 2.26 keV, well below the lines of interest and near the Mo-L series arising from the FIB sample carrier.)

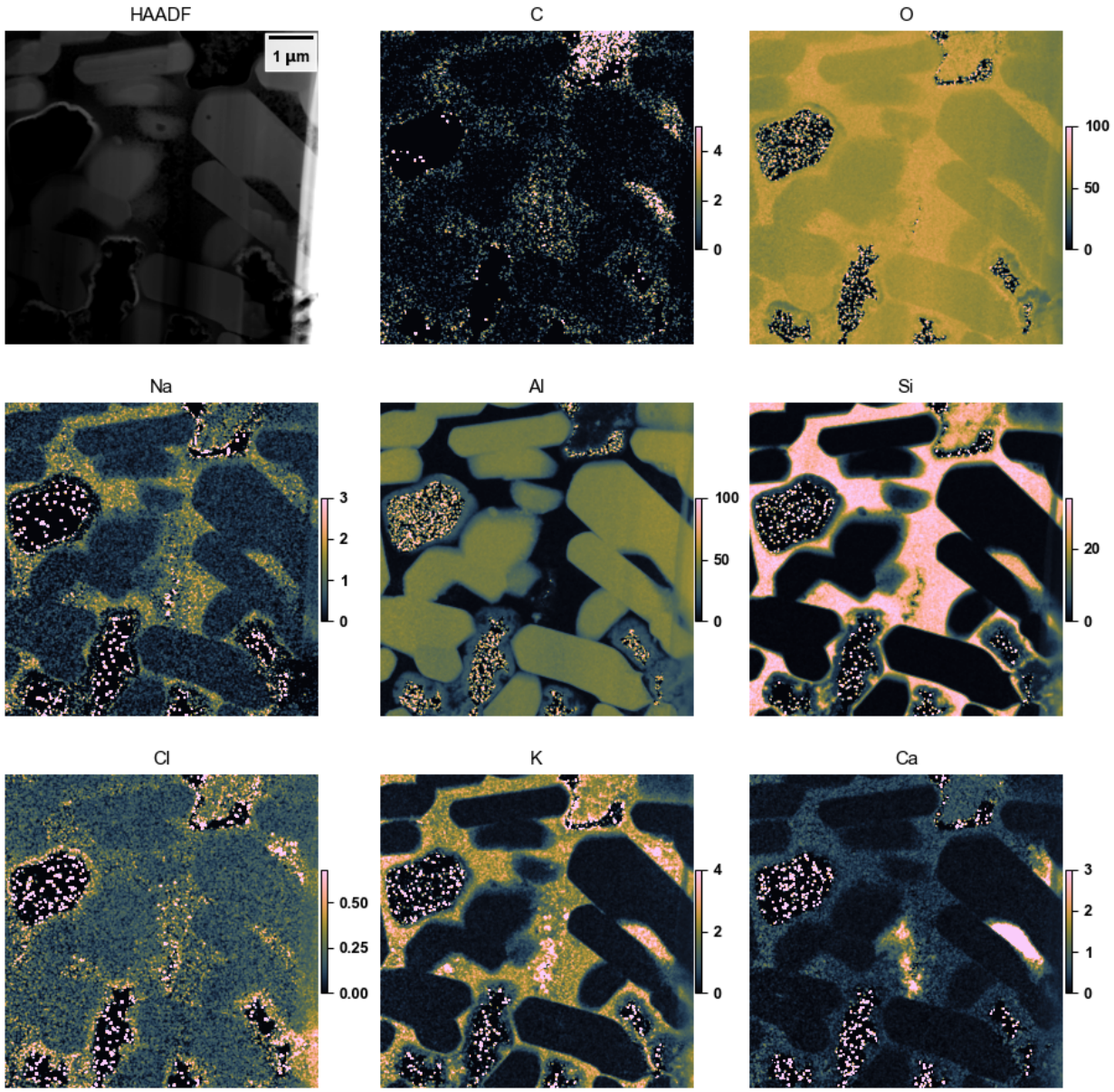


**Figure 4. X-ray maps, presented as estimated atom%, of the region of Figure 2. Speckle in the vacuum area is a quantification artifact and should be ignored.**

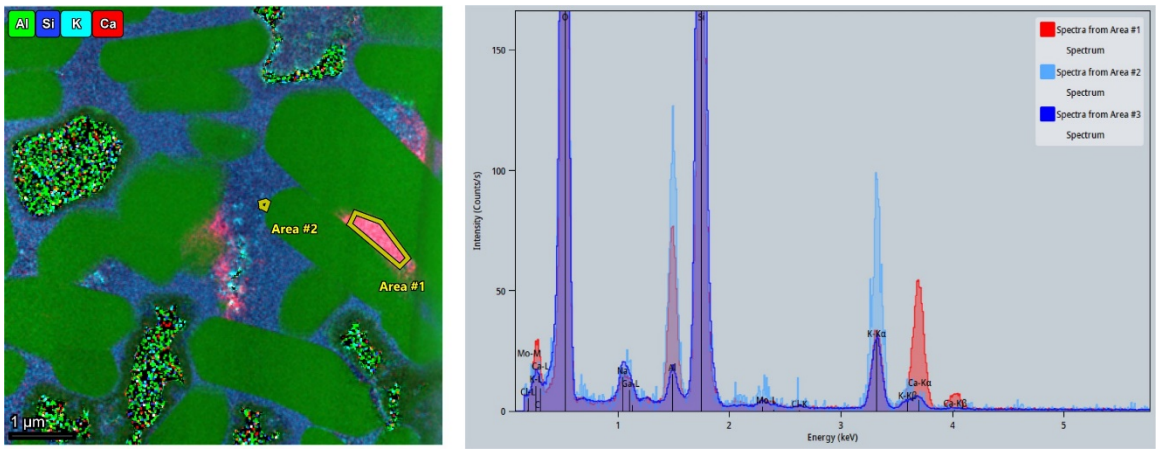


**Figure 5. Left: Color overlay of the data in Figure 4, with three areal spectra marked. Right: extracted spectra from the three areas, showing strong K and Ca peaks. Speckle in the vacuum area is a quantification artifact and should be ignored.**

The detailed area of Figure 3 is X-ray mapped in Figure 6. The overall details are fully consistent with the lower-magnification map of Figure 4. However, a few new details also emerge. Particularly, a strong K-rich layer is seen at the edge of the sample, and Ca-rich films are seen on a grain boundary (nearly horizontal) and on the interior face of the hexagonal-shaped triple-point pore. This indicates that although the alumina grains are Ca-poor, Ca is appearing on the internal interfaces, presumably during processing to consolidate the bonding layers. Small amounts of Na are also present in the Si-rich layer and at the cavity. The bright region at the bottom of the HAADF panel is Ga-rich, and is due to redeposition of sputtered material on the bottom-facing side of a prior-pore region.

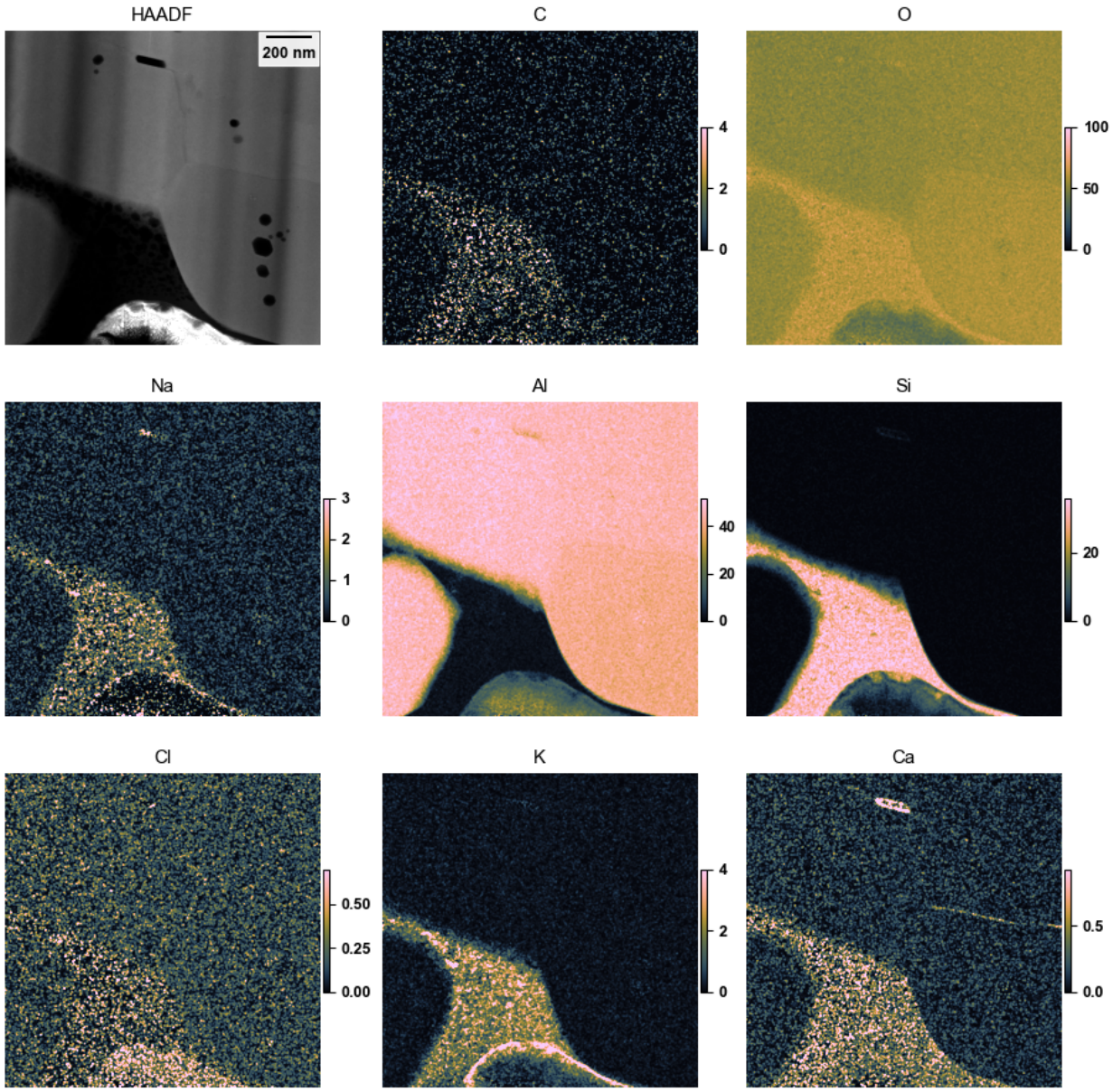


**Figure 6. X-ray maps, presented as estimated atom%, of the region of Figure 3.**

A triple-point pocket of the matrix material surrounded by three of the alumina grains is shown in Figure 7, with the associated X-ray mapping data in Figure 8. The details are consistent with the other maps above, although no grain boundary films (e.g., Ca) are observed on the clean grain boundaries between the alumina grains. The triangular Si-O pocket, containing significant amounts of Na, Ca, and K, also runs down the left-side alumina grain boundary, indicating some three-dimensional shape that was captured by milling the sample into a thin foil via FIB.

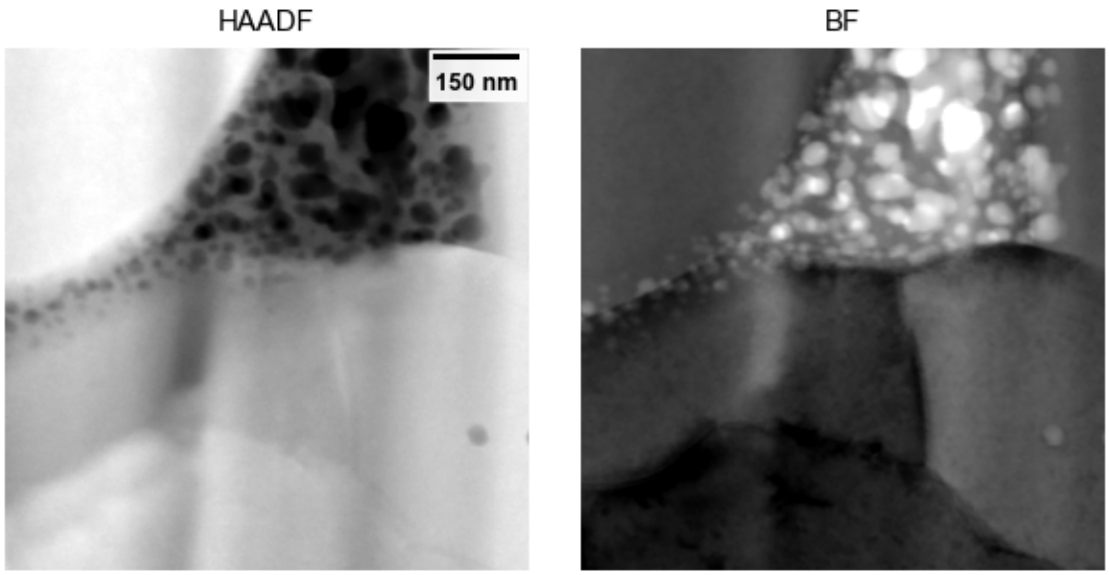


**Figure 7. A detailed view of matrix material near a triple-point between alumina grains.**

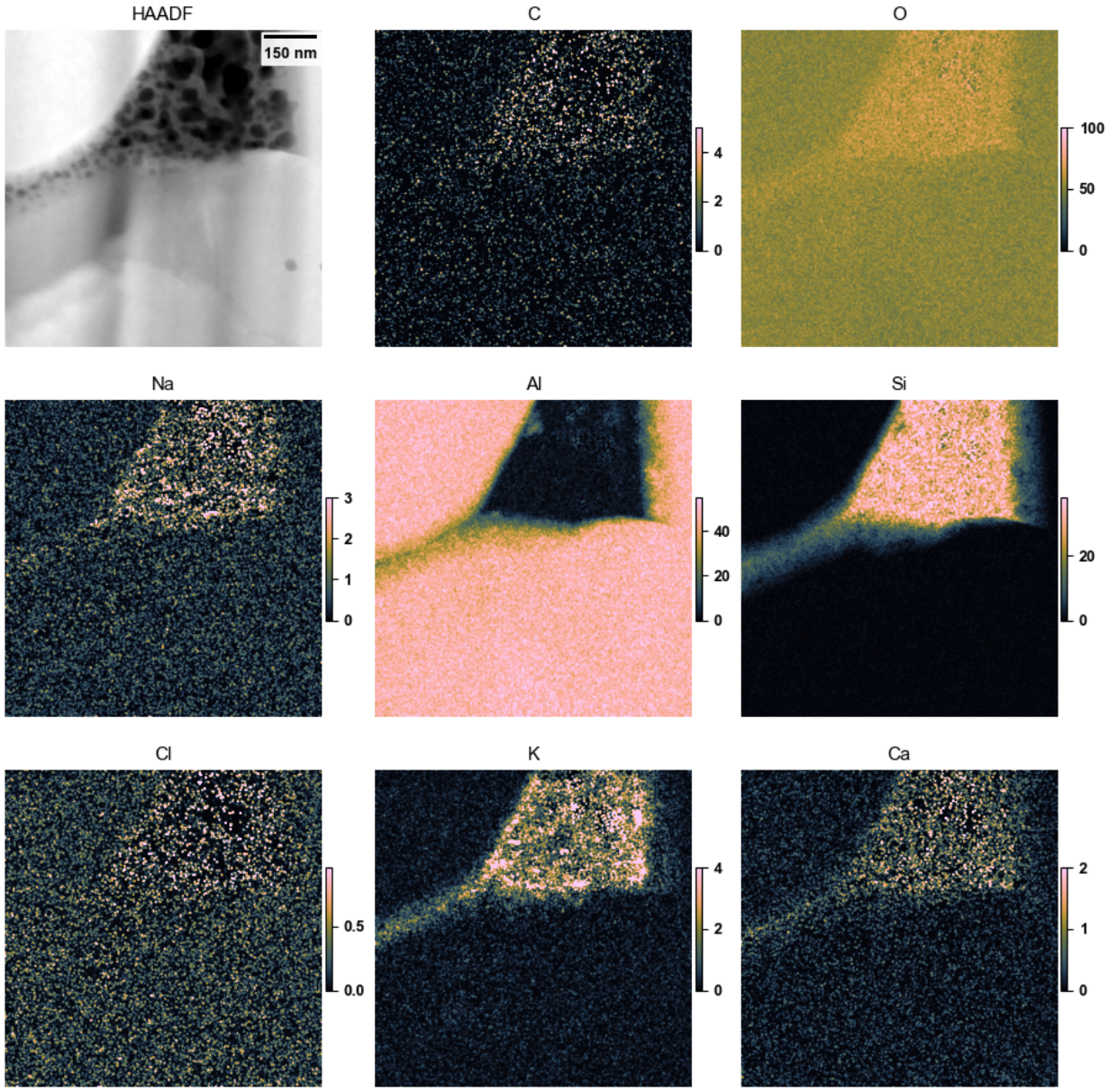


**Figure 8. X-ray maps, presented as estimated atom%, of the region of Figure 7.**

A second FIB foil, Figure 9, of the same sample provides consistent results with the above. Blocky grains are seen in the enfolding matrix again, along with tears and voids in the matrix regions. Small cavities are visible within individual grains. X-ray mapping at moderate magnification, Figure 10, is again consistent with above results, specifically blocky Al-O grains in a Si-O matrix containing some Na, K, and Ca. At even higher magnification, Figure 11, these same features are seen in more detail but with visibility of more Ca along Al-O grain boundaries and some pockets of strong Ca at the edges of Al-O grains.

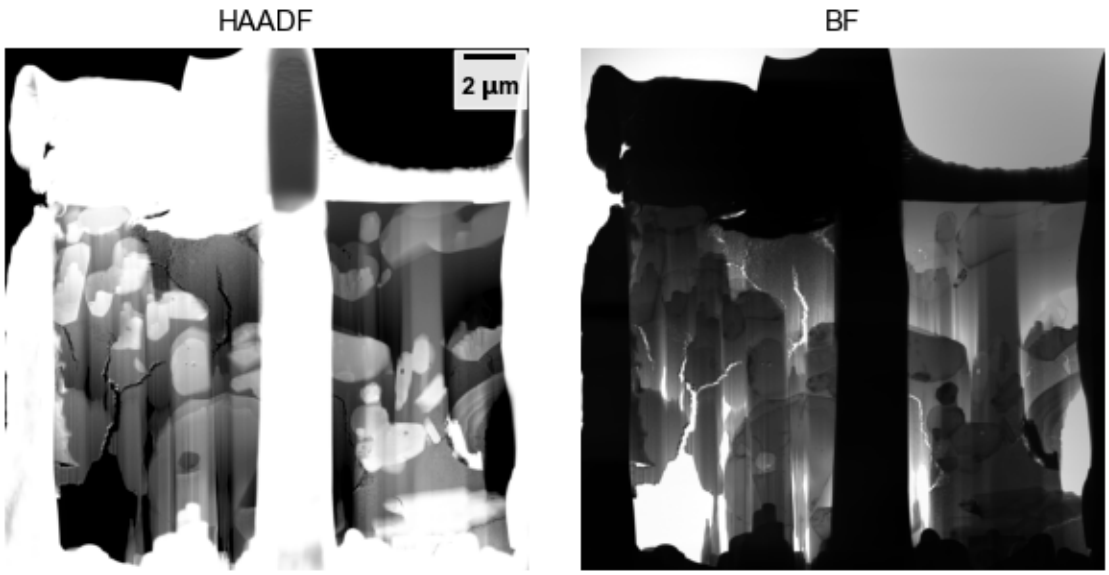


**Figure 9. Low-magnification STEM images of a FIB liftout from Unirradiated Sample 1.**

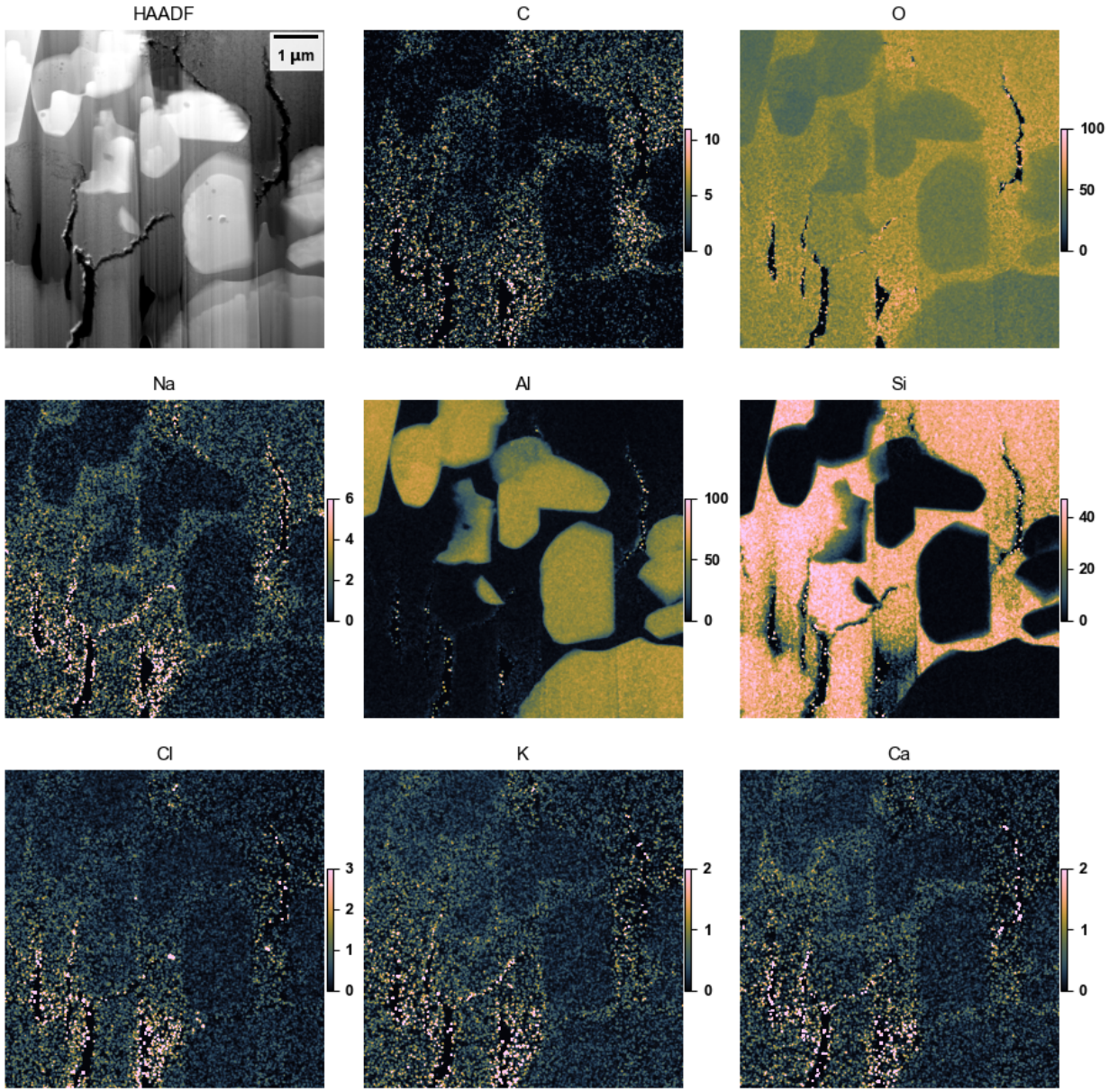


**Figure 10. X-ray maps, presented as estimated atom%, of a subregion of Figure 9. Speckle in the vacuum area is a quantification artifact and should be ignored.**

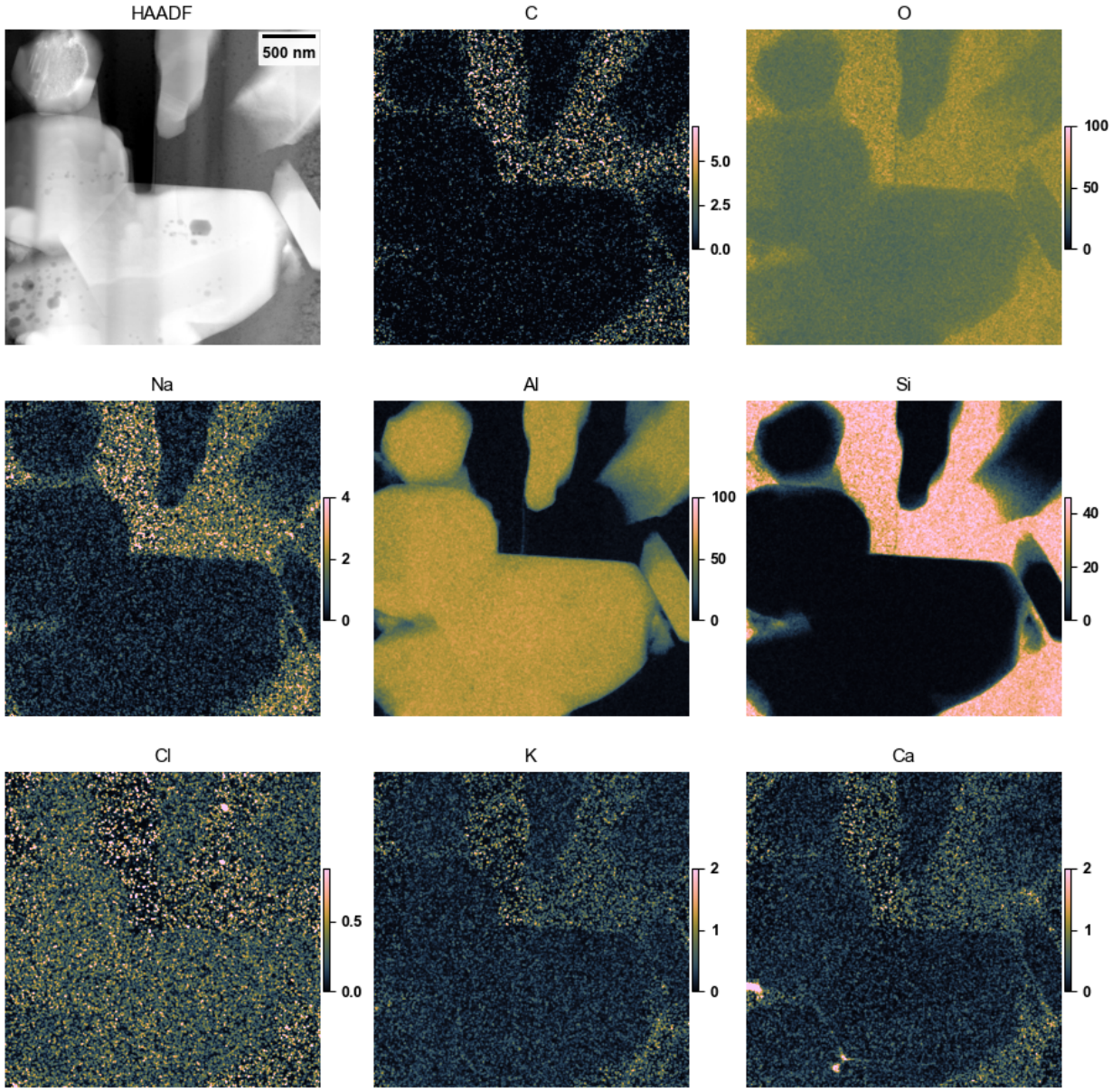


**Figure 11. X-ray maps, presented as estimated atom%, of a subregion of Figure 9.**

Overall, then, this Unirradiated Sample 1 is consistent with the prior SEM results, showing blocky alumina in a matrix of Si-Na-Ca-K-oxides. Soda- or alkali-lime type glasses have improved properties and easier melting/fabrication compared to pure silica glasses and the alumina fraction will produce further composite effects. The Ca on grain boundaries and coating pores in the alumina is indicative of interactions between the Si-K-Ca-O matrix and the Al-O grains.

### 3.1.2 Sample 5: AlSiNaO

Unirradiated Sample 5 showed large, blocky $Al_2O_3$ grains via SEM-EBSD with minor Si, Na, and C surrounding the $Al_2O_3$ grains [1]. In Figure 12, a low-magnification view of a liftout from the layer is visible. Large and medium blocky grains are seen, along with pores and matrix material. More detail of

the edge grains is given in Figure 13, and the associated X-ray map in Figure 14. The grains are blocky and contain small hexagonal pores, as in Unirradiated Sample 1 above. The X-ray maps indicate essentially pure Al-O in the grains, and predominantly Si-O in the surrounding matrix, with small regions of very minor Ca and K content. No Na was observed; whether this means this region was Na-free, or if the high dose of electrons from SEM-FIB and STEM caused the Na to migrate, or some other factor, is difficult to say.

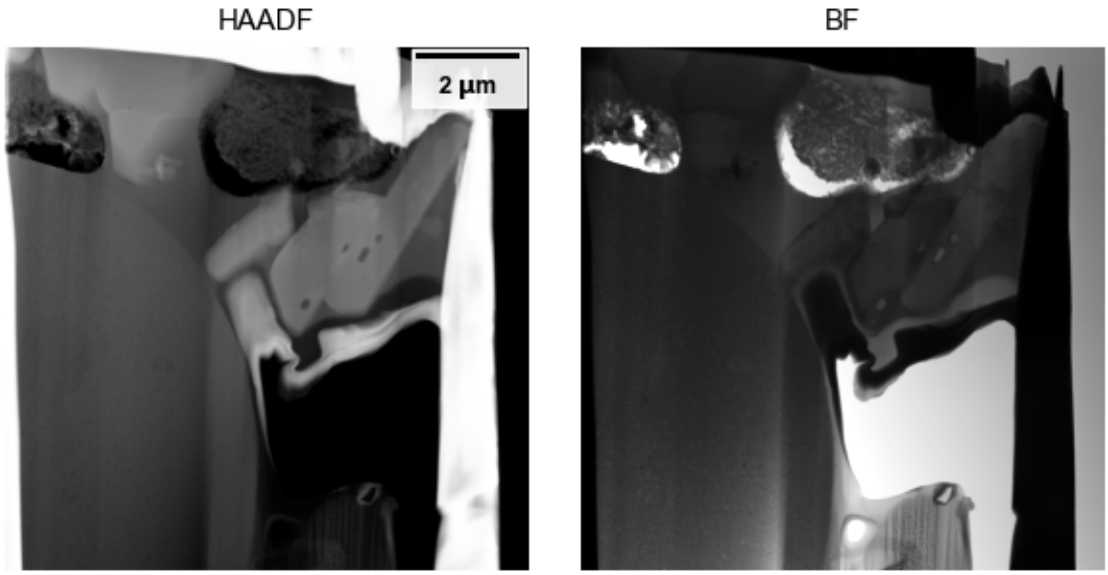


**Figure 12. Low-magnification STEM images of a FIB liftout from Unirradiated Sample 5.**

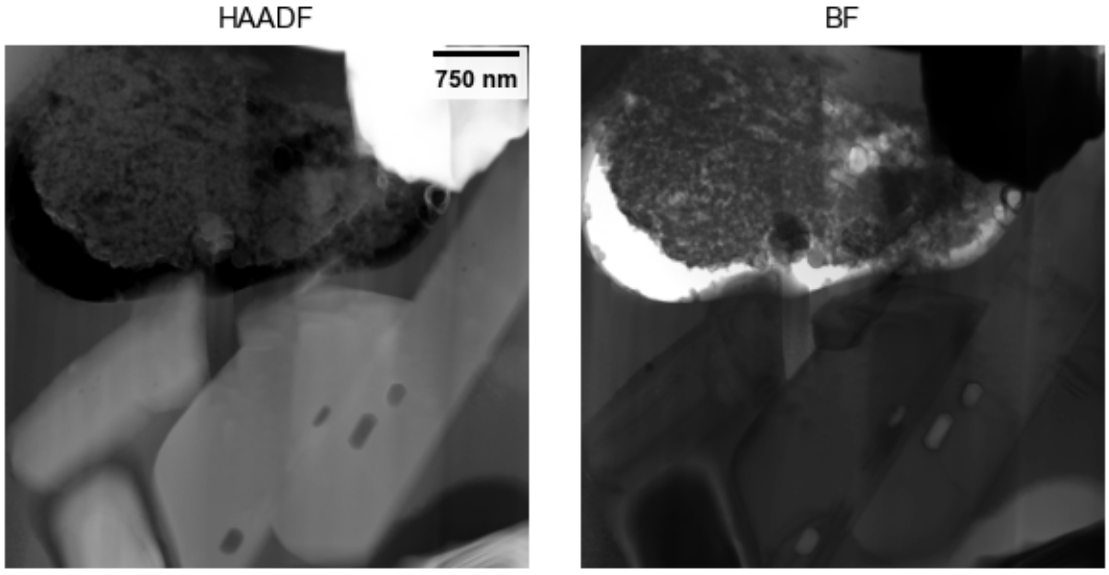


**Figure 13. Moderate-magnification STEM images of a FIB liftout from Unirradiated Sample 5.**

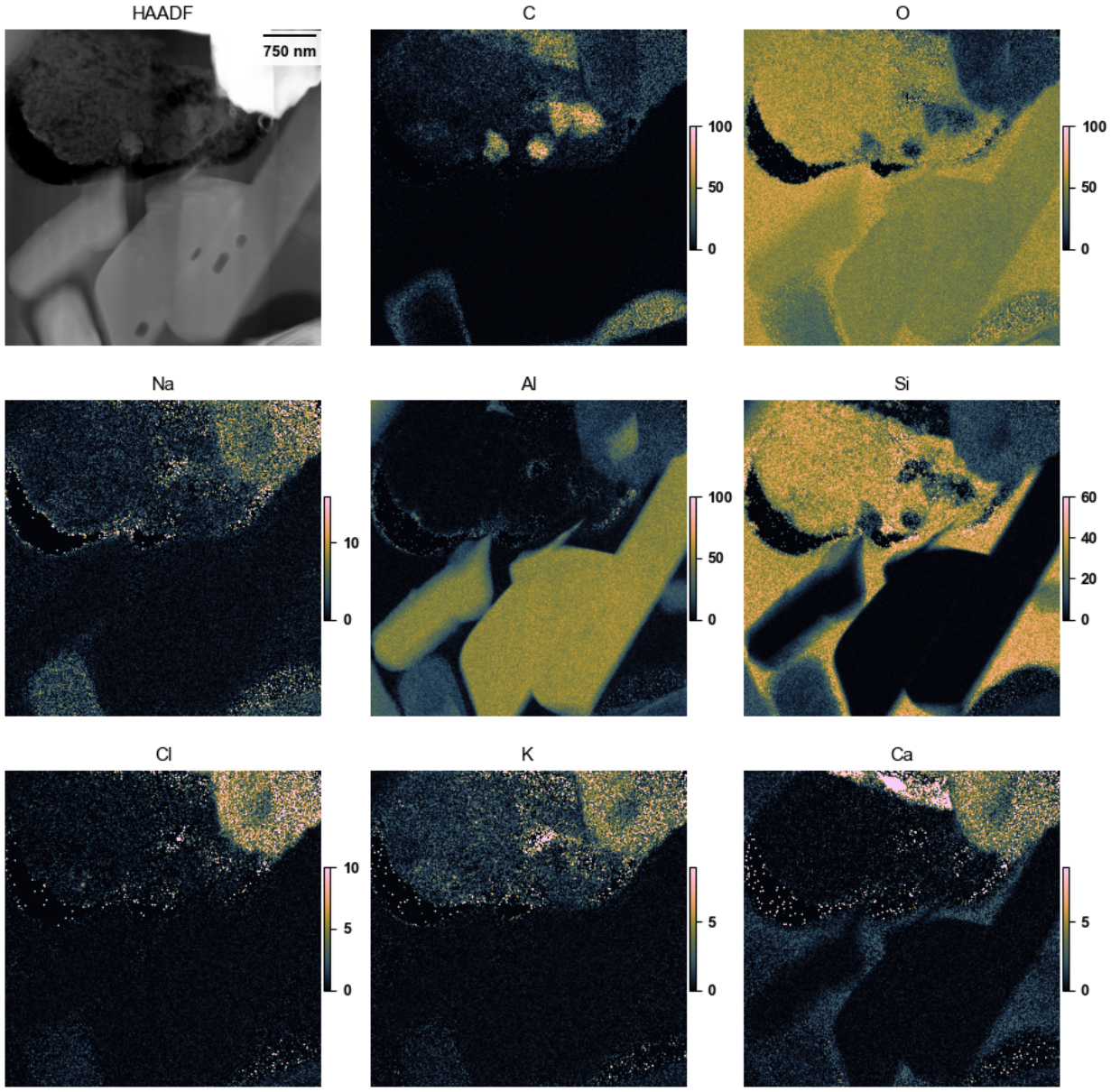


**Figure 14. X-ray maps, presented as estimated atom%, of a subregion of Figure 14. Speckle in the vacuum area is a quantification artifact and should be ignored.**

Further detail of these blocky grains and the hexagonal pores are seen in Figure 15 and in X-ray mapping in Figure 16. The blocky grains are, again, Al-O, as expected. The surrounding matrix shows Si-O with a very small amount of Ca; no to very little Na was observed above the noise level. This is confirmed in an extracted areal spectrum from the matrix region, Figure 17, where minor Ca and no Na were observed.

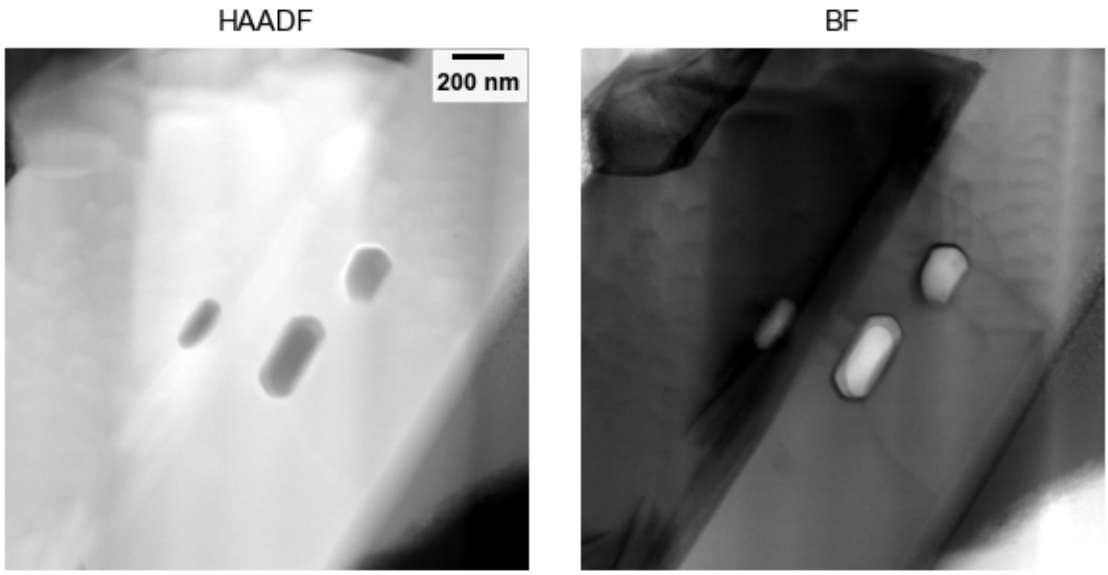


**Figure 15. High-magnification STEM images of a FIB liftout from Unirradiated Sample 5.**

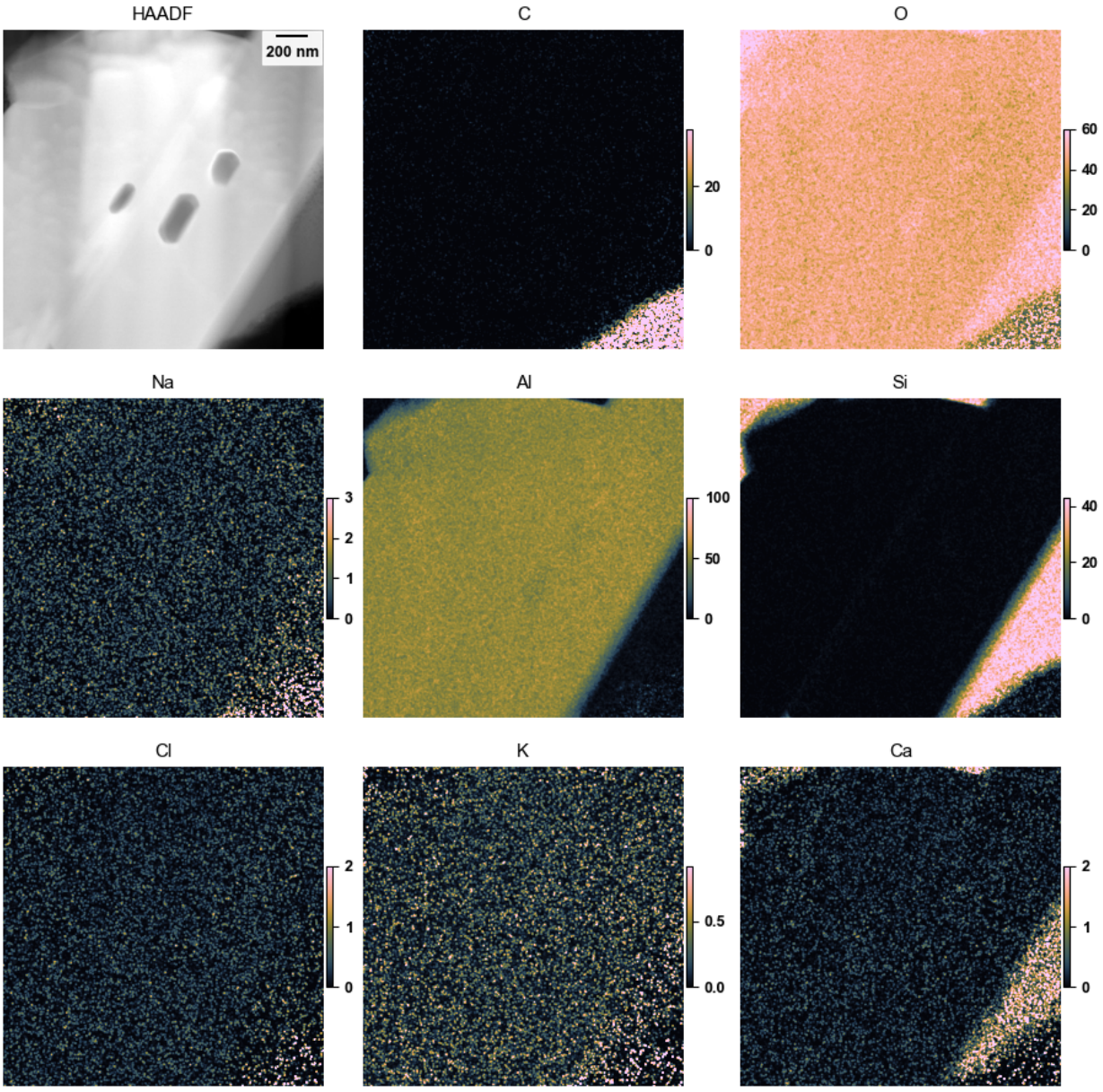


**Figure 16. X-ray maps, presented as estimated atom%, of a subregion of Figure 15. Speckle in the vacuum area is a quantification artifact and should be ignored.**

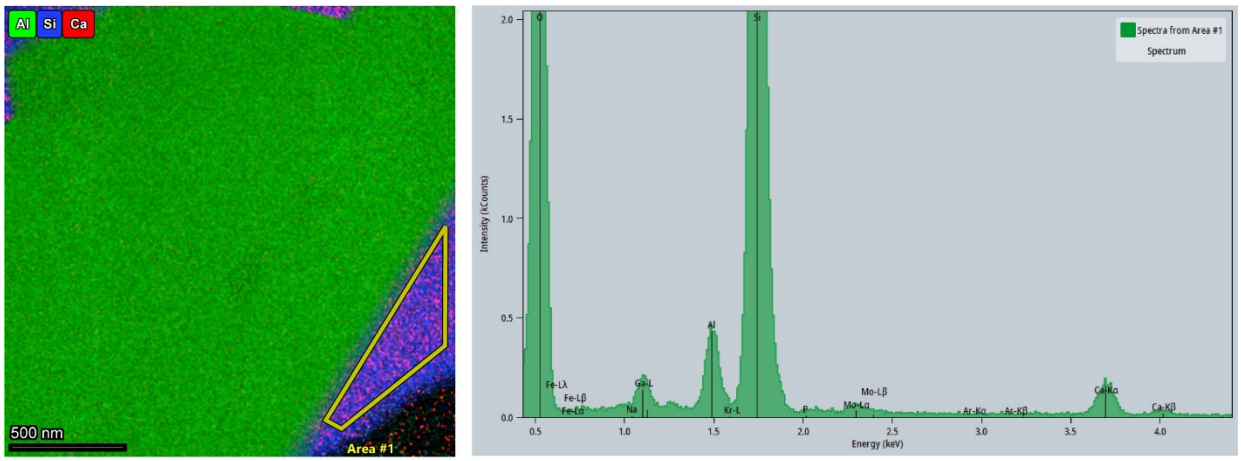


**Figure 17. Left: Color overlay of the data in Figure 16, with two areal spectra marked. Right: extracted spectra from the two areas, showing strong K and Ca peaks.**

Another liftout, Figure 18, shows large and blocky grains again. Smaller fragmented grains are also seen embedded in the background matrix and near the intersections of the larger grains. Cavities are also seen, with FIB redeposition on the edges of the cavities, a consequence of FIB milling of porous materials. Examining a detailed region near the top of the foil, Figure 19 and Figure 20, shows the Al-O grains and Si-O matrix, as expected, but also significant regions of C-rich material, which are likely embedding epoxy from the sample preparation process or else residual organics from initial fabrication, or both.

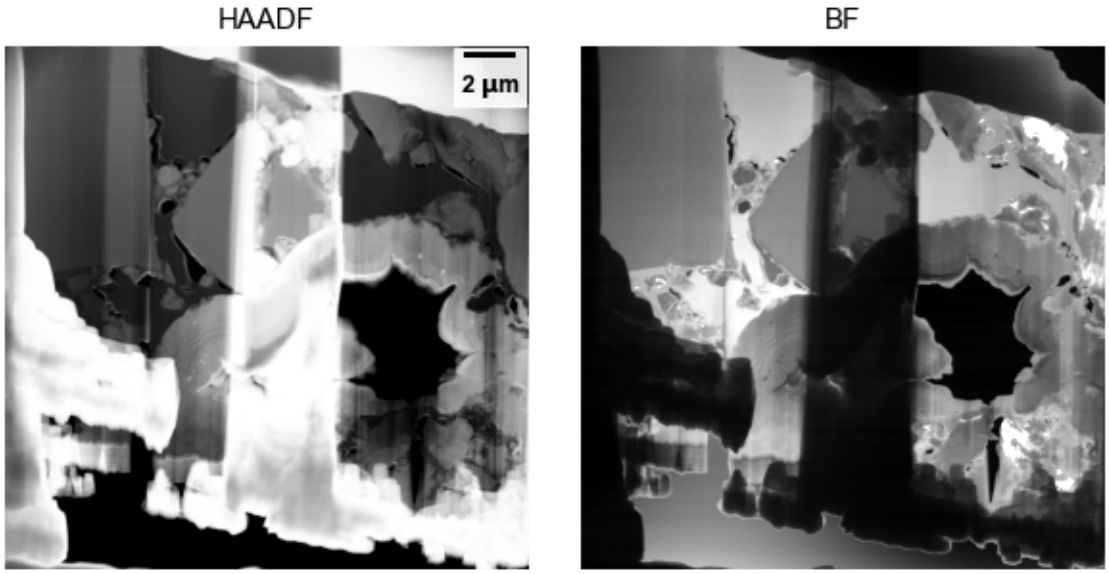


**Figure 18. Low-magnification STEM images of a FIB liftout from Unirradiated Sample 5.**

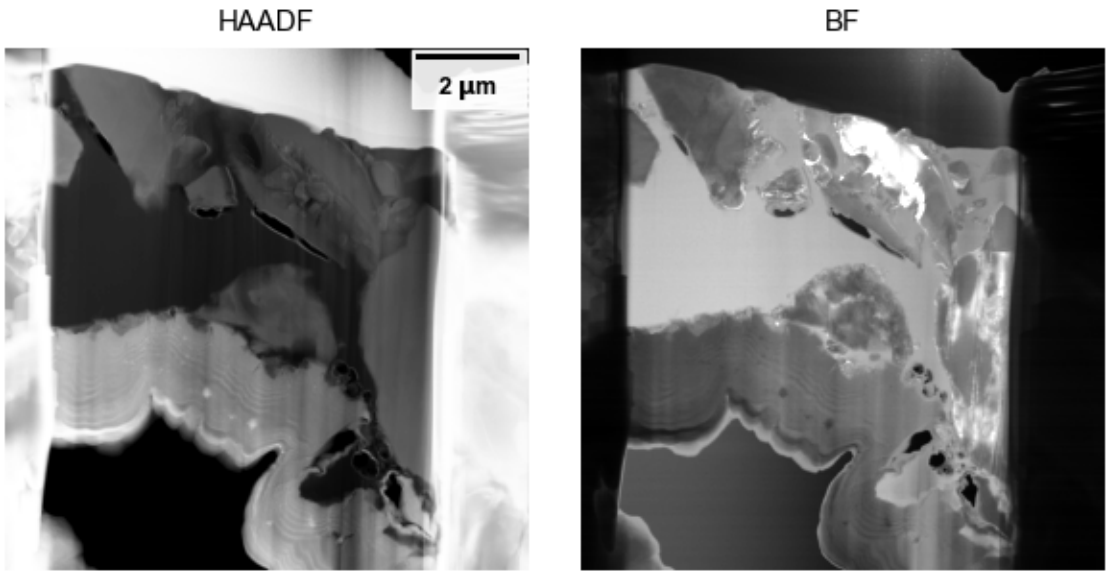


**Figure 19. Moderate-magnification STEM images of a FIB liftout from Unirradiated Sample 5.**

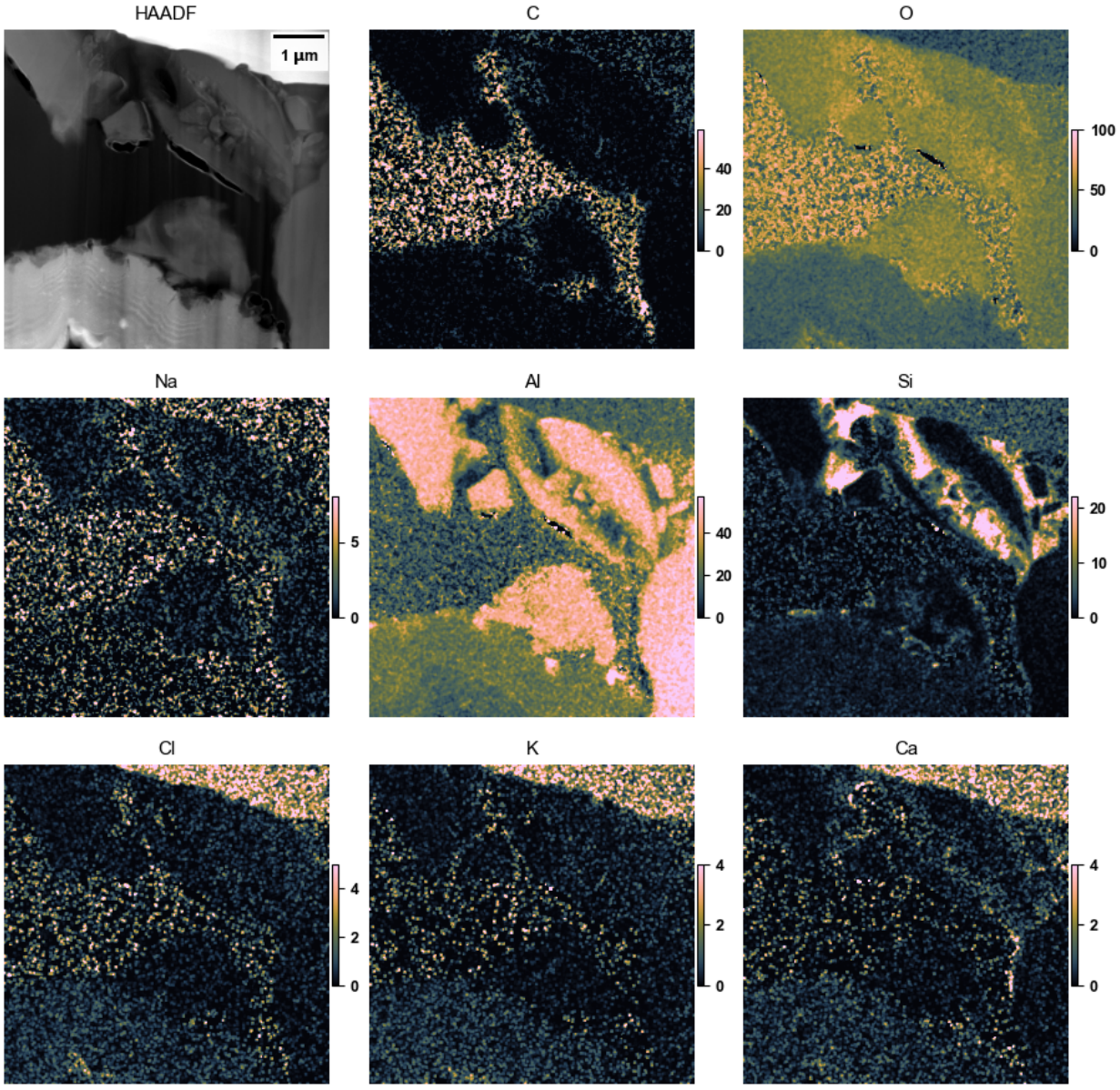


**Figure 20. X-ray maps, presented as estimated atom%, of a subregion of Figure 19.**

The intersection between two large grains, and containing many small grains, of alumina is seen in Figure 21. The vertical contrast is due to differences in thickness arising from the inhomogeneities in the sample resulting in non-uniform FIB removal. An important subsidiary point to keep in mind is that X-ray EDS "quantification" algorithms make assumptions about absorption of X-rays in the foil prior to reaching the detector. The subtle changes in thickness result in these assumptions' validity varying, and the resulting changes in Al to O ratio seen in the X-ray maps, Figure 22. Of more relevance in Figure 22, C is seen surrounding the areas, presumably infiltrated epoxy. The Si-O binder/matrix is seen where the Al-O grains and small particles all meet in the center of the map. This indicates even small alumina pockets are still broadly consistent with the large ones in terms of chemistry and surrounding binder/matrix.

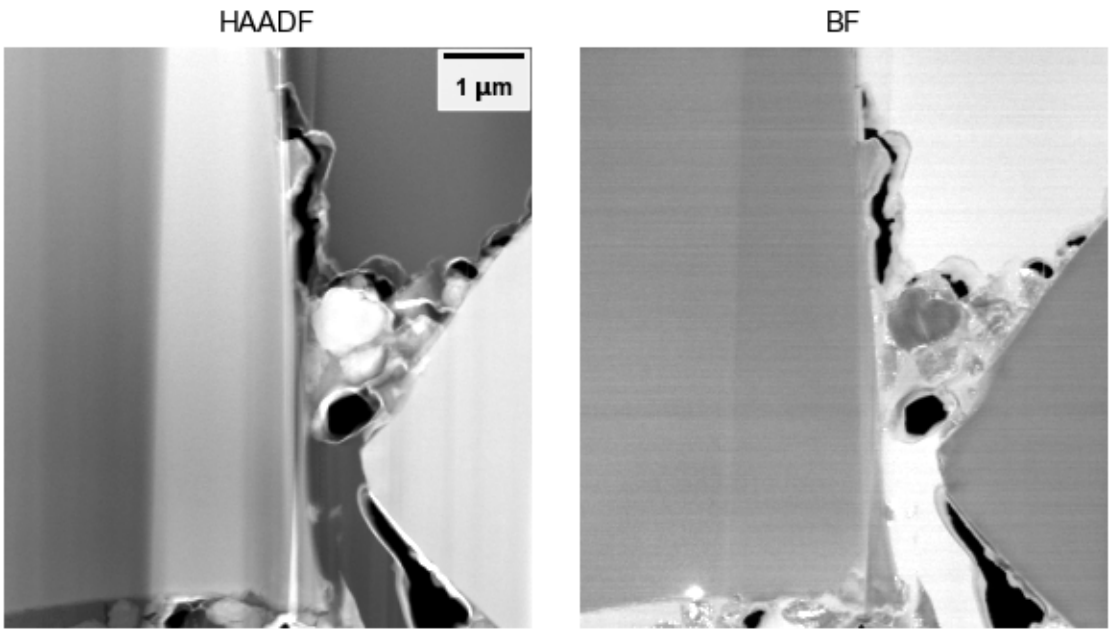


**Figure 21. Moderate-magnification STEM images of a FIB liftout from Unirradiated Sample 5. Vertical contrast in HAADF is a thickness effect due to uneven FIB milling.**

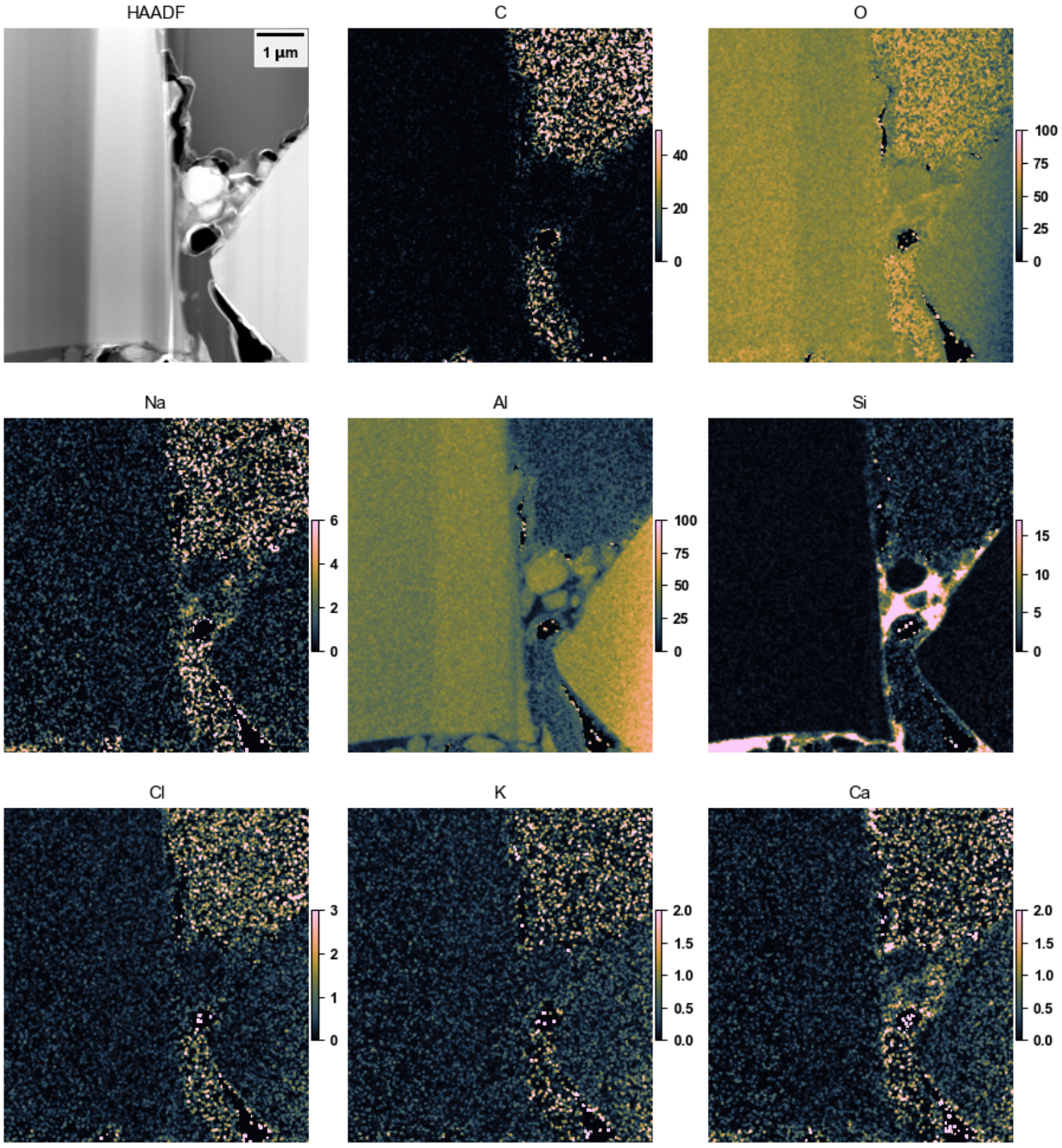


**Figure 22. X-ray maps, presented as estimated atom%, of the region of Figure 21. Speckle in the vacuum area is a quantification artifact and should be ignored. Changes in Al:O stoichiometry with thickness are a quantification artifact due to preferential absorption of soft O X-rays.**

Overall, Unirradiated Sample 5 showed the large alumina grains and a Si-O binder/matrix, without the major tertiary element contributions of Unirradiated Sample 1, other than a small contribution of Ca to the matrix.

### 3.1.3 Sample 11: AlO

Prior results show Unirradiated Sample 11 to consist of blocky alumina grains in a mostly Si-O binding matrix with relatively little content of other elements [1]. This is consistent with the more detailed STEM results here. Blocky grains, with the prior-observed small pores, are visible in Figure 23 and in more detail in Figure 24. As above, both grain-grain and grain-matrix interfaces are present. The X-ray mapping data, Figure 25. Three broad types of regions are seen in Figure 25: first, the Al-O blocky grains; second, the Si-O rich matrix/binder, containing a small amount of K; third, a carbonaceous phase, possibly an infiltrated organic.

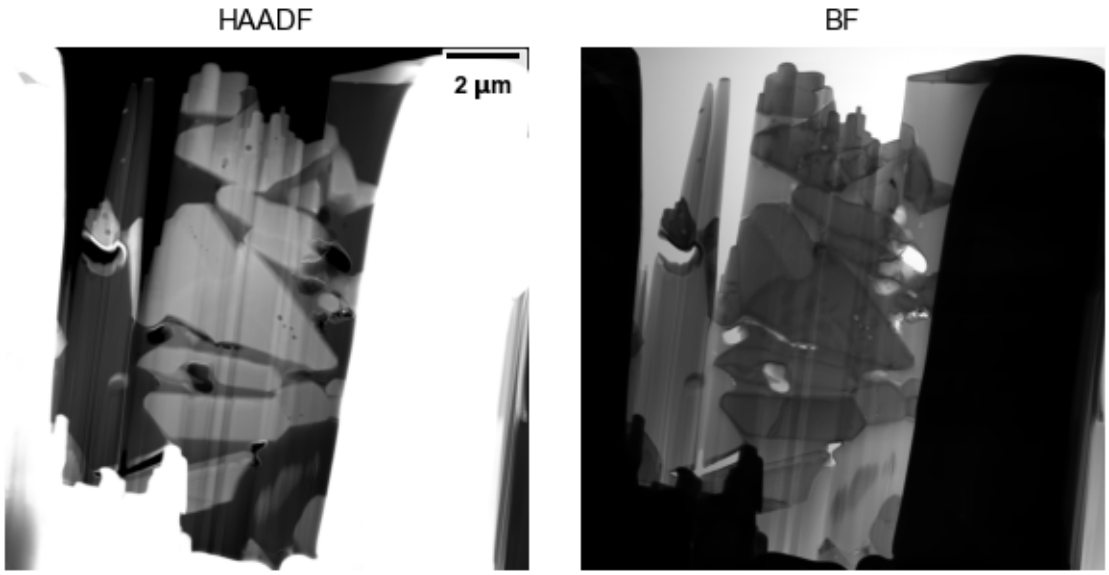


**Figure 23. Low-magnification STEM images of a FIB liftout from Unirradiated Sample 11.**

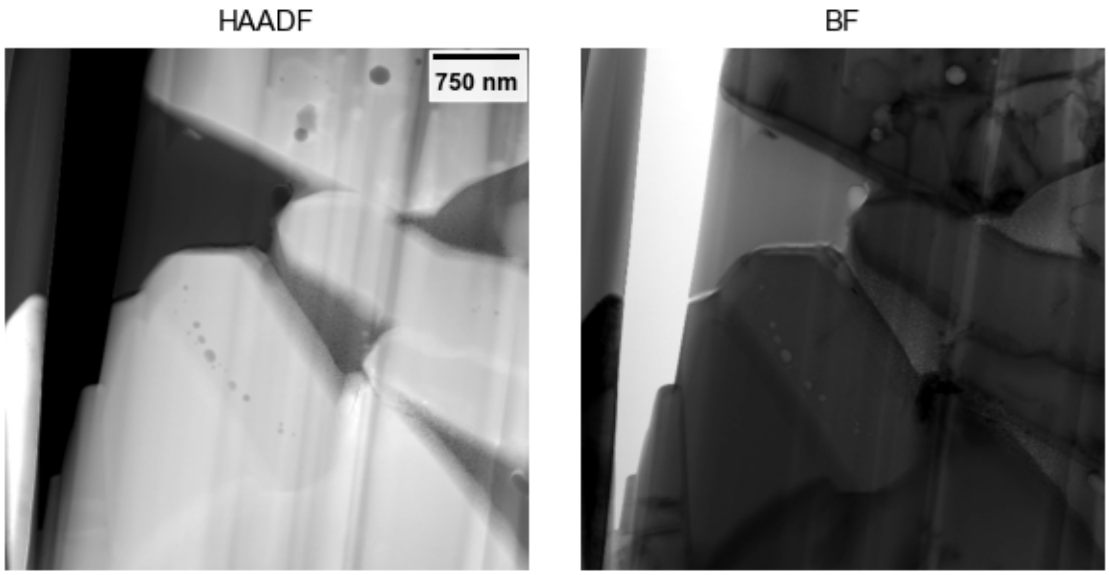


**Figure 24. Moderate-magnification STEM images of a FIB liftout from Unirradiated Sample 11.**

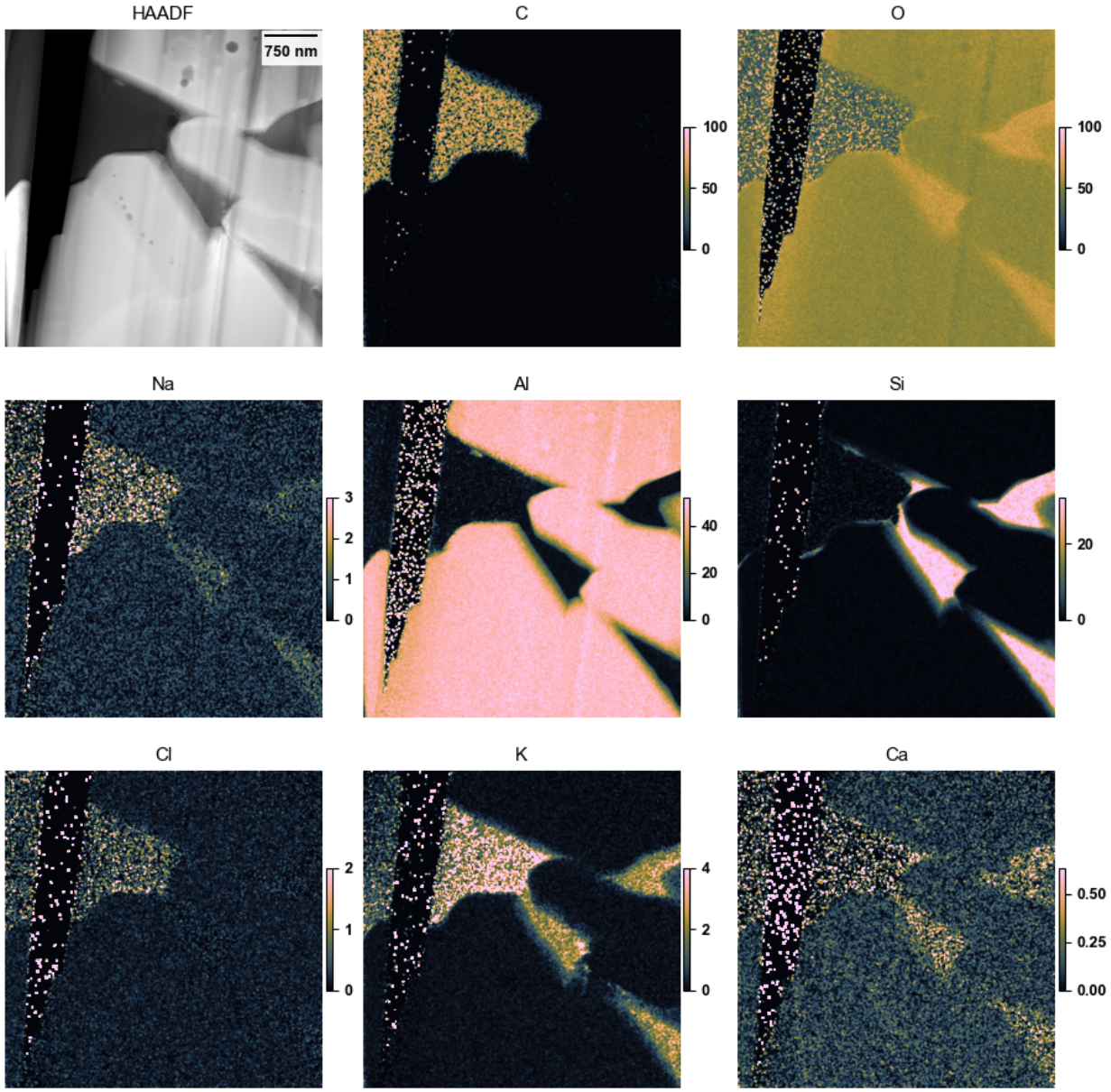


**Figure 25. X-ray maps, presented as estimated atom%, of Figure 24. Speckle in the vacuum area is a quantification artifact and should be ignored.**

As the view becomes more detailed, Figure 26, the small pores in the alumina grains are seen clearly and the Si-O binder/matrix is also seen to connect the alumina grains. The C-rich region is black in HAADF (very low average atomic number). The Al-O and Si-O regions are seen by the X-ray mapping, Figure 27, to be sharply defined and contain only small quantities of the other elements.

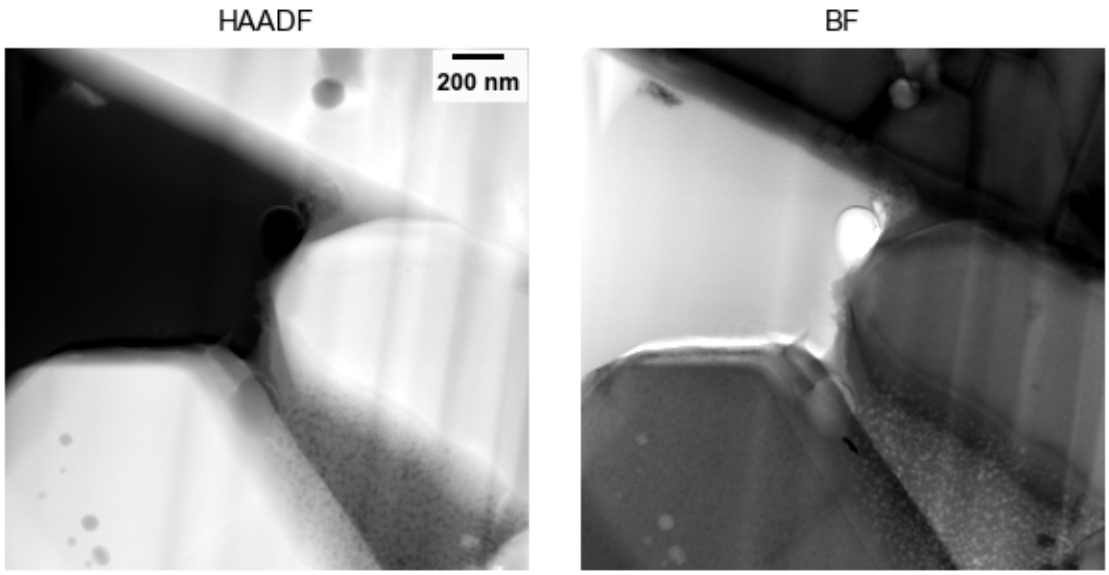


**Figure 26. Higher-magnification STEM images of a FIB liftout from Unirradiated Sample 11.**

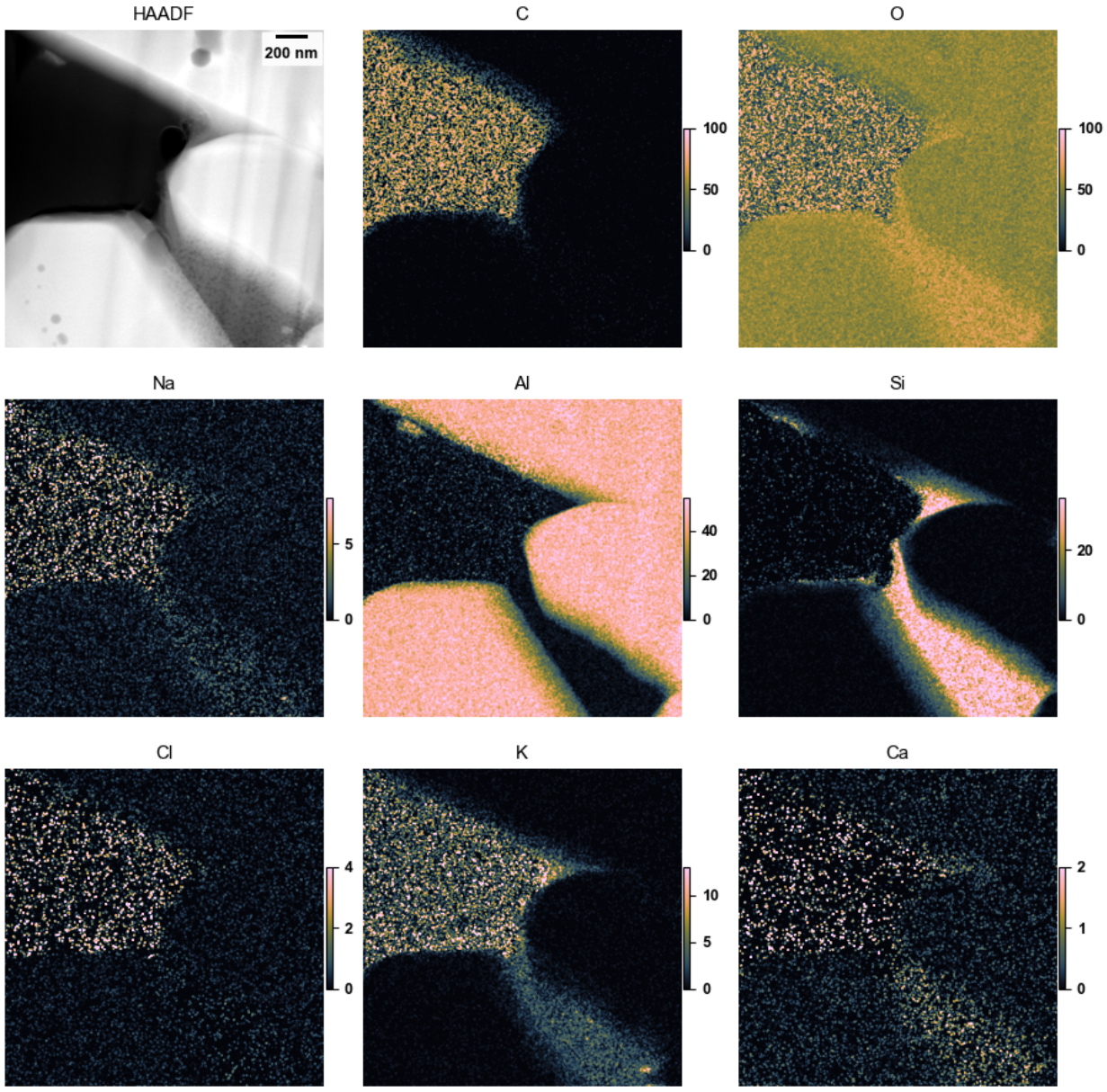


**Figure 27. X-ray maps, presented as estimated atom%, region of Figure 26.**

A second liftout from this sample showed a surprising behavior; in Figure 28, for instance, the low-atomic-number regions show round spots of higher atomic number. In more detail, Figure 29, these round features are seen in much more detail and cover the sample regions at high density.

X-ray mapping shows a number of surprising features, Figure 30. Specifically, the round features sit on the Si-O binder matrix, and consist of potassium-chlorine rich areas. This specimen was not handled or prepared differently than any of the other samples, so the anomalous presence of K-Cl ~~regoins~~regions is surprising. Possible sources of these elements are difficult to ascertain, but could presumably be residues from the sample fabrication, or from metallographic polishing.

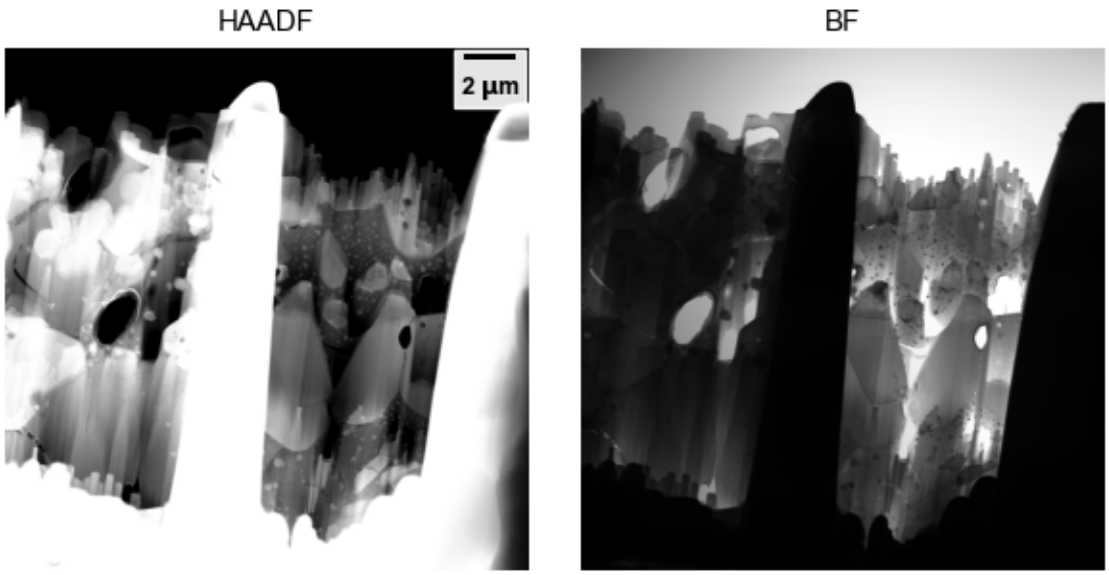


**Figure 28. Low-magnification STEM images of a FIB liftout from Unirradiated Sample 11.**

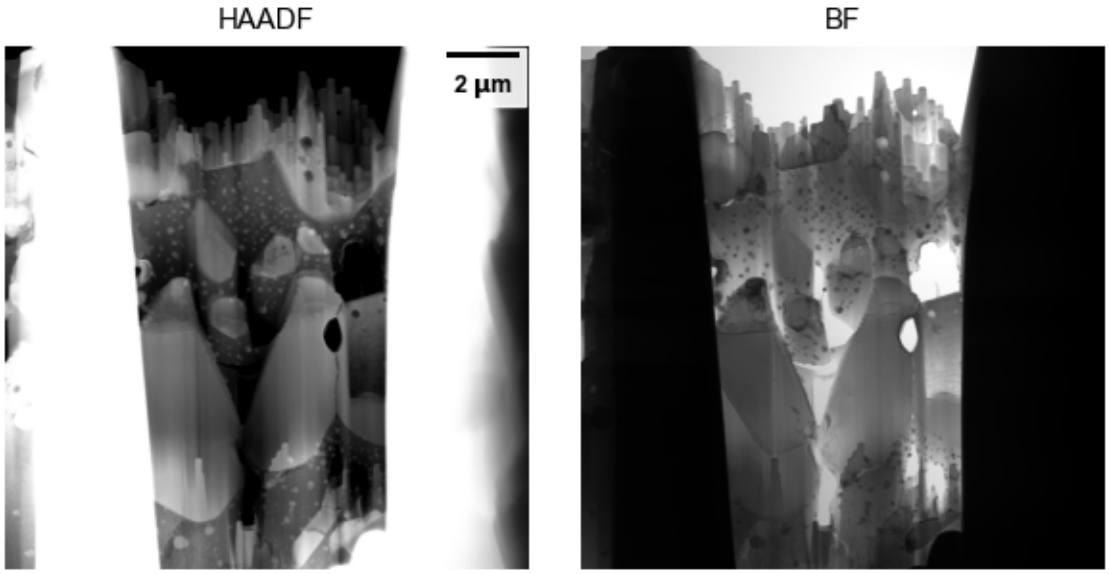


**Figure 29. Moderate-magnification STEM images of a FIB liftout from Unirradiated Sample 11.**

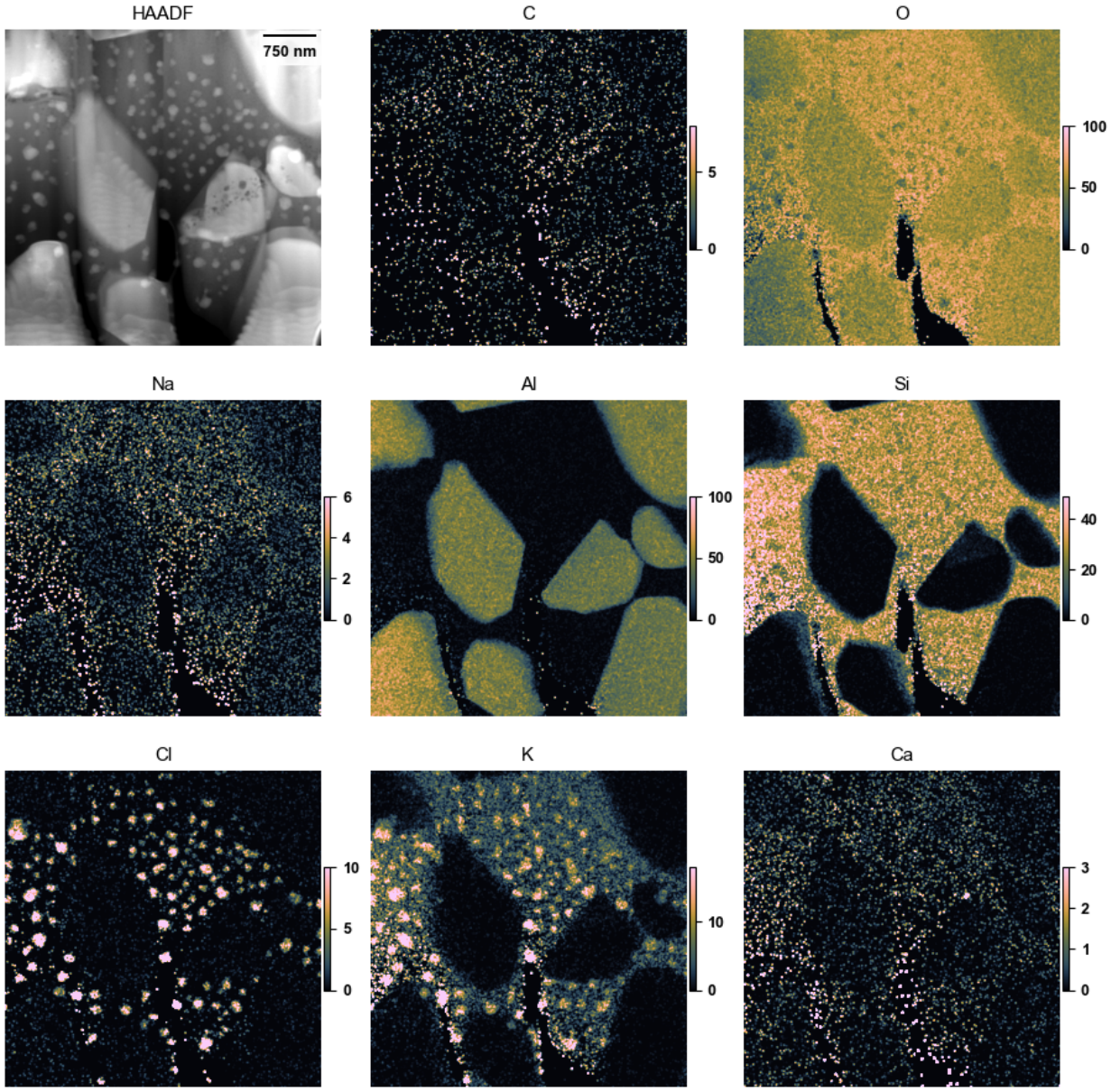


**Figure 30. X-ray maps, presented as estimated atom%, region of Figure 29.**

At high magnification, Figure 31, these K-Cl features are seen to be very round and show significant contrast compared to the amorphous Si-O layer around them, perhaps indicating crystallinity. The X-ray map of Figure 32 shows these features in elemental ~~d~~detail, and a small Ca-rich pocket, consistent with the other samples, is also seen to be present at the Si-O/Al-O interface. However, the most surprising part of the dataset in Figure 32 was what happened after the ~10 minute integration, Figure 33, where STEM imaging of the same region showed significantly reduced quantities of the these K-Cl features, indicating they were sublimed or diffused away by the action of the intense X-ray mapping electron beam.

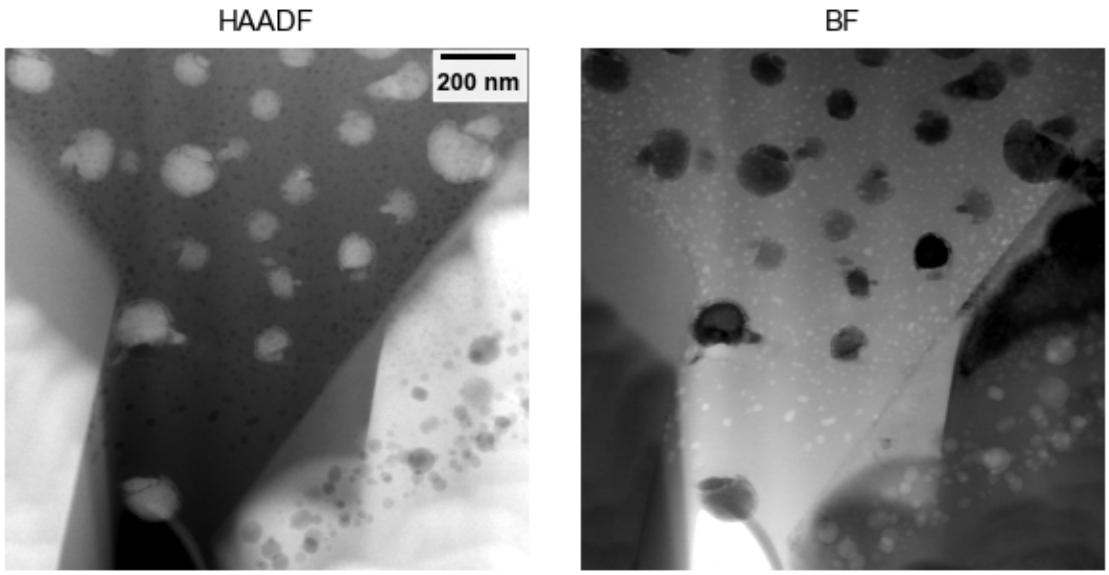


**Figure 31. Higher-magnification STEM images of a FIB liftout from Unirradiated Sample 11, showing anomalous round features.**

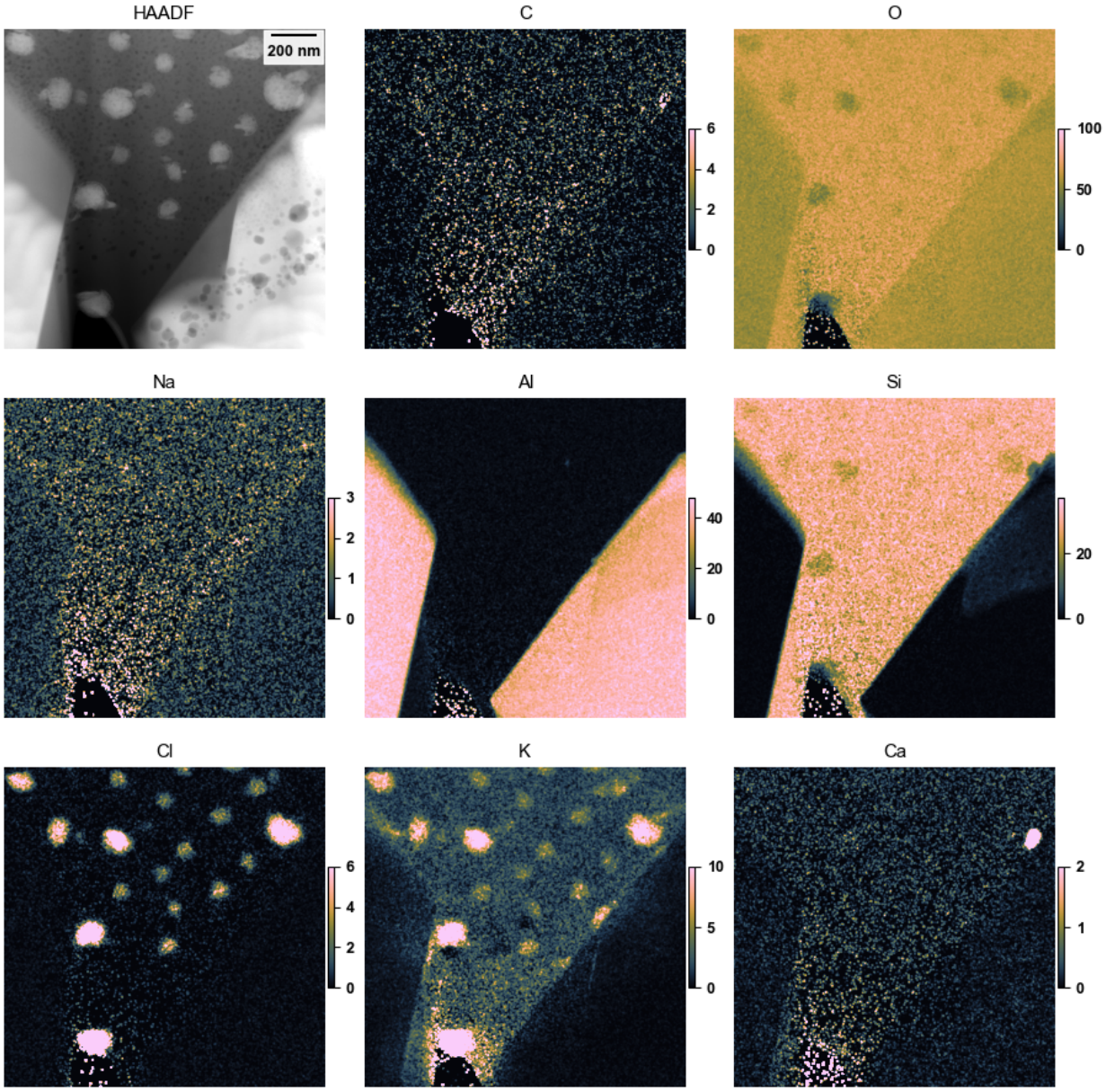


**Figure 32. X-ray maps, presented as estimated atom%, of Figure 31. Speckle in the vacuum area is a quantification artifact and should be ignored.**

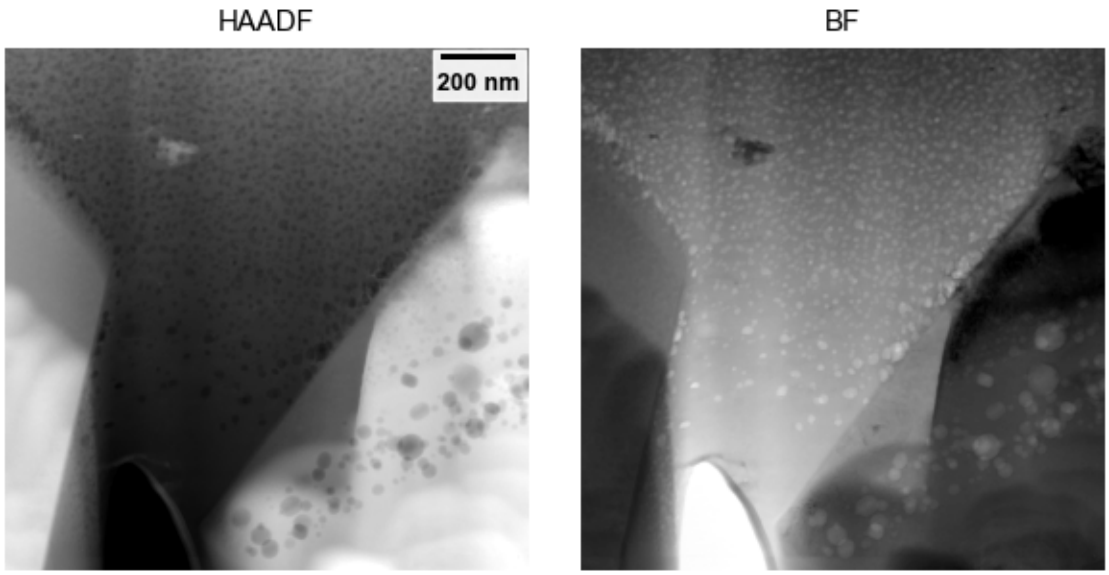


**Figure 33. The region of Figure 31, after X-ray map integration.**

Because the software Velox was used to acquire the X-ray mapping spectrum images, it is possible to use software to prepare snapshots from the integration. 50 frames (individual spectrum images) were integrated together to create the aggregate dataset in Figure 32. Using the Velox post-processing features, five sub-maps were acquired, Figure 34, from the five quintiles of integration time: e.g., the first quintile consists of frames 1-10, the second 11-20, etc., to frames 41-50 in the fifth quintile. This provides semi-static snapshots of the progress of the integration, and it's clear that the number and density of the K-Cl rich regions is markedly reduced in each quintile of the integration time, indicating that, indeed, the K-Cl features are reduced steadily with increasing electron fluence.

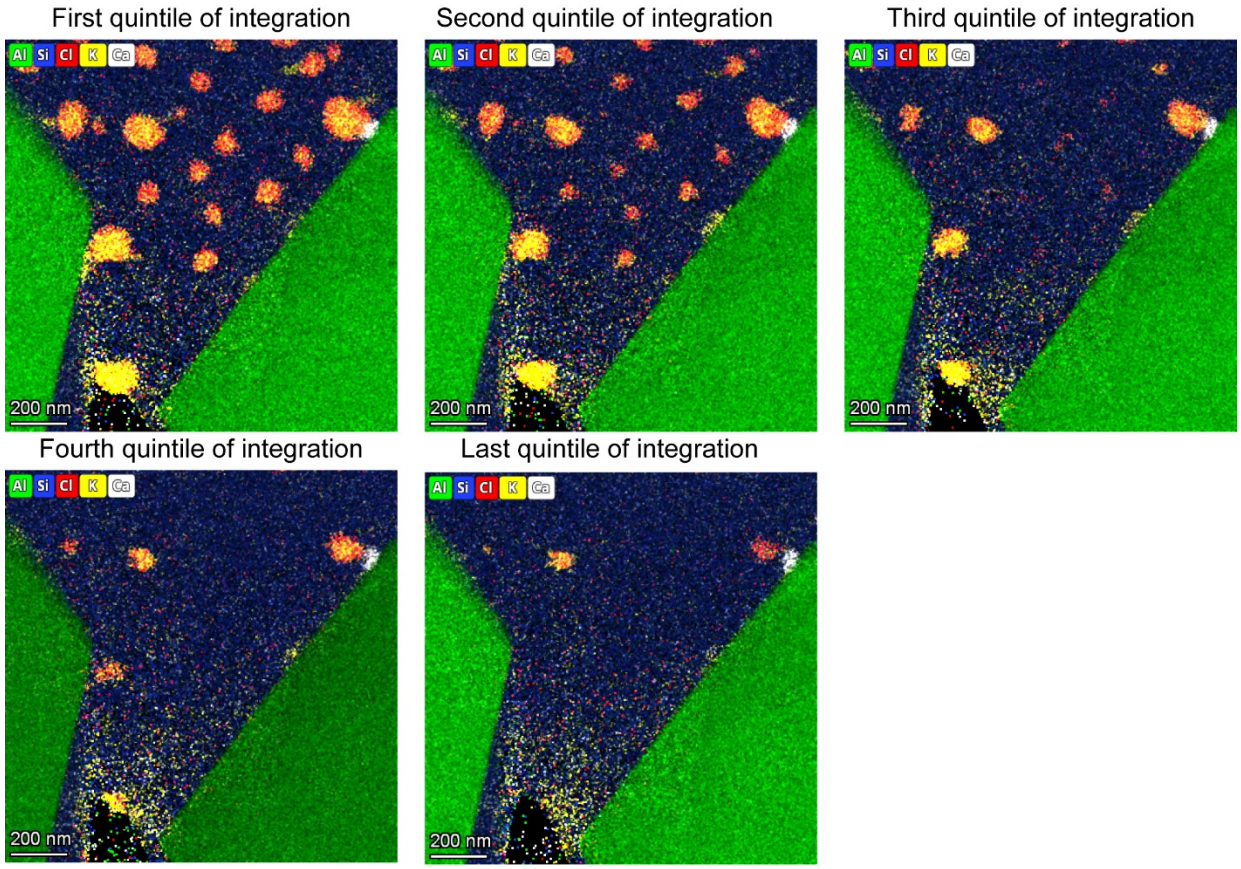


**Figure 34. Color-overlay maps of the data in Figure 32, but each from a different 20% of the aggregated data.**

Overall, Unirradiated Sample 11 is broadly consistent with the prior results and with the Unirradiated Samples 1 and 5 in that large, blocky Al-O grain are present in a Si-O binder matrix. Regions enriched in K-Cl were observed and were volatile against the electron beam; why regions of this sample showed this behavior, and no other samples or regions did, is unclear, but probably arising due to inhomegeneities that captured transient elements.

### 3.1.4 Sample 12: ZrO

In the prior work [1], Unirradiated Sample 12 was observed to consist of large, blocky $ZrO_2$ grains. In this work, the STEM results are consistent with this, Figure 35, in that large blocky high-atomic number grains are observed in a low-atomic number matrix region.

In greater detail, Figure 36 and Figure 37, large and small ceramic grains are visible in the complex binder regions. From the X-ray data, Figure 38, shows both the expected features and unexpected features. In terms of expected, the matrix consists primarily of Zr-O grains with small amounts of Si-O binder or matrix around them, and infiltration of C-rich regions. However, unexpectedly, both Ca and Hf were observed in the Zr-O grains. These elemental identifications are confirmed by EDS area spectra in Figure 39. Ultimately, calcia-stabilized zirconia is a common technological material, one of the class of partially stabilized zirconias (PSZs) [e.g., 4], so a small amount (~few percent) of Ca in zirconia is not

unreasonable to find. Hf is generally present in zirconium feedstocks due to the elements' similar chemistry and colocation of hafnium in zirconium ore; unless specifically nuclear-grade zirconium is purchased, Zr:Hf at a ratio of 50:1 is often found in zircon ores [5]. If Zr-based ceramics are used in-reactor in the future, it might be worthwhile to specify low-Hf feedstock, due to hafnium's high neutron absorption compared to zirconium.

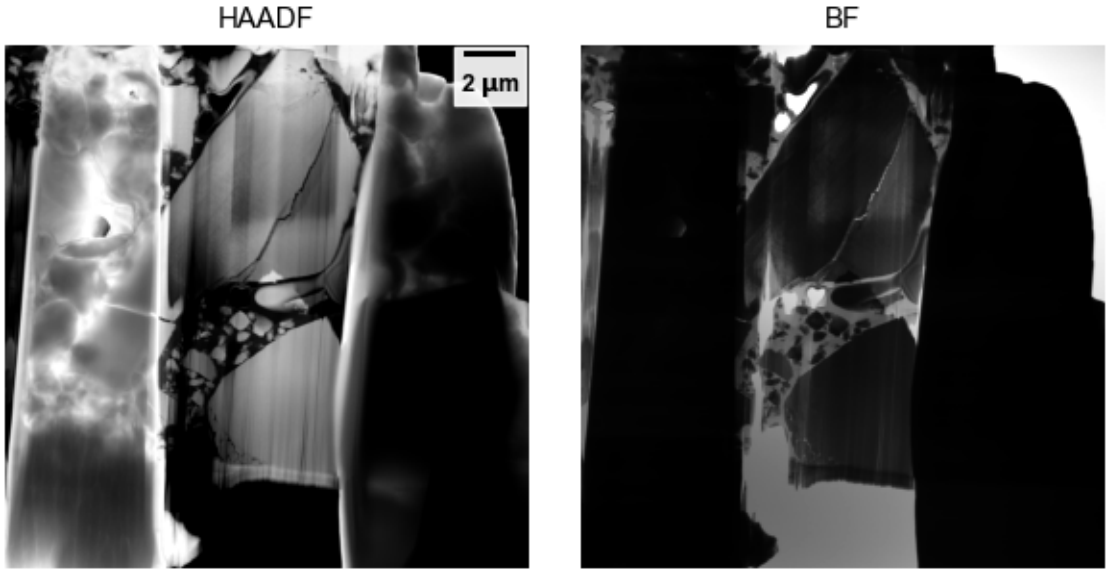


**Figure 35. Low-magnification STEM images of a FIB liftout from Unirradiated Sample 12.**

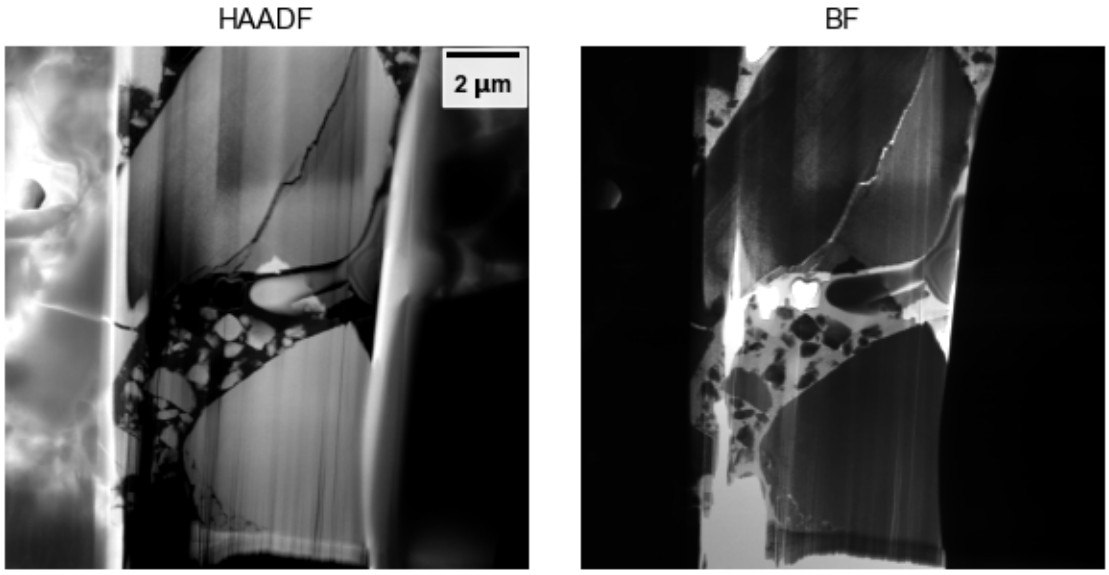


**Figure 36. Medium-magnification STEM images of a FIB liftout from Unirradiated Sample 12.**

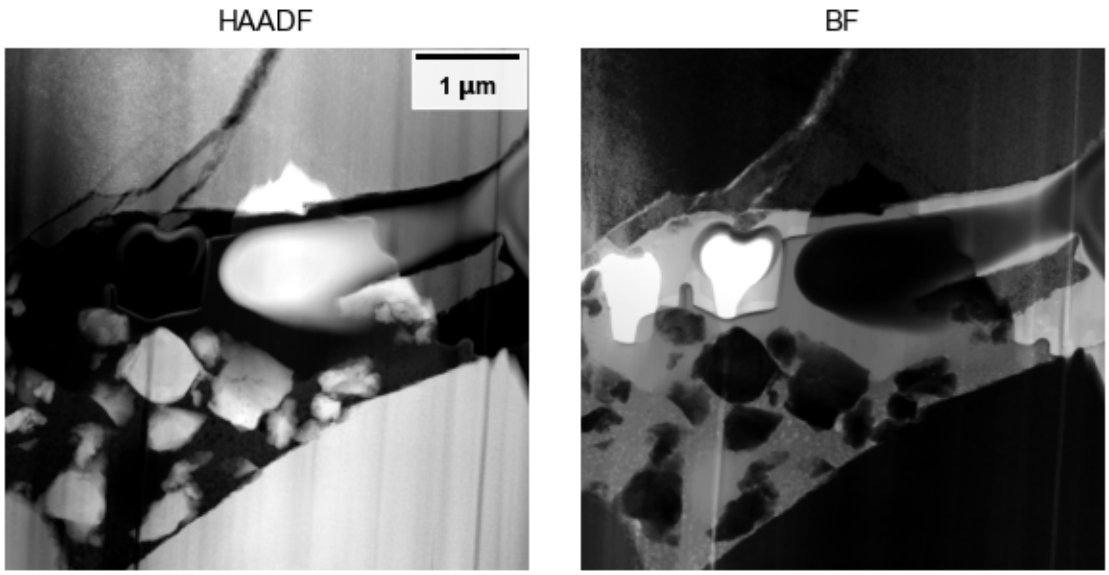


**Figure 37. Medium-magnification STEM images of a FIB liftout from Unirradiated Sample 12.**

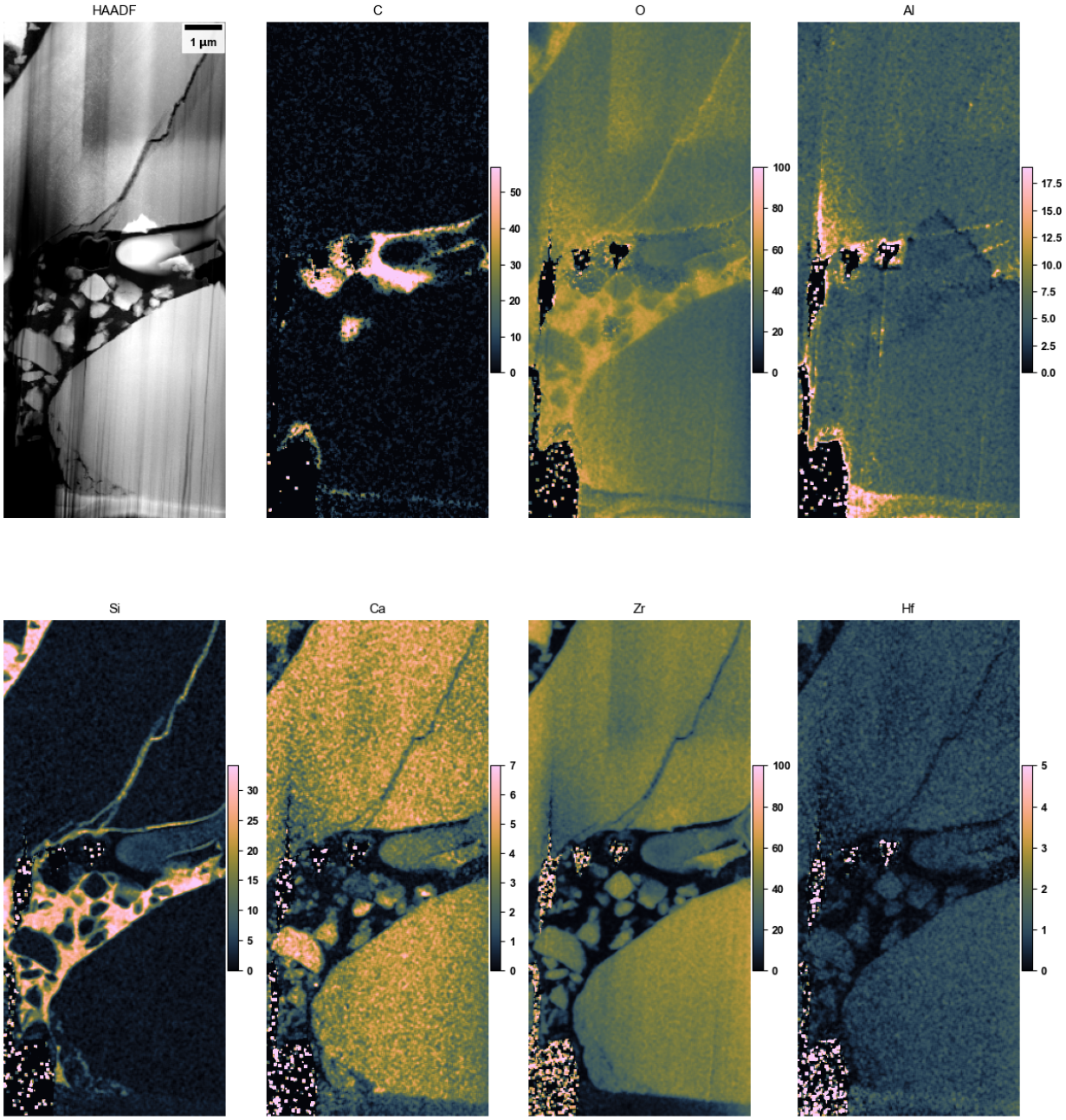


**Figure 38. X-ray maps, presented as estimated atom%, of Figure 36. Speckle in the vacuum area is a quantification artifact and should be ignored.**

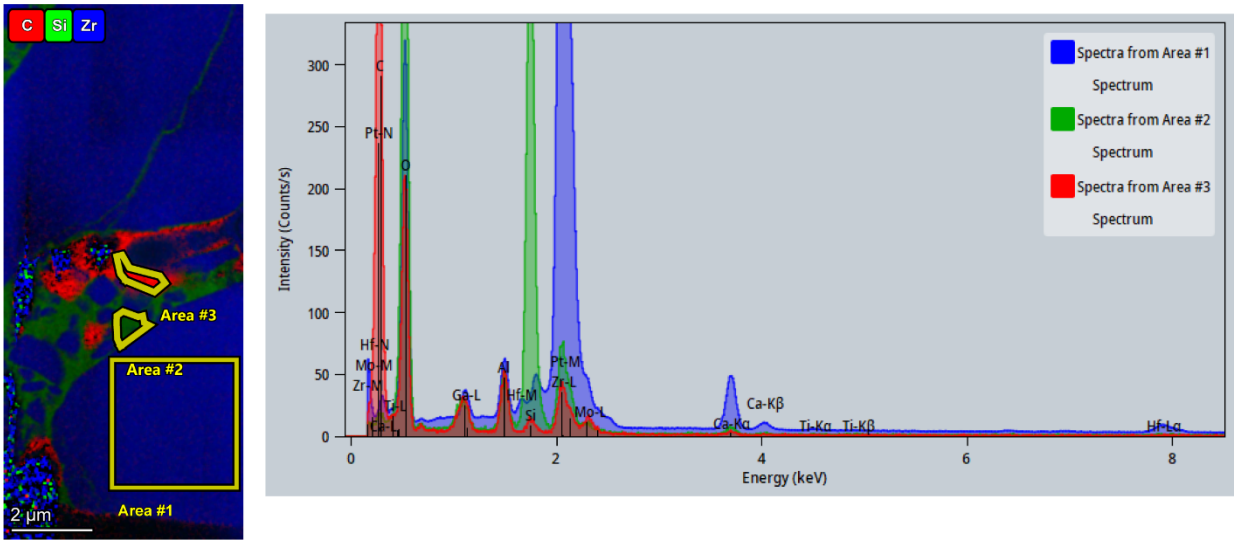


**Figure 39. Left: Color overlay of the data in Figure 38, with three areal spectra marked. Right: extracted spectra from the three areas.**

If the small zirconia grains and edges of the large grains are examined in more detail, Figure 40, with the X-ray mapping data, Figure 41, beginning to show some interesting fine-scale features invisible in the broader X-ray mapping data above in Figure 38. Specifically, in Figure 40 there are dark, round features in the HAADF image within the large zirconia grains. These consist of both black and dark gray contrast, indicating very low (black) and low (gray) atomic number. From the X-ray map, the gray (low atomic number) features appear to be Al-rich, presumably aluminum oxides. The black (very low atomic number) features appear to be cavities, because no elements other than the surrounding Zr-O are observed at those locations. Further, the Ca maps in Figure 41 begin to show a fine periodicity in the large Zr-O grain, in addition to a few blocky ~100 nm or so sized regions much richer in Ca than the surrounding areas. Although the Ca-rich and Ca-poor regions in the Ca map are all very low (less than about 5 at%), the variations are clearly observed. Variations in the Hf map are not seen and the Hf appears to distributed uniformly in the Zr, although given its low content, small variations would be invisible under the noise level.

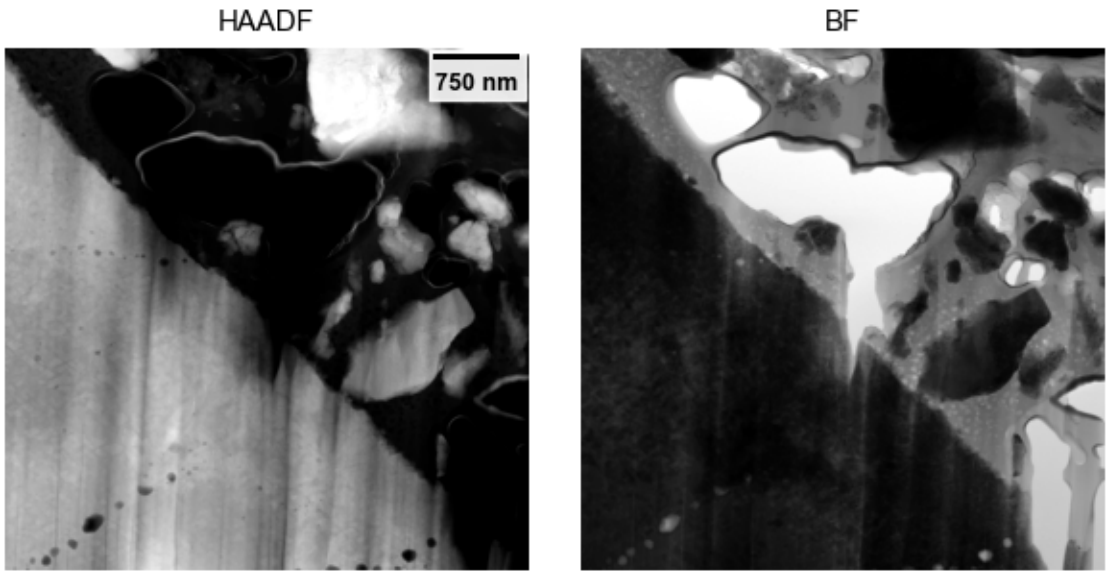


**Figure 40. High-magnification STEM images of a FIB liftout from Unirradiated Sample 12.**

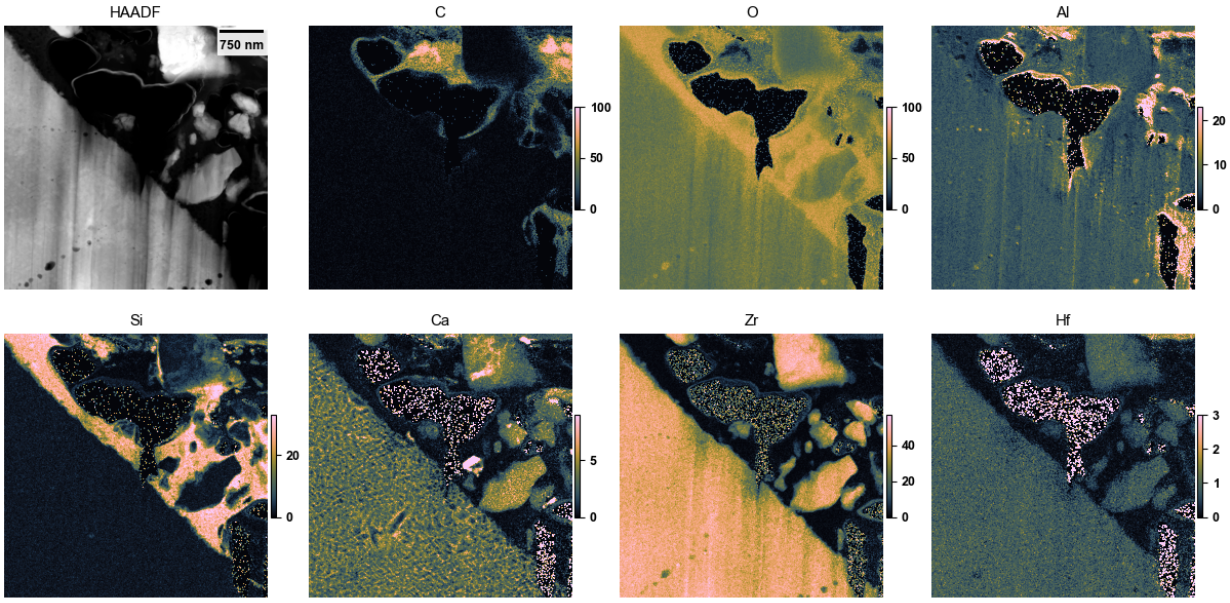


**Figure 41. X-ray maps, presented as estimated atom%, of Figure 40. Speckle in the vacuum area is a quantification artifact and should be ignored.**

Another FIB foil is imaged in Figure 42-Figure 43, with the foil being taken from a monolithic area of zirconia without apparent binder or infiltrated organic regions. Large cavities ~100 nm are visible in the zirconia grains, Figure 43. X-ray mapping shows a uniform structure, with a single alumina particle near the top-right corner, Figure 44.

However, as the level of detail increases, Figure 45, more features become apparent. Both large and small voids are apparent, and regions of brighter and darker matrix are also visible, likely related to the variations in Ca/Zr ratio, which are visible in the X-ray mapping data, Figure 46. Noticeably, there are a few “V” or chevron-shaped regions of low Ca content visible in Figure 46; overlaying the Ca map onto the HAADF image, Figure 47, shows that voids coincide with the edges of these chevrons, but not all voids are associated with one of the chevron-shapes. The cause of these small Ca-poor regions, and the association of the voids, if any, is unclear. A few small pockets of Al were also observed, Figure 46.

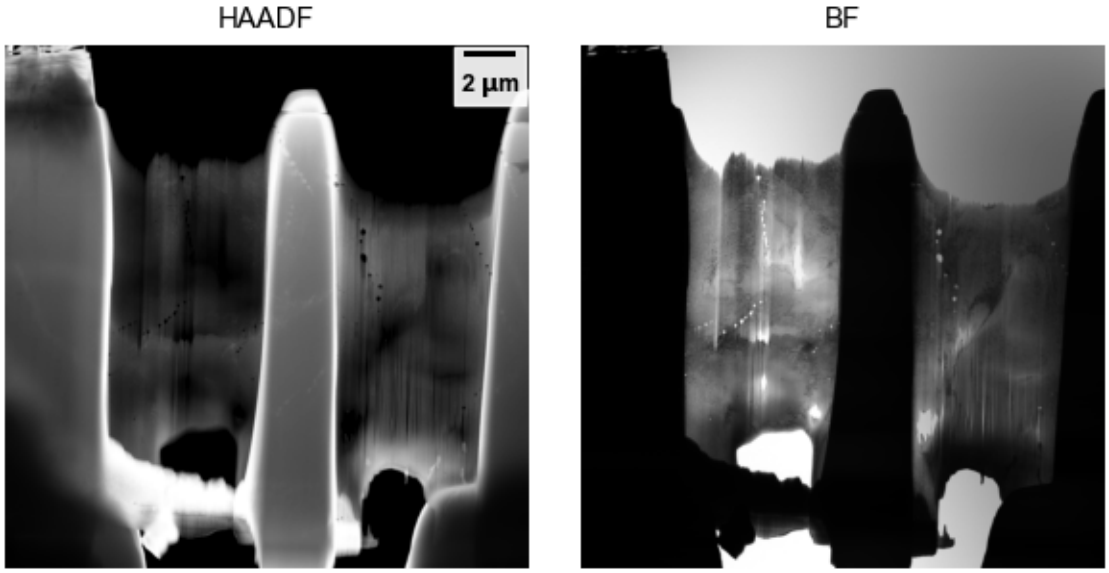


**Figure 42. Low-magnification STEM images of a FIB liftout from Unirradiated Sample 12.**

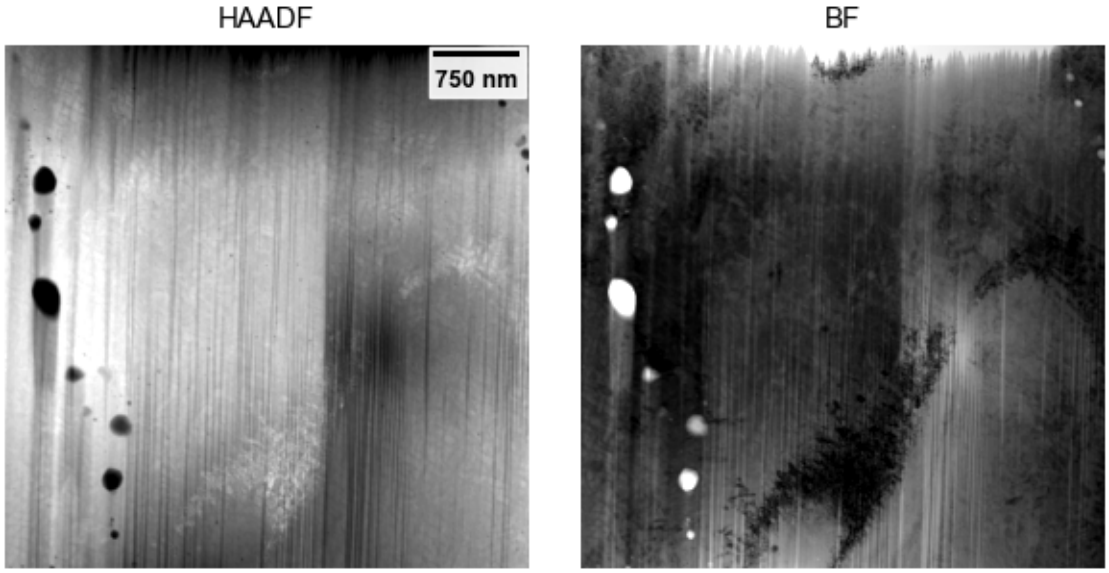


**Figure 43. Medium-magnification STEM images of a FIB liftout from Unirradiated Sample 12.**

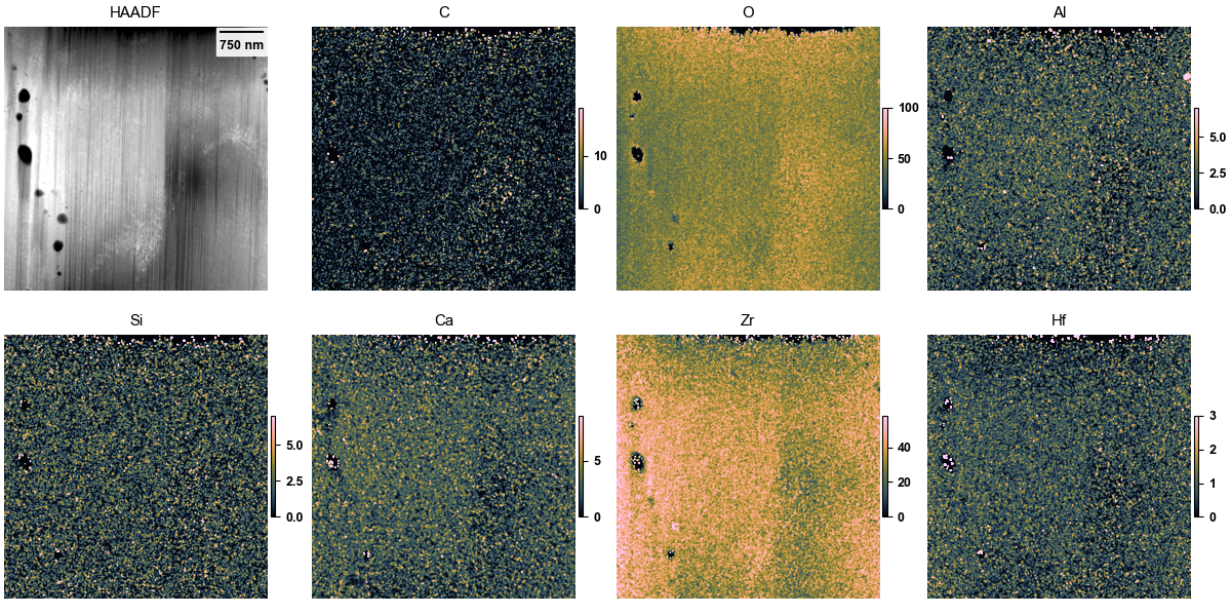


**Figure 44. X-ray maps, presented as estimated atom%, of Figure 43. Speckle in the vacuum area is a quantification artifact and should be ignored.**

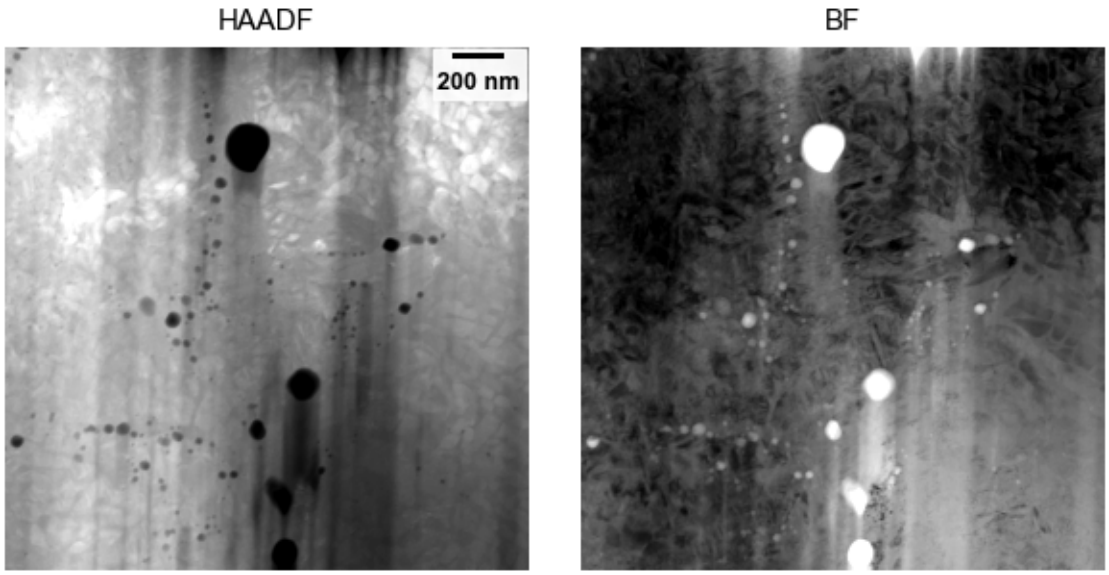


**Figure 45. High-magnification STEM images of a FIB liftout from Unirradiated Sample 12.**

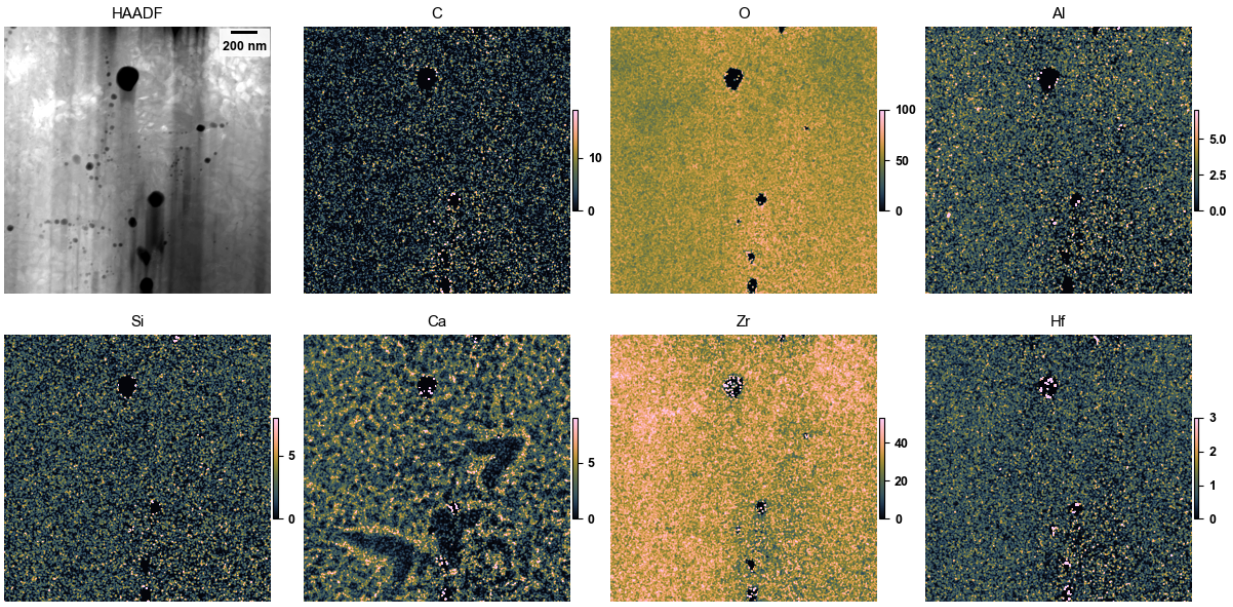


**Figure 46. X-ray maps, presented as estimated atom%, of Figure 45. Speckle in the vacuum area is a quantification artifact and should be ignored.**

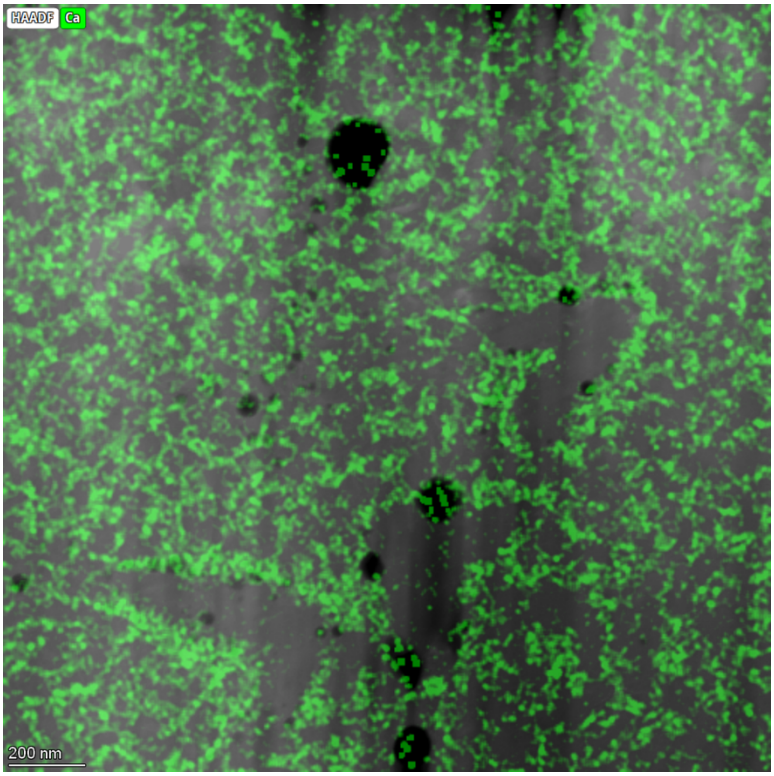


**Figure 47. Color overlay of the HAADF and Ca data in Figure 46. Ca in estimated atom%.**

At very high magnification, the zirconia grains show regions of high and low contrast, probably related to the different atomic number between Ca and Zr but also possibly some small misorientations resulting in subtle diffraction contrast, along with large (~50 nm) and small (~10 nm) round low-atomic-number features, Figure 48-Figure 49. From the X-ray mapping data, Figure 50, many small (<≈10 nm) Al-rich spherical precipitates are seen, and the Ca/Zr regions are present in a blocky square pattern with characteristic side sizes of ~50-100 nm. The Hf map is very noisy at ~1 at%, but no obvious segregation to or away from the Ca or Al is visible in the Hf data at the noise level. These observations are further seen in more detail in Figure 51-Figure 52. The results of the mapping are confirmed via extracted area spectra in Figure 53, where the Zr-O matrix is present in all three examined regions, the Ca-rich regions shows an increase in Ca while still remaining mostly Zr-O, and the Al-rich particles also show significant Zr contribution because the Al-rich particles are embedded in the surrounding Zr-O matrix and the electron beam must excite surrounding Zr to reach the Al.

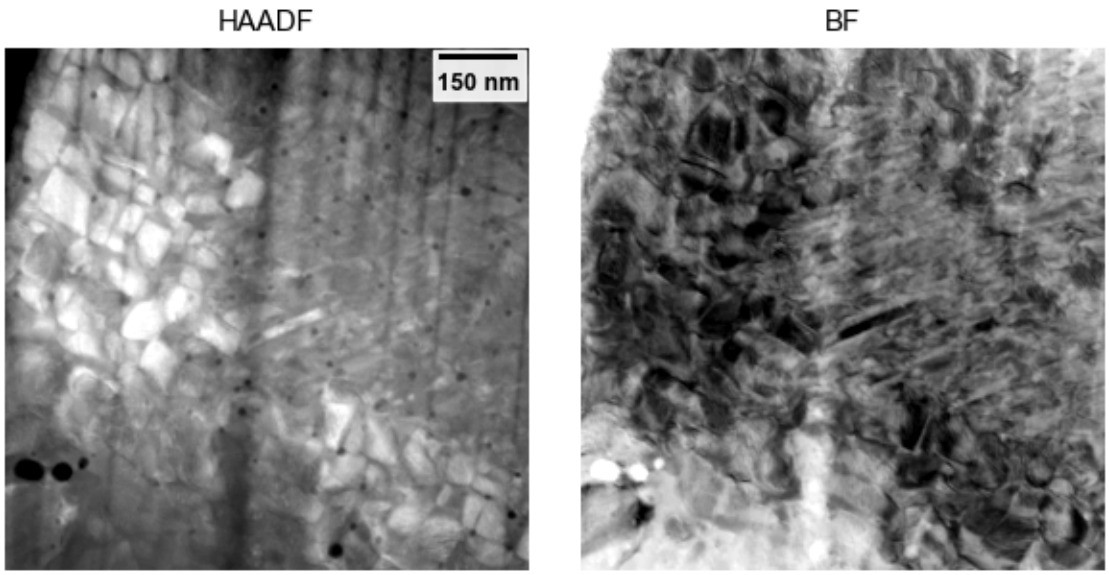


**Figure 48. High-magnification STEM images of a FIB liftout from Unirradiated Sample 12.**

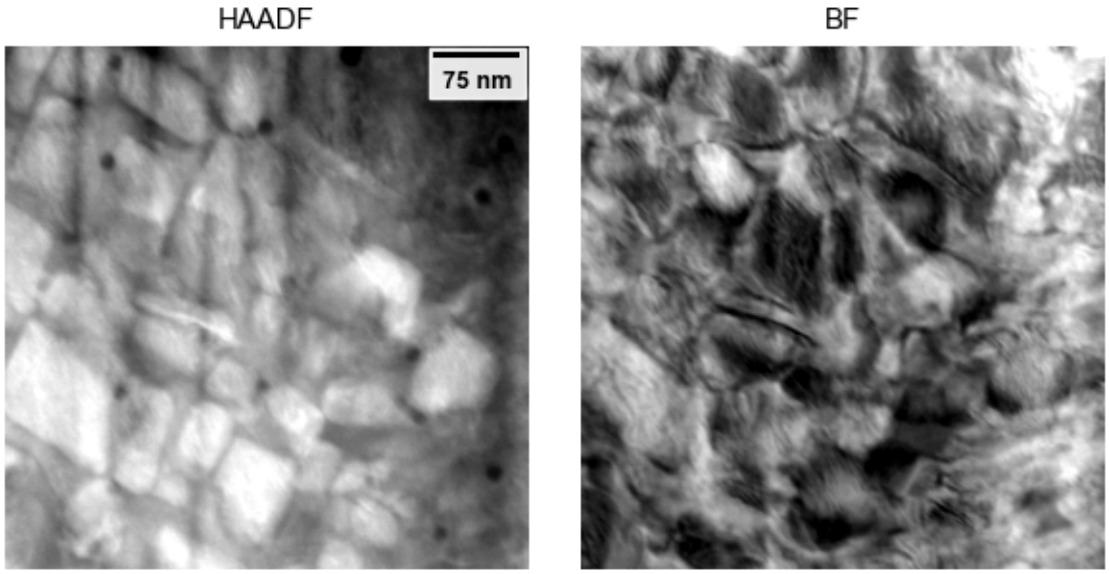


**Figure 49. High-magnification STEM images of a FIB liftout from Unirradiated Sample 12.**

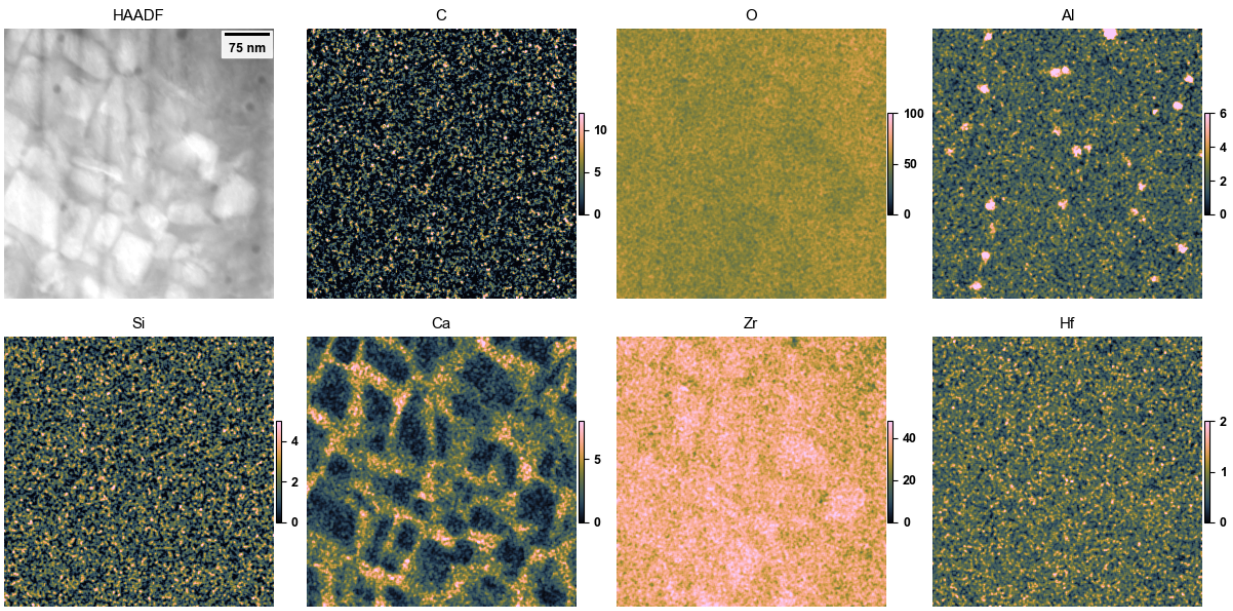


**Figure 50. X-ray maps, presented as estimated atom%, of Figure 49. Speckle in the vacuum area is a quantification artifact and should be ignored.**

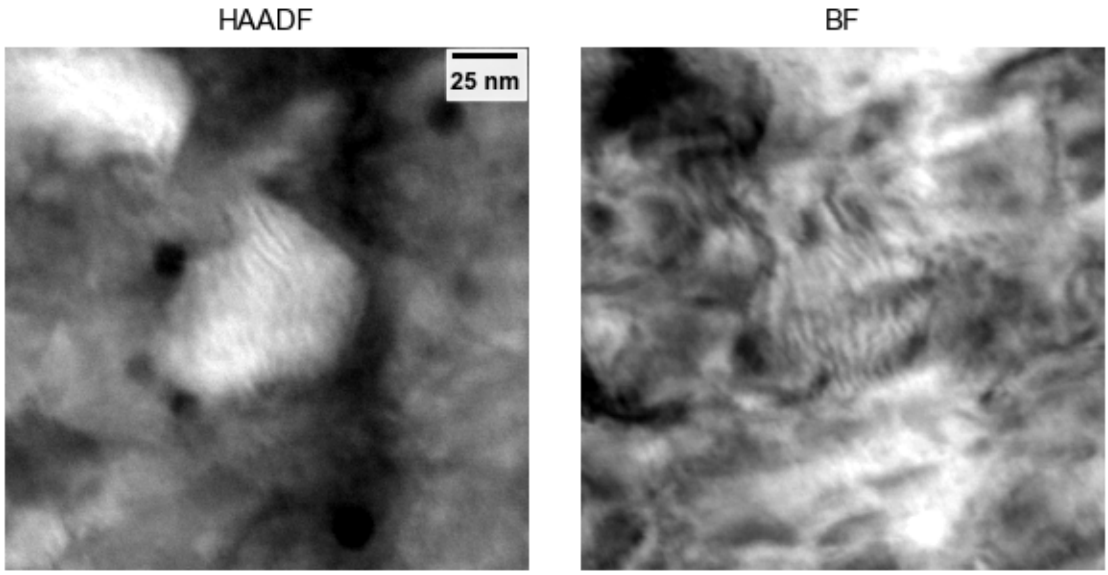


**Figure 51. High-magnification STEM images of a FIB liftout from Unirradiated Sample 12.**

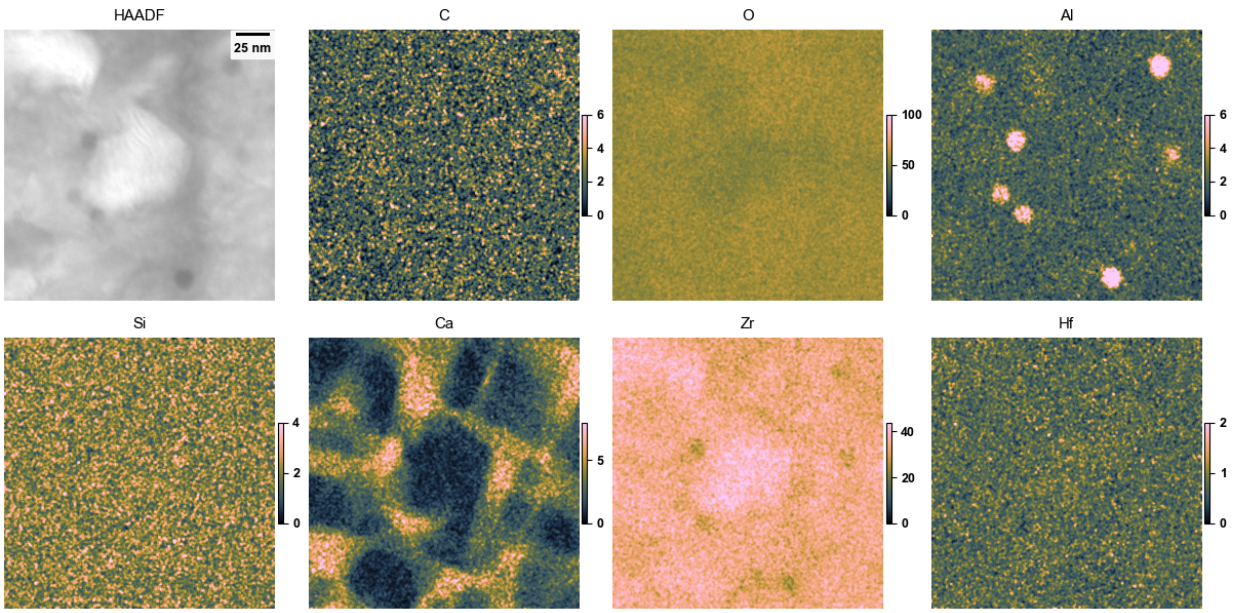


**Figure 52. X-ray maps, presented as estimated atom%, of Figure 51. Speckle in the vacuum area is a quantification artifact and should be ignored.**

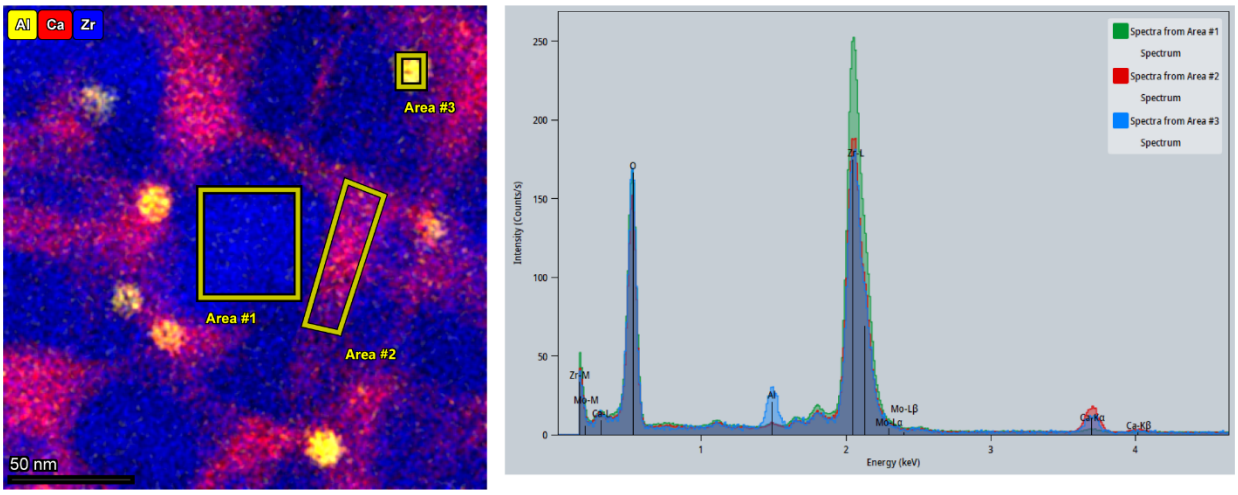


**Figure 53. Left: Color overlay of the data in Figure 52, with three areal spectra marked. Right: extracted spectra from the three areas.**

Overall, the examination of Unirradiated Sample 12 indicates the grains are partially-stabilized zirconia, stabilized with calcia, and non-nuclear-grade, Hf-containing Zr feedstock was used. The binder is a Si-O rich material with infiltration of C-rich materials. The zirconia consists of large and small grains, and the grains contain high densities of both voids and Al-rich inclusions, probably aluminum oxides. The zirconia itself shows domains of almost pure Zr-O with boundaries of Ca-Zr-O, where Ca reaches a few at% in the domain edges. The effects of Ca and Hf on irradiation effects and ultrasonic transmission are not clear a priori but could potentially become significant at high neutron doses.

## 3.2 IRRADIATED

### 3.2.1 Sample 1: Alkali Slurry

Sample EPRI-1 is comparable to a baseline of sample Unirradiated 1. The prior work [1] on Irradiated Sample 1 indicated regions of Al-O and Si-K-O, consistent with what was observed here in Unirradiated Sample 1.

In Irradiated Sample 1, a structure like in Unirradiated Sample 1 above is seen, Figure 54. Here, a low-atomic-number background containing blocky ceramic grains is present, and the grains show small intragranular and grain-boundary cavities. Higher magnification, Figure 55, shows a detail of an area where several of the blocky ceramic grains and small pockets of the amorphous filler phases are present. The X-ray mapping, Figure 56, of the same area shows the expected Al-O grains with Si-O rich matrix binder filling gaps between the alumina grains. Small amounts of Na-K-Ca are observed in the Si-O rich region, both in the maps of Figure 56 and from an extracted areal spectrum in Figure 57. The extracted spectra of Figure 57 show the clean Al-O spectrum in the ceramic grains and Si-Na-Ca with perhaps a small peak at K in the binder phase. There appears to be an increase in C, Cl, Na, etc., in a few regions of Figure 56's maps, but are primarily a quantification artifacts due to low count rates on C-rich regions that produce few X-ray counts, as seen in the Area #3 spectrum in Figure 57. Small Ca+Na rich regions were also seen to coincide with the low-atomic-number (dark) features in HAADF, either indicating Na+Ca coating internal surfaces on cavities, or Na+Ca rich precipitates.

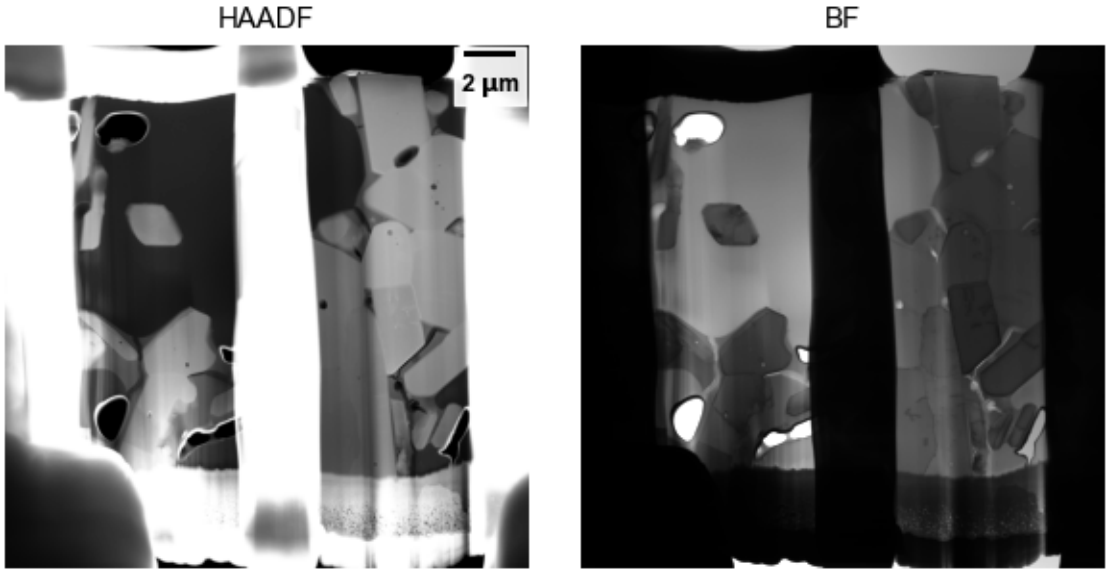


**Figure 54. Low-magnification STEM images of a FIB liftout from Irradiated Sample EPRI-1.**

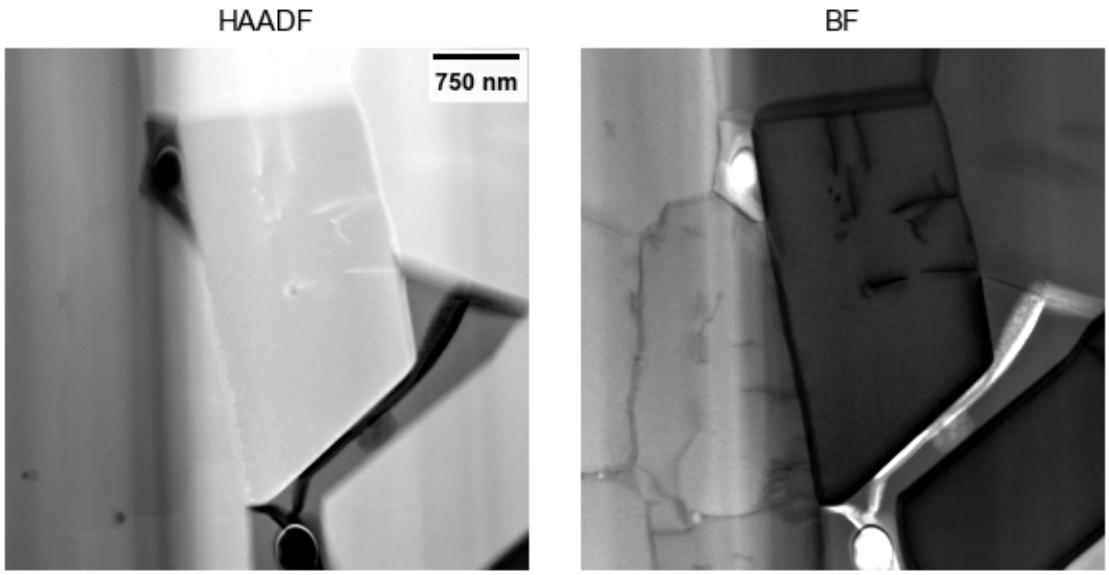


**Figure 55. Medium-magnification STEM images of a FIB liftout from Irradiated Sample EPRI-1.**

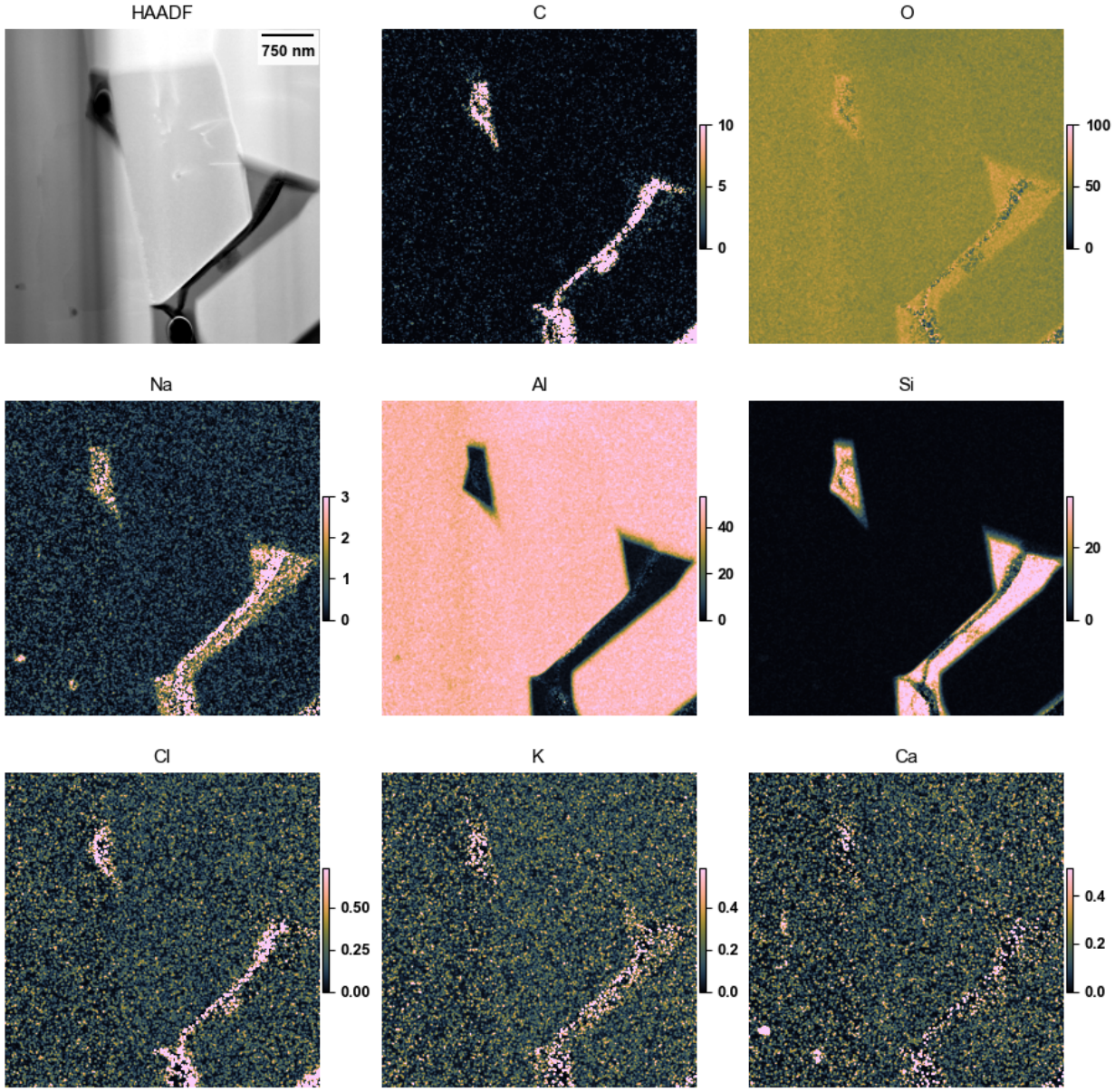


**Figure 56. X-ray maps, presented as estimated atom%, of the region of Figure 55. Speckle in the vacuum area is a quantification artifact and should be ignored.**

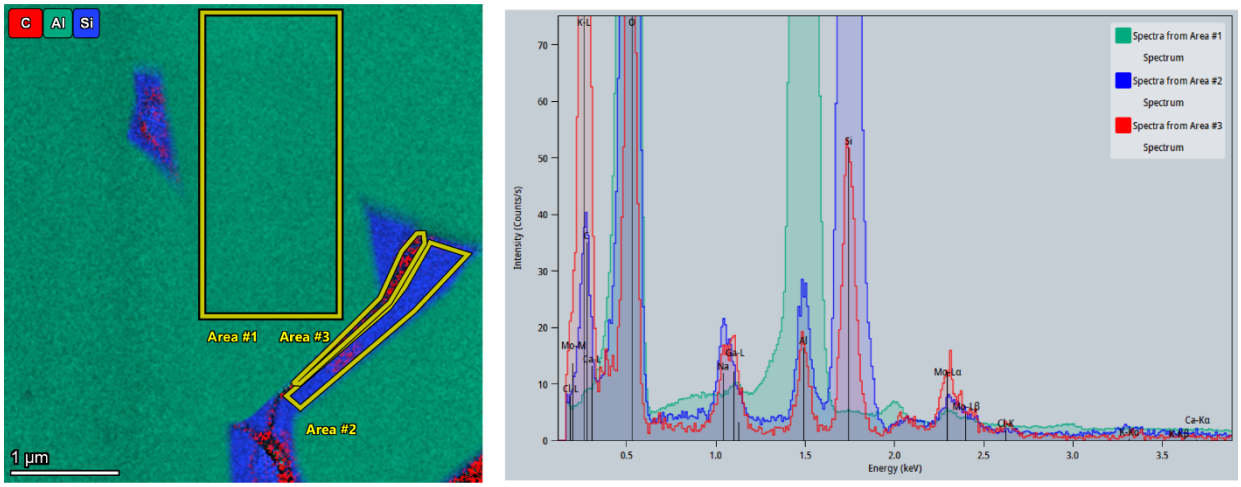


**Figure 57. Left: Color overlay of the data in Figure 56, with three areal spectra marked. Right: extracted spectra from the three areas.**

In the low-magnification image of Figure 54, a single isolated roughly rhombohedral grain was observed in the surrounding matrix, seen in more detail in Figure 58. The X-ray mapping results, Figure 59, indicate this alumina grain was surrounded by carbonaceous material, perhaps epoxy, rather than the Si-O binder material. Interestingly, the alumina grains observed have significant Si on their surface, perhaps due to wetting of the alumina grains during fabrication of the mixed-material couplant layer.

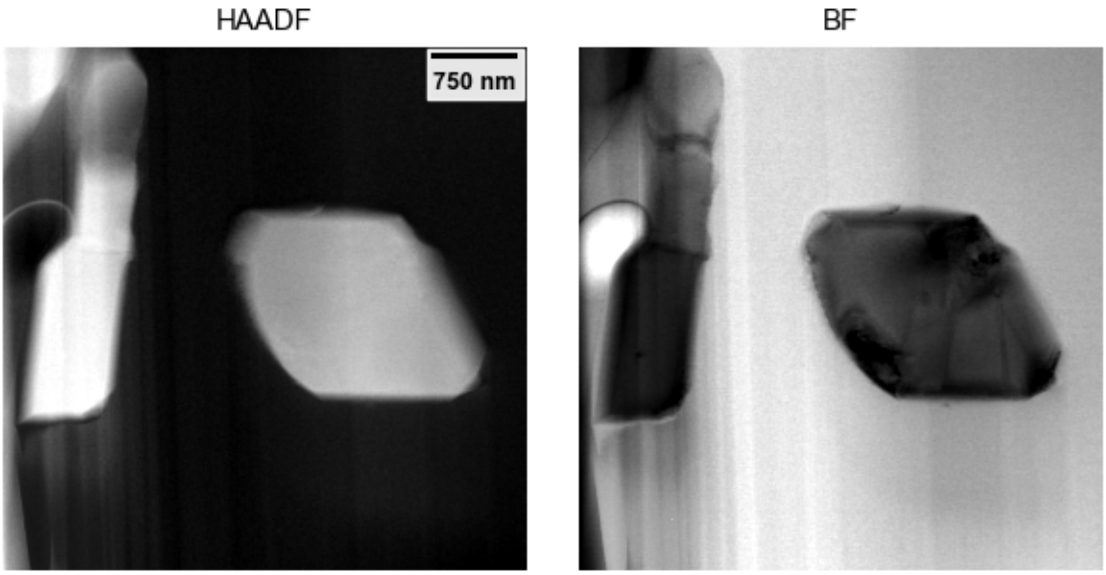


**Figure 58. High-magnification STEM images of a FIB liftout from Irradiated Sample 1.**

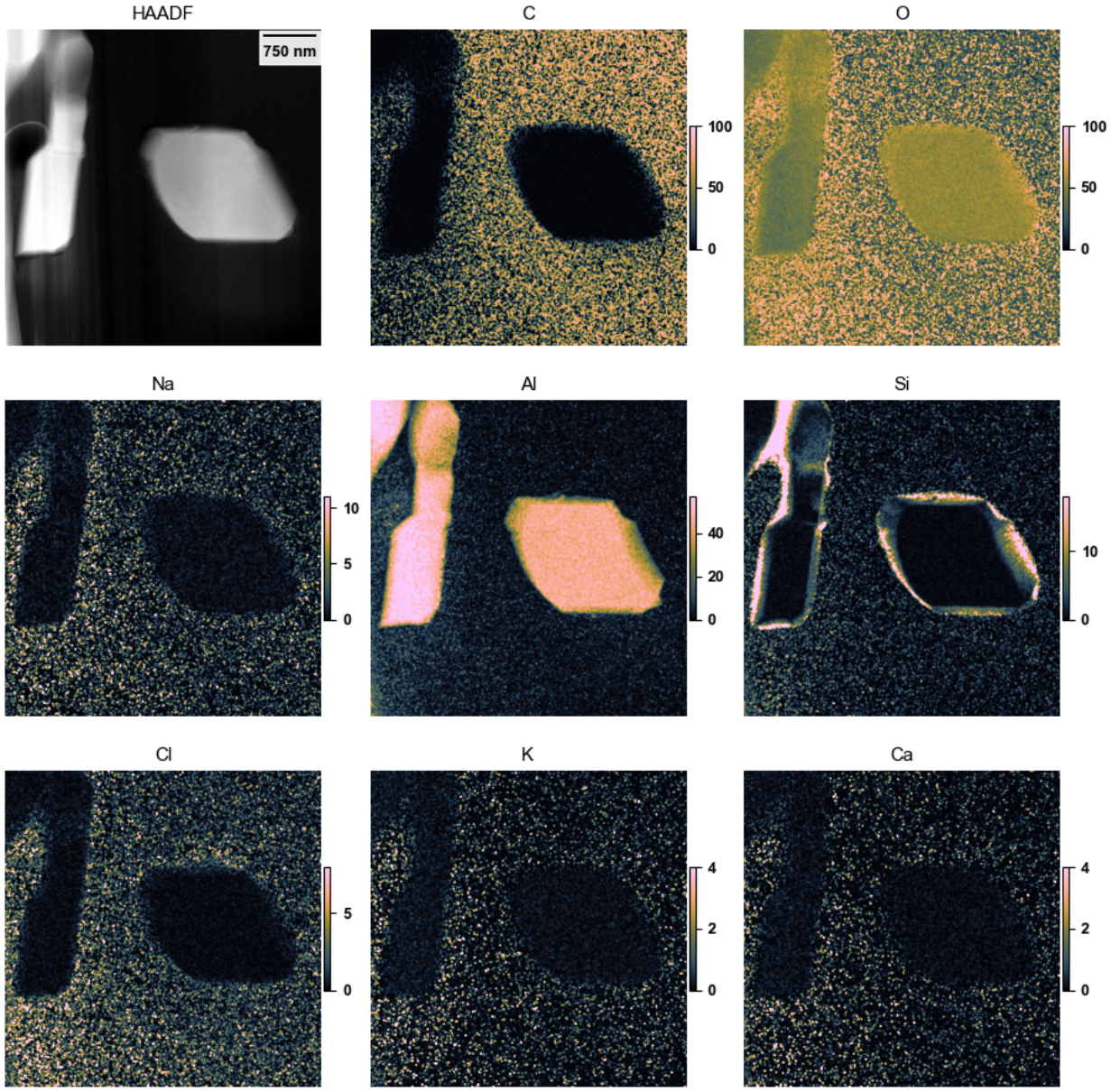


**Figure 59. X-ray maps, presented as estimated atom%, of the region of Figure 58.**

Towards the bottom-left of the foil in Figure 54 is the region of Figure 60. In Figure 60, we observe large blocky alumina grains, containing angular cavities or other low-atomic-number regions, as well as a large cavity (vacuum region), and regions of dark and moderate-contrast in HAADF matrix, indicating low and moderate atomic number regions. From the X-ray mapping data, Figure 61, the Si-O-(Na-K-Ca) matrix binder again surrounds the alumina grains, and the infiltrated carbonaceous phase fills in above the Si-O and into the cracks through the Si-O phase. Small pockets of Ca-rich and K-rich areas are observed, likely similar to those seen in Unirradiated Sample 1, Figure 4 - Figure 5, and resulting from processing / fabrication inhomogeneities.

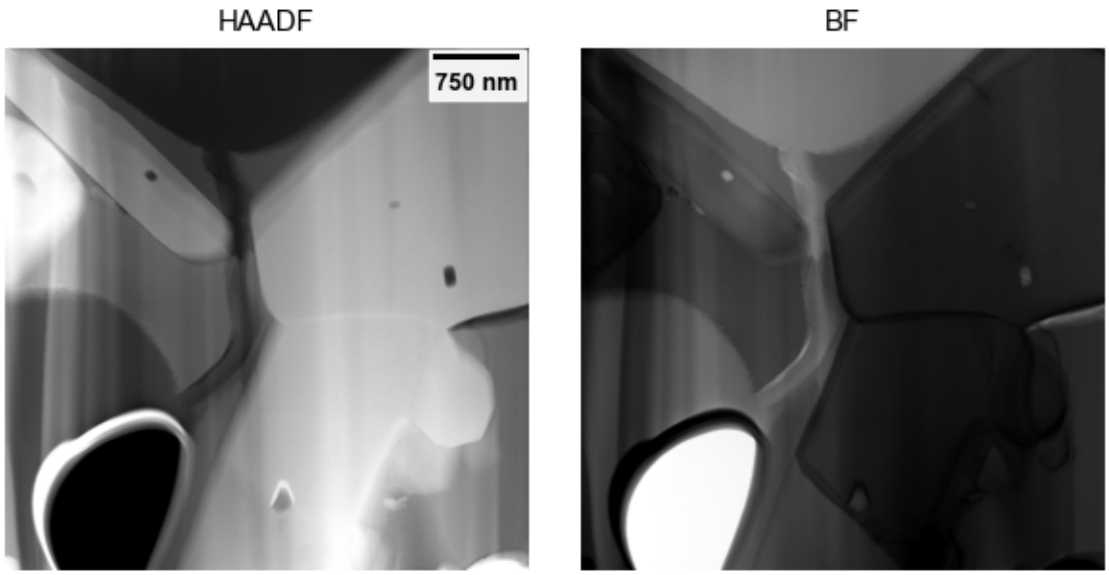


**Figure 60. High-magnification STEM images of a FIB liftout from Irradiated Sample EPRI-1.**

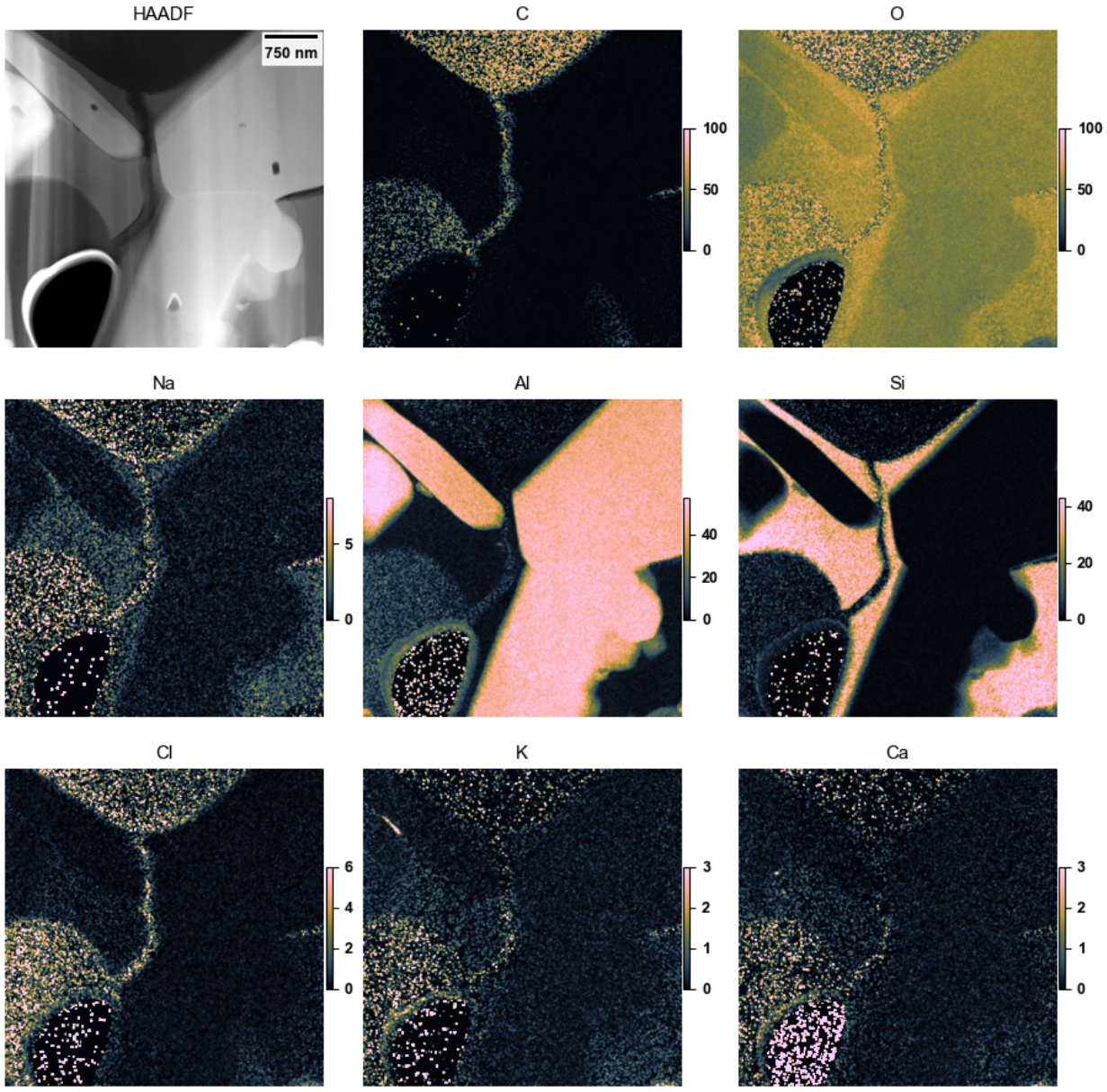


**Figure 61. X-ray maps, presented as estimated atom%, of the region of Figure 59. Speckle in the vacuum area is a quantification artifact and should be ignored.**

Examining the center of this region in more detail, we yield Figure 62. This region is from the very bottom of the FIB foil in Figure 54 with consequently some redeposition (speckled contrast) at the bottom due to resputtered material from the bottom of the foil, but the interpretation from the X-ray mapping, Figure 63, is substantially unchanged in comparison to the other region examined above. Which is to say, there are large blocky alumina grains with surrounding Si-O(-Ca-K-Na) and some carbon rich area as well.

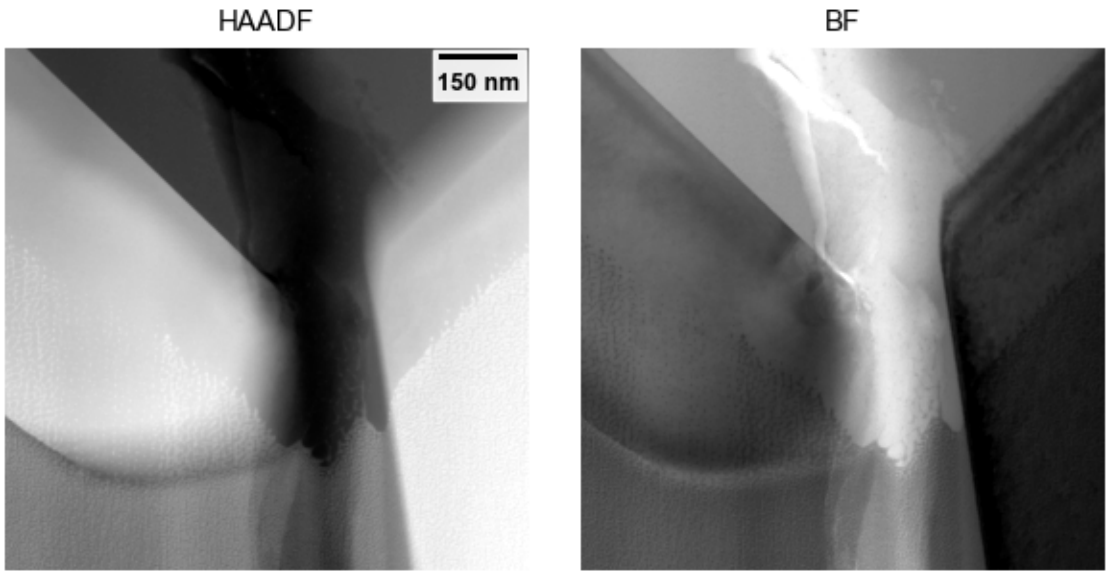


**Figure 62. High-magnification STEM images of a FIB liftout from Irradiated Sample EPRI-1. Specle towards the bottom is FIB redeposition.**

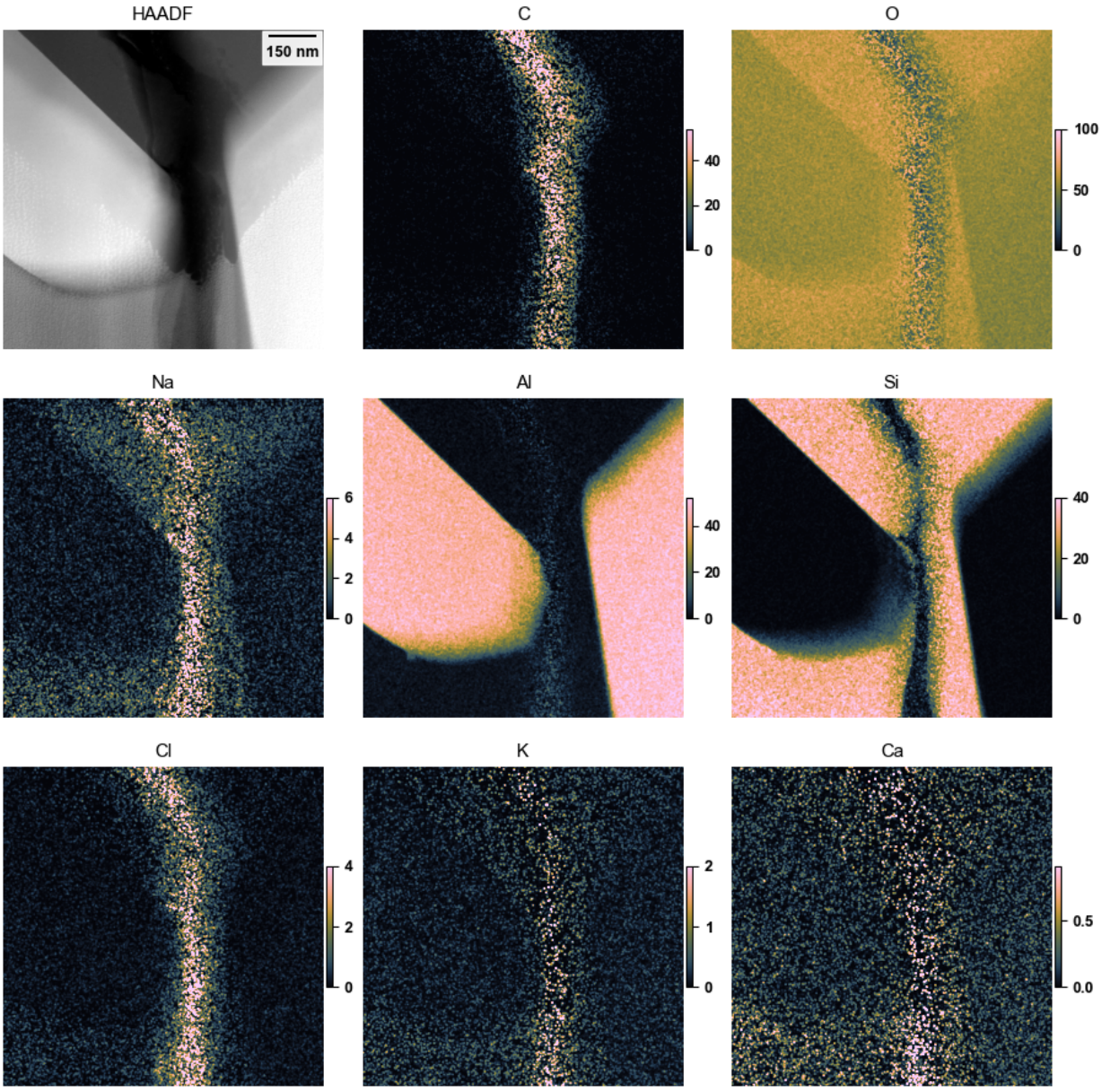


**Figure 63. X-ray maps, presented as estimated atom%, of the region of Figure 62.**

Another FIB foil of ~~Irradated~~IrradiatedIrradiated Sample EPRI-1 is seen in Figure 64. Again, regions of medium- and low-atomic-number matrix are visible, along with blocky ceramic grains containing, in turn, dark cavities or precipitates. From the right edge of Figure 64, the region of Figure 65-Figure 66 is found which contains large, blocky alumina grains and, between the grains, both porous and non-porous filler regions. The X-ray mapping data, Figure 67, shows the blocky grains are Al-O, as expected, and the filler along the grain-boundary gap is Si-O, both in the porous and non-porous regions, with slight Na and possibly very slight K-Ca content as well. At the bottom corner carbon is seen, and possibly a small amount of Cl, which could be consistent with an epoxy infiltration. A small amount of Ca is also apparent down the horizontal alumina-alumina grain boundary near the bottom of the map, which is consistent with the unirradiated observations as well.

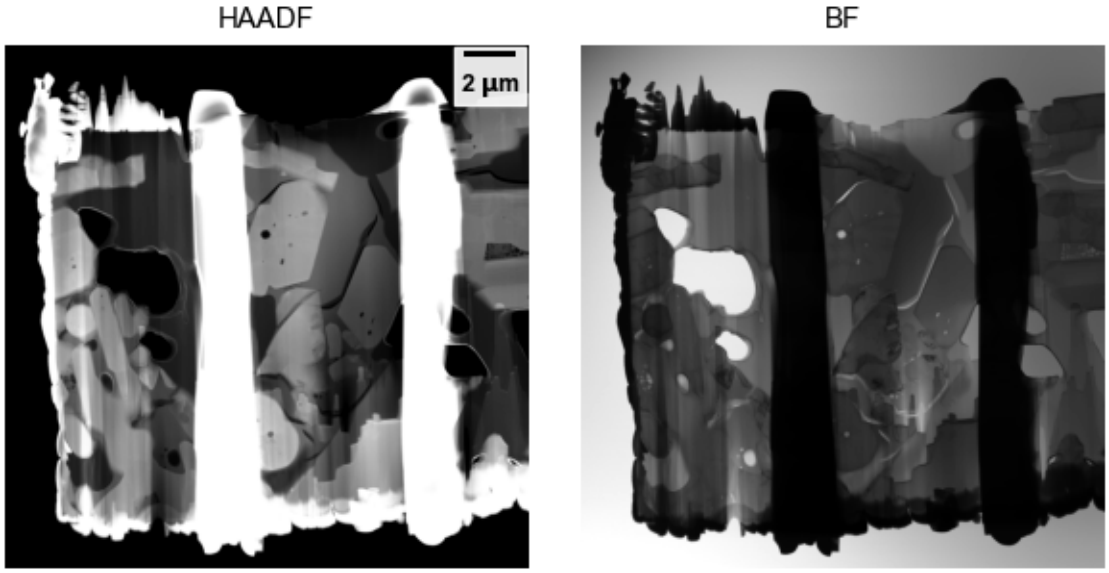


**Figure 64. Low-magnification STEM images of a FIB liftout from Irradiated Sample EPRI-1.**

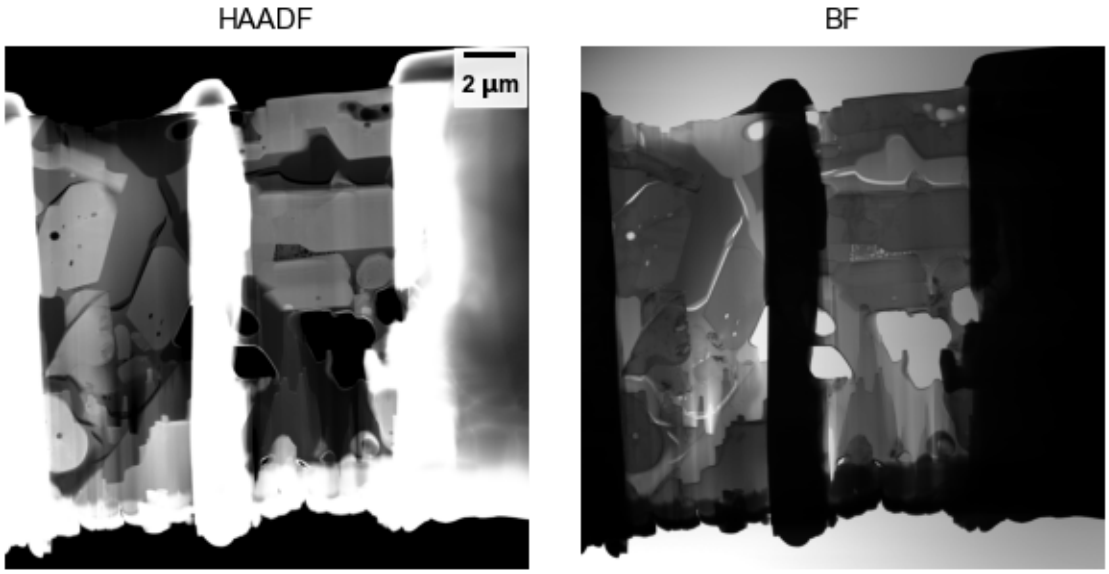


**Figure 65. Low-magnification STEM images of a FIB liftout from Irradiated Sample EPRI-1.**

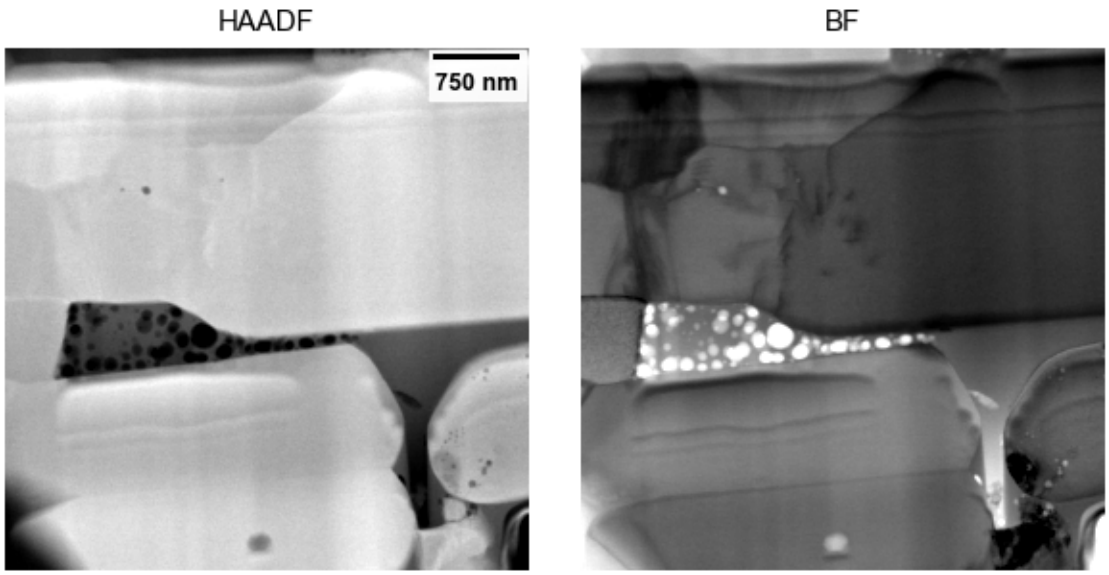


**Figure 66. Medium-magnification STEM images of a FIB liftout from Irradiated Sample EPRI-1.**

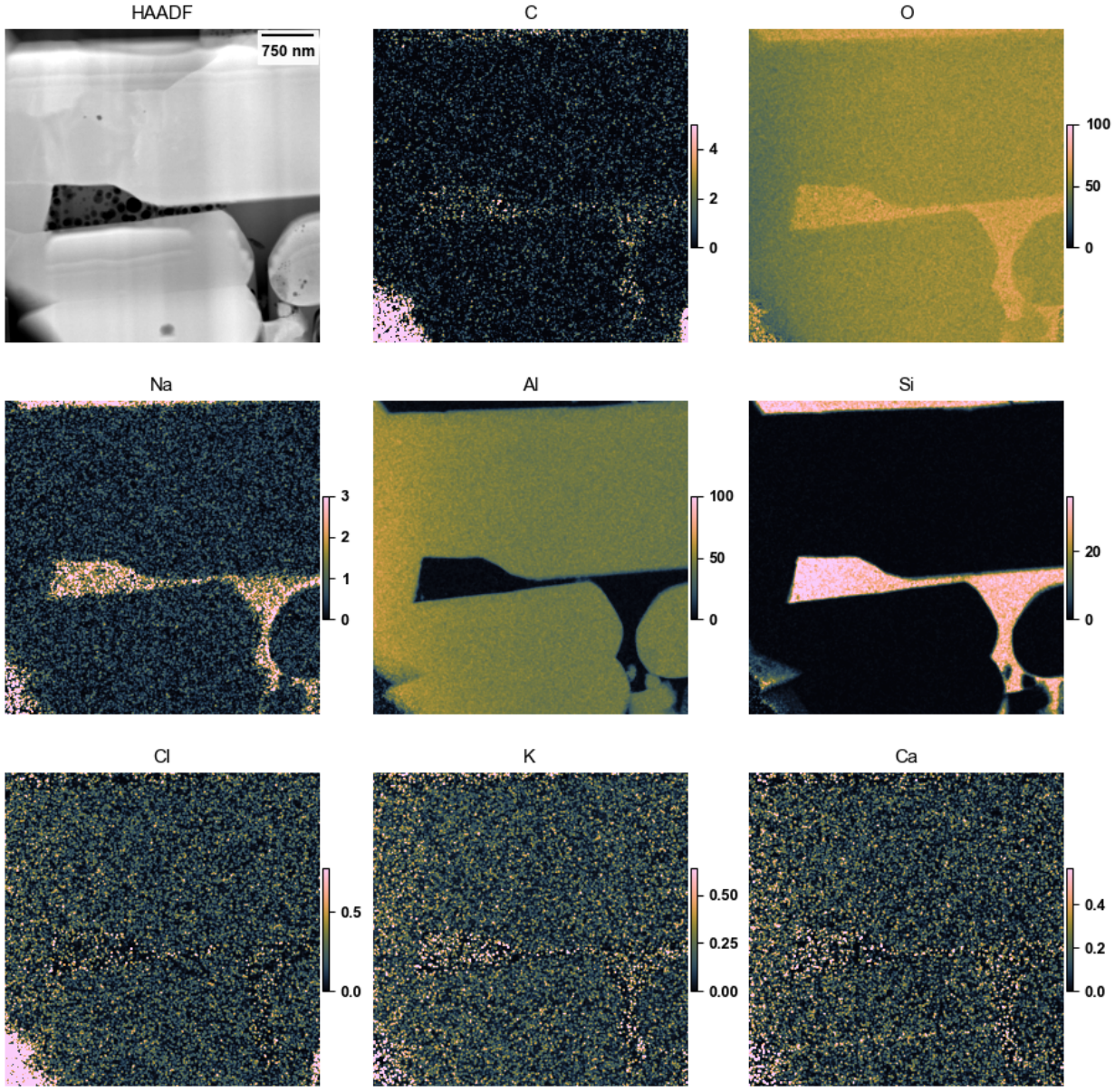


**Figure 67. X-ray maps, presented as estimated atom%, of the region of Figure 66. Speckle in the vacuum area is a quantification artifact and should be ignored.**

Another detailed region of the foil of Figure 64-Figure 65 is shown in Figure 68. The expected features — blocky ceramic grains, binding matrix, cavities in the ceramic — are again present. The X-ray mapping, Figure 69, is again consistent with the other regions, showing Al-O grains, Si-O(-Na-K-Ca) matrix binder, and small regions of C possibly containing Cl and Na.

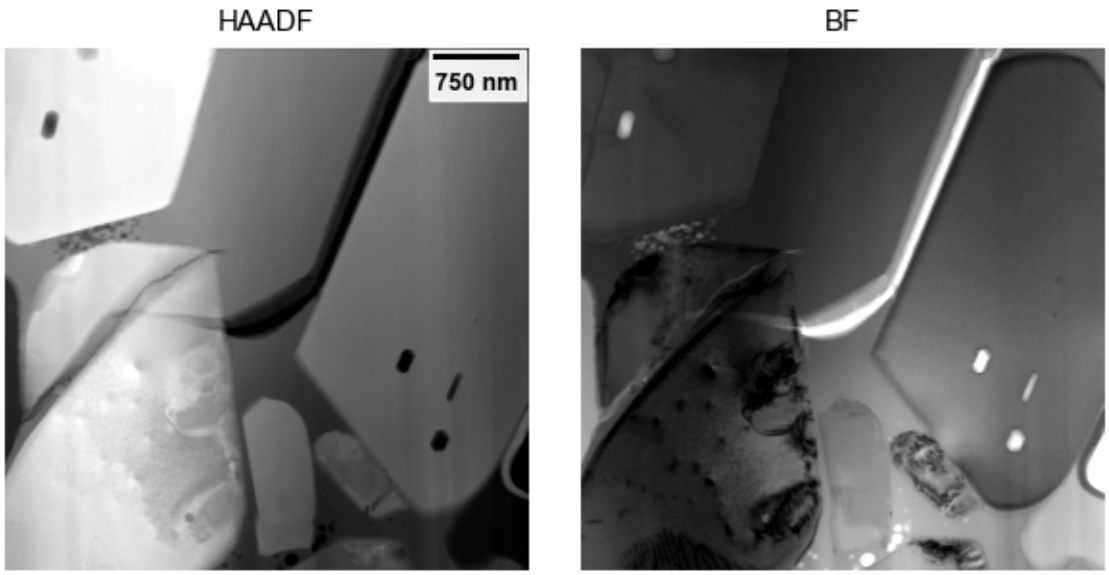


**Figure 68. High-magnification STEM images of a FIB liftout from Irradiated Sample EPRI-1.**

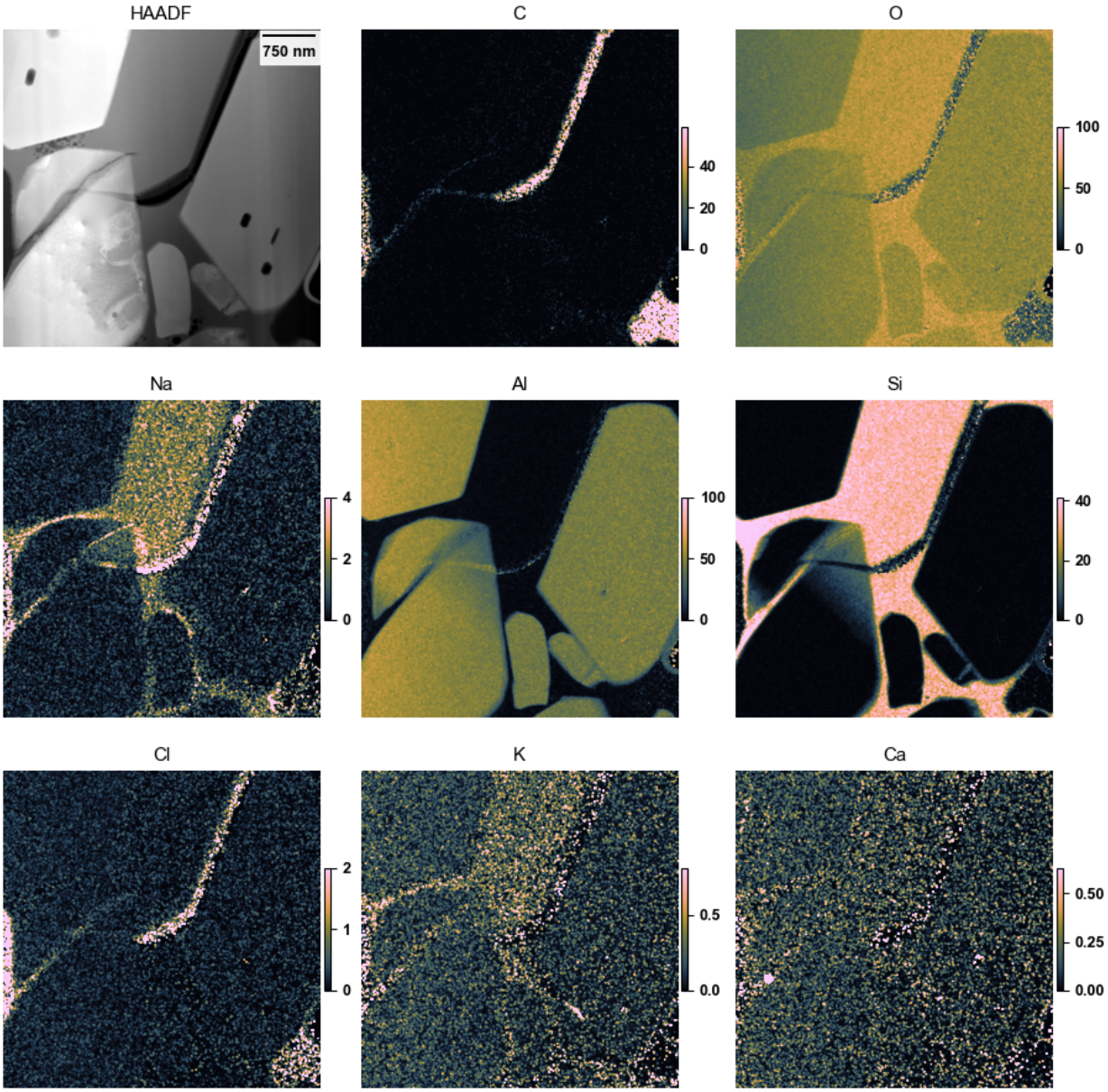


**Figure 69. X-ray maps, presented as estimated atom%, of the region of Figure 68. Speckle in the vacuum area is a quantification artifact and should be ignored.**

Overall, Irradiated Sample 1 is similar to, and shows no gross differences from, Unirradiated Sample 1. The alumina phase of blocky ceramic grains and silica-based, Na-K-Ca doped glass matrix phase are still present. Small regions of enhance Na-Ca or Si were seen, probably arising from fabrication.

### 3.2.2 Sample EPRI-4: AlSiNaO

Irradiated Sample EPRI-4 was seen in the prior work [1] to be similar to Unirradiated Sample 5, and to consist of large alumina grains and a Si-rich glass binder matrix with small Na. It's worth recalling from the prior work that Irradiated Sample EPRI-4 showed Na-O-rich surface growths; in this work, the sample

was polished and then immediately placed in the FIB-SEM tool vacuum, so these Na-rich growths were not observed.

A FIB foil from Irradiated Sample EPRI-4, Figure 71, shows part of a large monolithic ceramic particle with sharp crystallographic internal interfaces present as well as a cavity. The internal crystallographic interfaces are seen in more detail in Figure 71, and X-ray mapping of a subregion from the interface in Figure 72. In this region, as expected, only Al and O are seen above the noise level, and no discernable segregation is present on the internal interfaces.

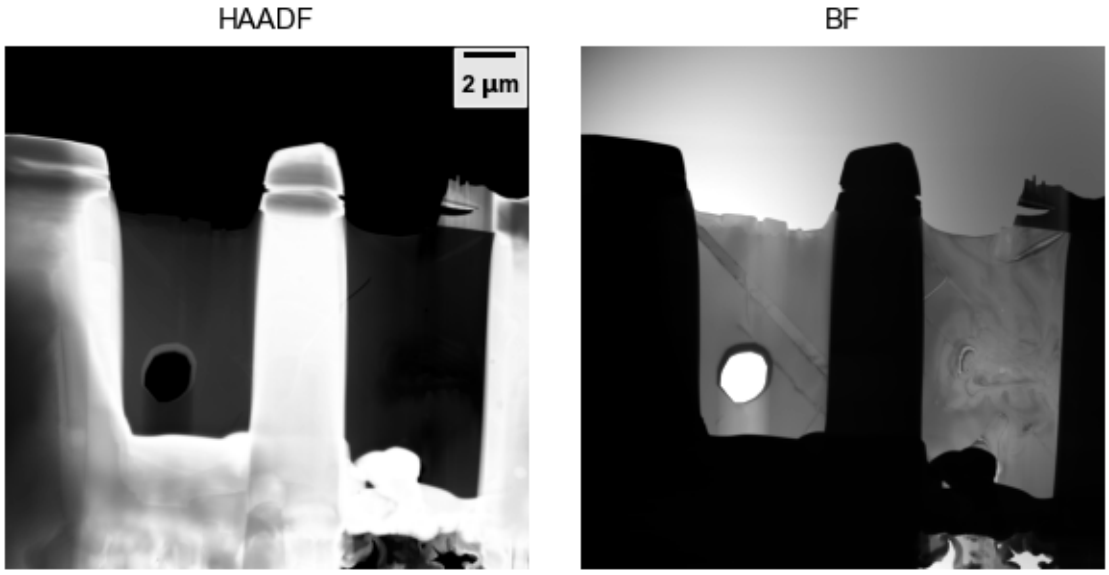


**Figure 70. Low-magnification STEM images of a FIB liftout from Irradiated Sample EPRI-4.**

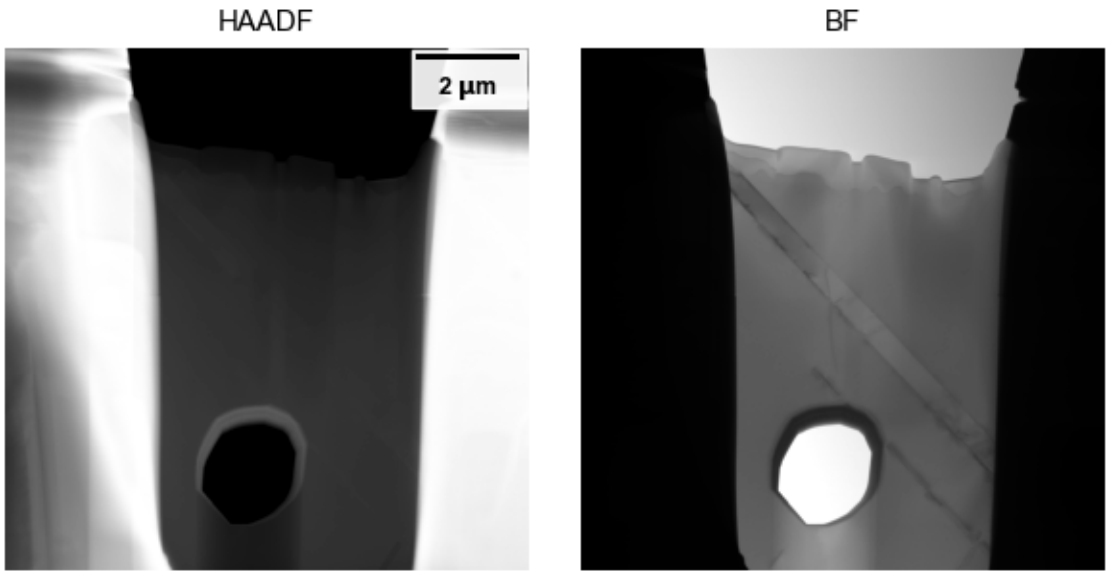


**Figure 71. Low-magnification STEM images of a FIB liftout from Irradiated Sample EPRI-4.**

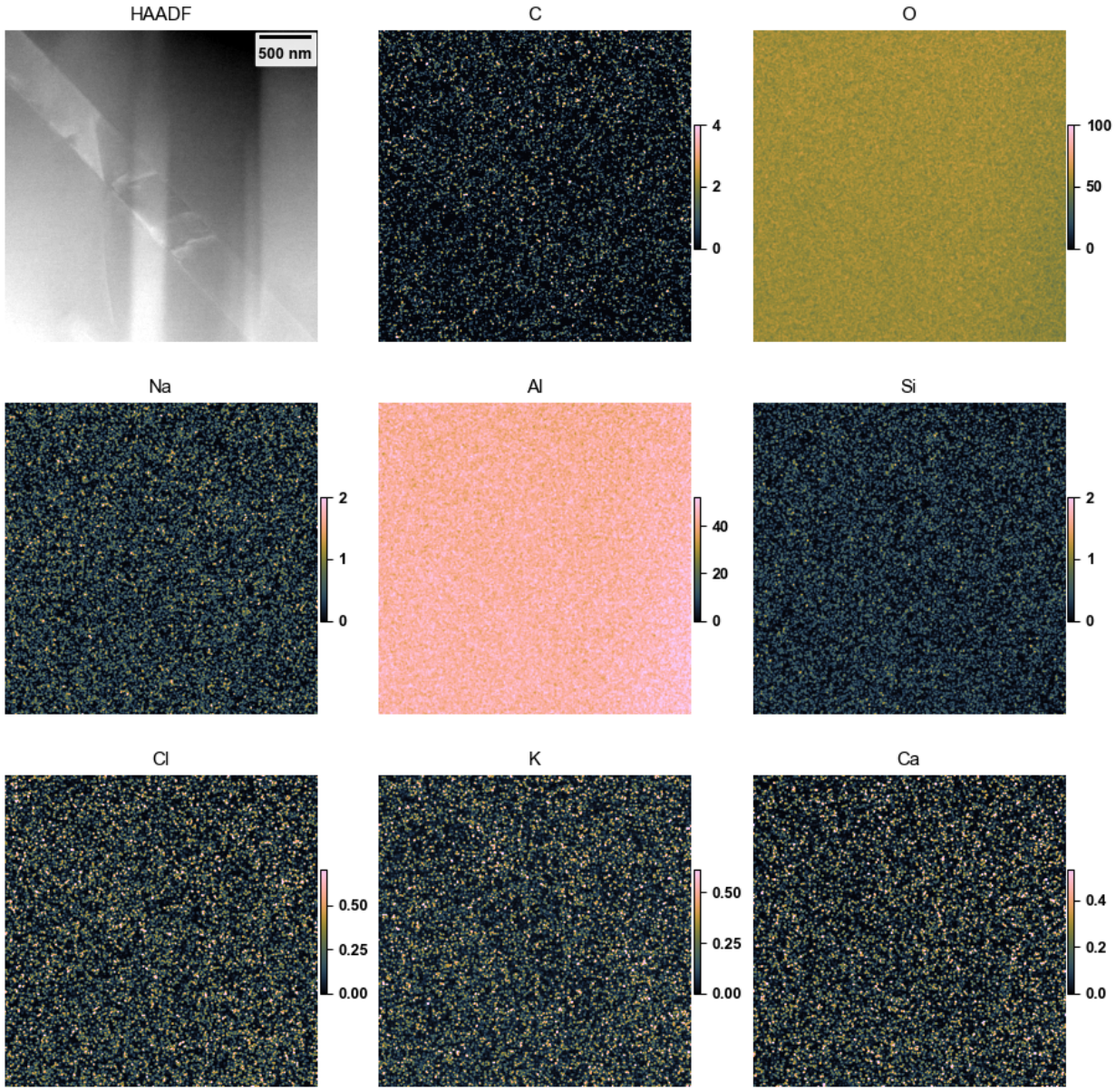


**Figure 72. X-ray maps, presented as estimated atom%, of the region of Figure 70.**

Results more like Irradiated Sample EPRI-1 are seen in the region of Figure 73~~Figure 73~~ and Figure 74.~~Figure 74.~~ Open space between alumina grains is filled with a porous Si-O-rich region; Na is at the noise level, and interference between the Ga-L lines and Na-K lines make it difficult to be sure when both Ga (from the FIB beam) and Na are present at less than the ~1% level, and might not be present. However, extraction of the areal spectrum from the Si-rich region yields Figure 75.~~Figure 75.~~ If both Na-K and Ga-L are modeled, the ~1.1 keV peak residual is very small, whereas if only Ga-L is modeled, the residual is larger and asymmetric towards the left, where the Na-K line sits. Although not definitive, this indicates a *very* small Na content may be present.

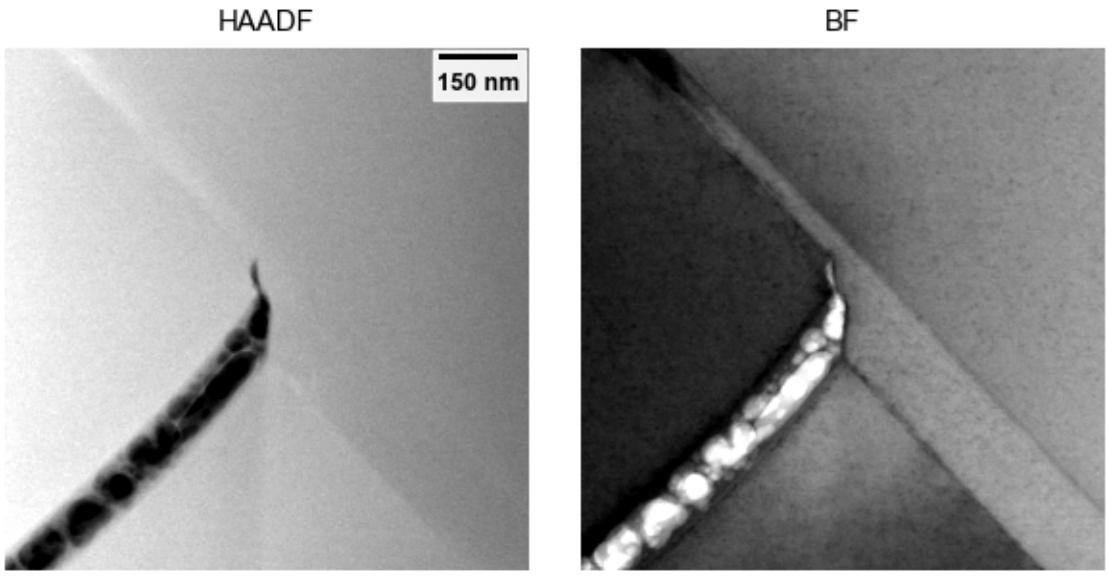


**Figure 73. High-magnification STEM images of a FIB liftout from Irradiated Sample EPRI-4.**

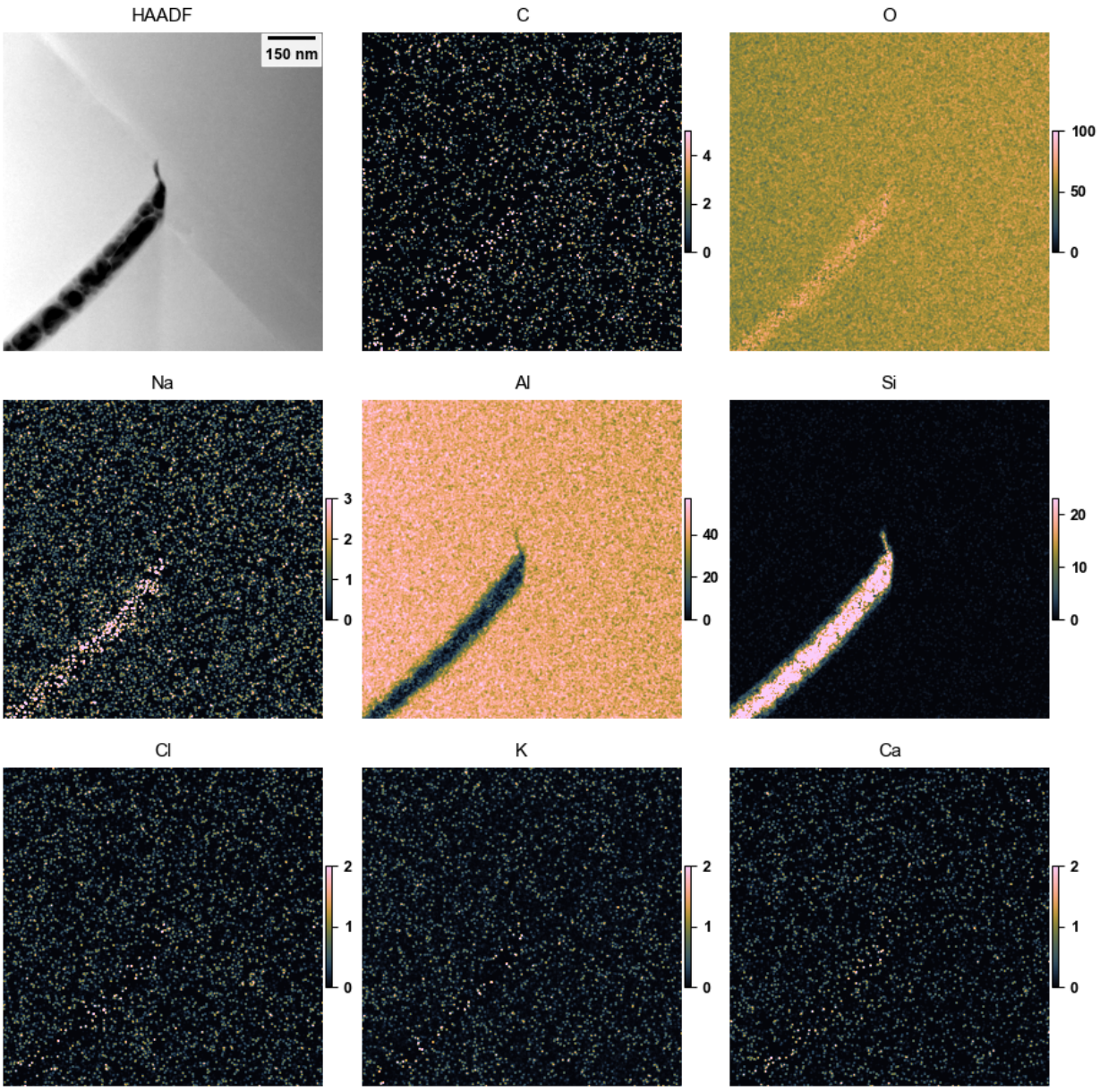


**Figure 74. X-ray maps, presented as estimated atom%, of the region of Figure 73. Speckle in the vacuum area is a quantification artifact and should be ignored.**

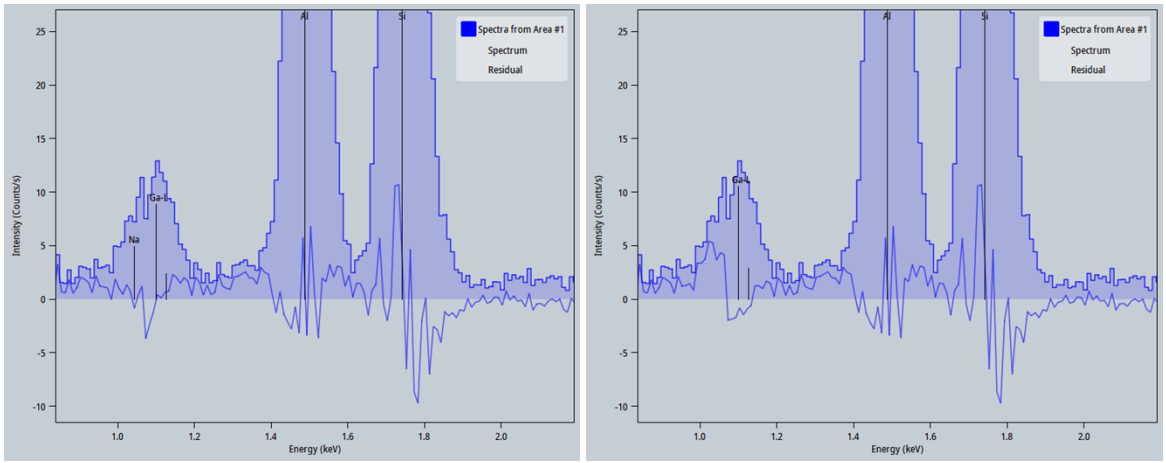


**Figure 75. Spectrum extracted from the Si-O-rich region of Figure 74. The residual of the model, thin blue line, is much smaller if Na+Ga is modelled (left) than if only Ga is modelled (right).**

Another FIB foil from this sample Irradiated Sample EPRI-4 is seen in Figure 76. A large monolithic ceramic grain cuts across the top of the foil, with smaller grains and the binder matrix below. The bottom edge of the left side of the monolithic grain is seen in Figure 77 and Figure 78. The large alumina grain and small grains below it are visible in the X-ray maps, with the Si-O based glass coating the small grains and bottom surface of the large grain, and with adventitious filler around them. The same results, in more detail, are in Figure 79-Figure 80.

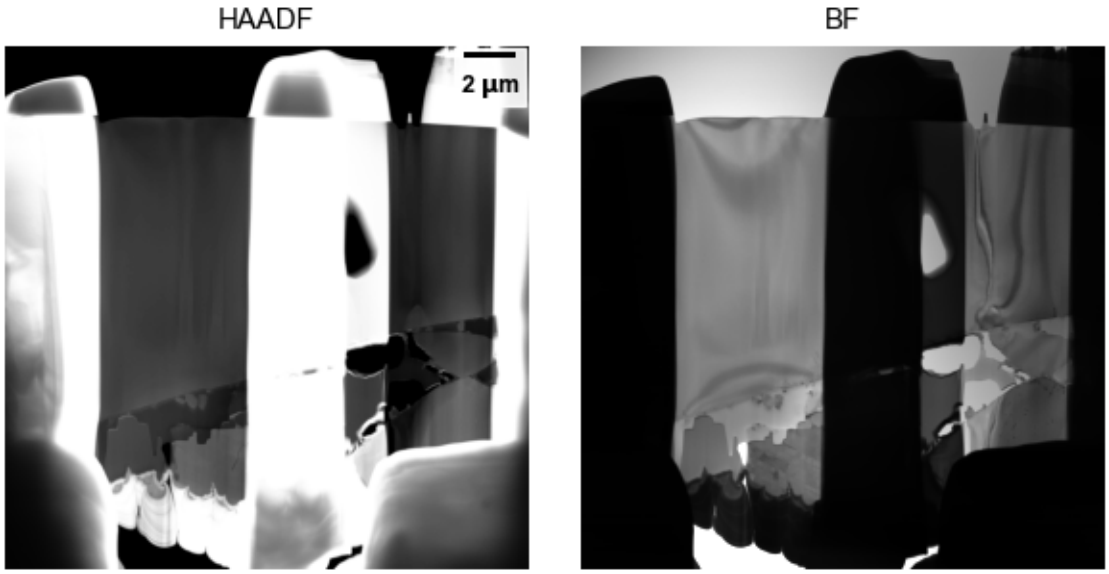


**Figure 76. Low-magnification STEM images of a FIB liftout from Irradiated Sample EPRI-4.**

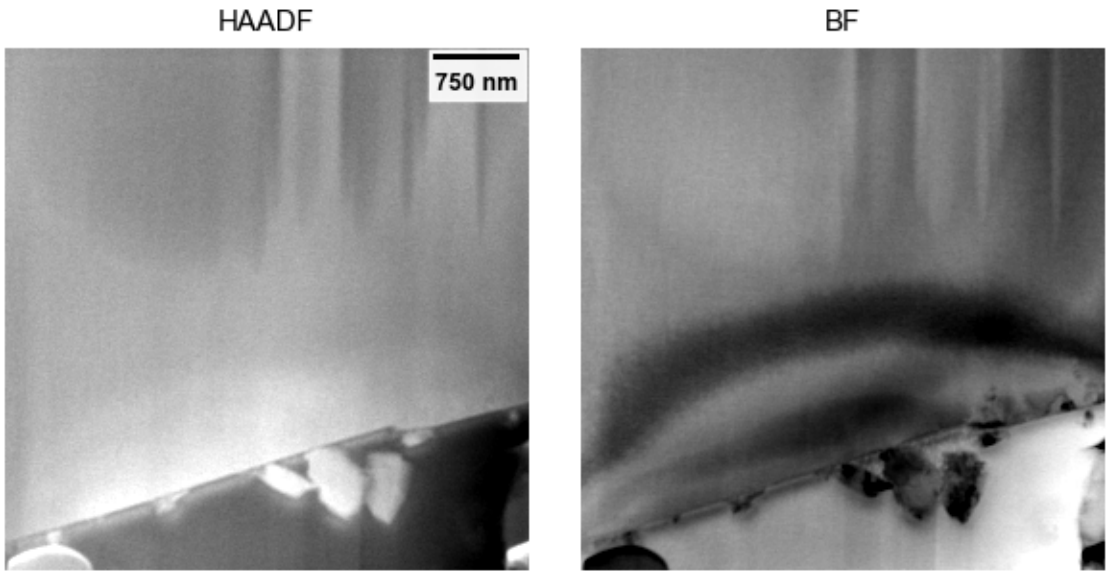


**Figure 77. High-magnification STEM images of a FIB liftout from Irradiated Sample EPRI-4.**

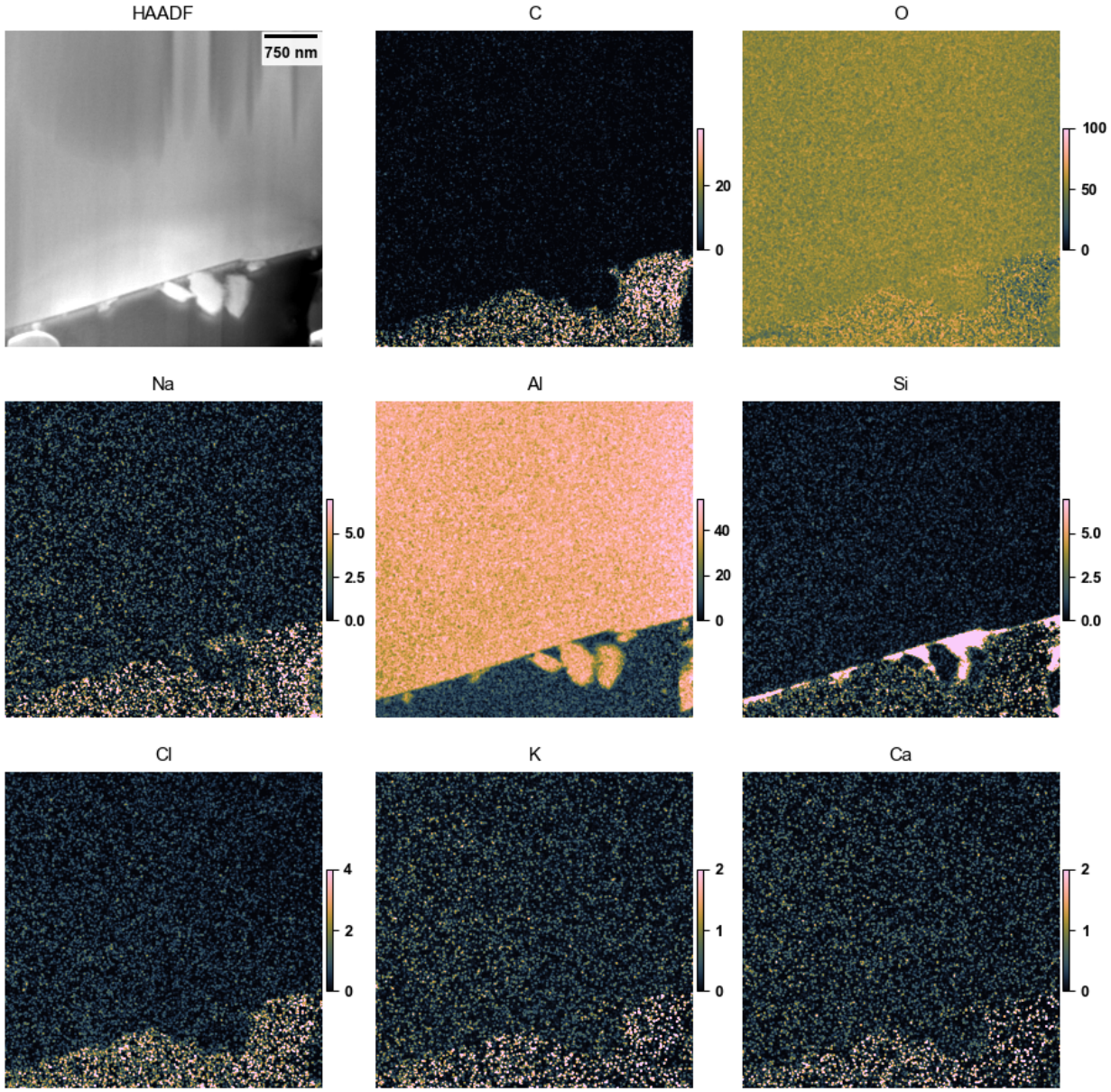


**Figure 78. X-ray maps, presented as estimated atom%, of the region of Figure 77. Speckle in the vacuum area is a quantification artifact and should be ignored.**

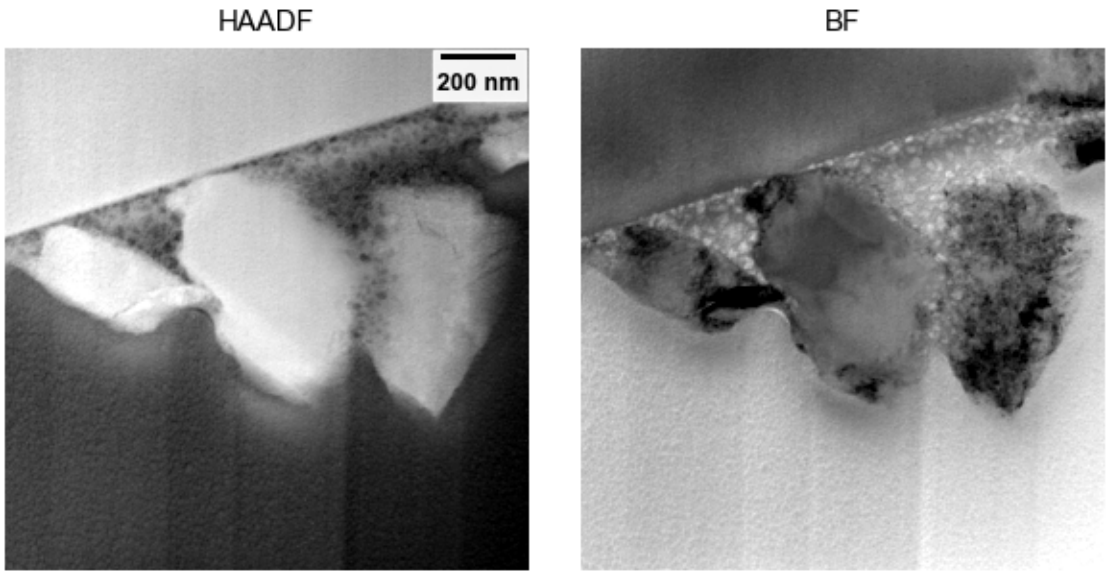


**Figure 79. High-magnification STEM images of a FIB liftout from Irradiated Sample EPRI-4.**

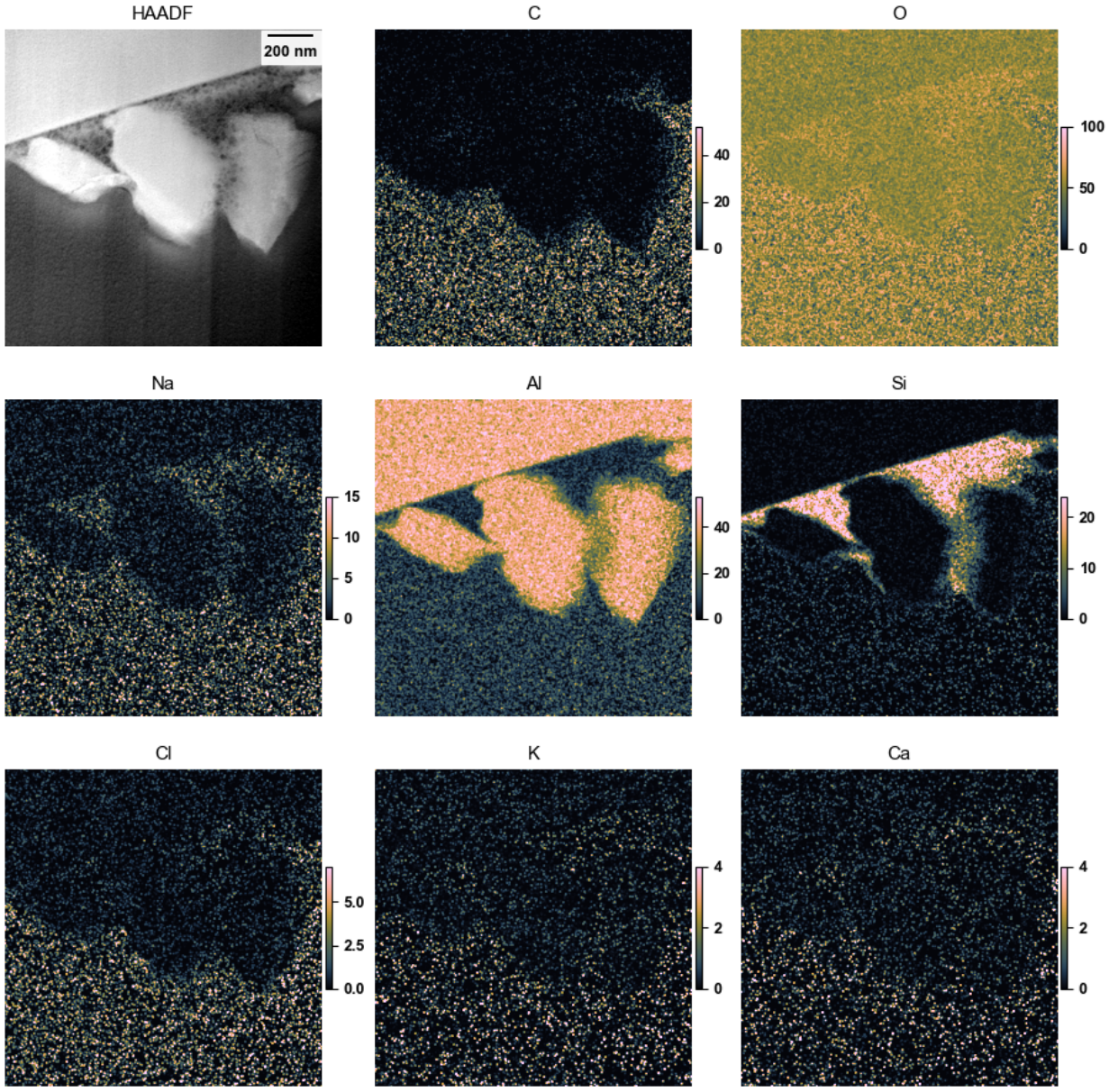


**Figure 80. X-ray maps, presented as estimated atom%, of the region of Figure 79. Speckle in the vacuum area is a quantification artifact and should be ignored.**

The right side of the monolithic grain cutting across the foil is shown again in Figure 81, and the center of the large grain is X-ray mapping in Figure 82. Once again, the center of the grain is seen to be pure Al-O to the limits of EDS detection.

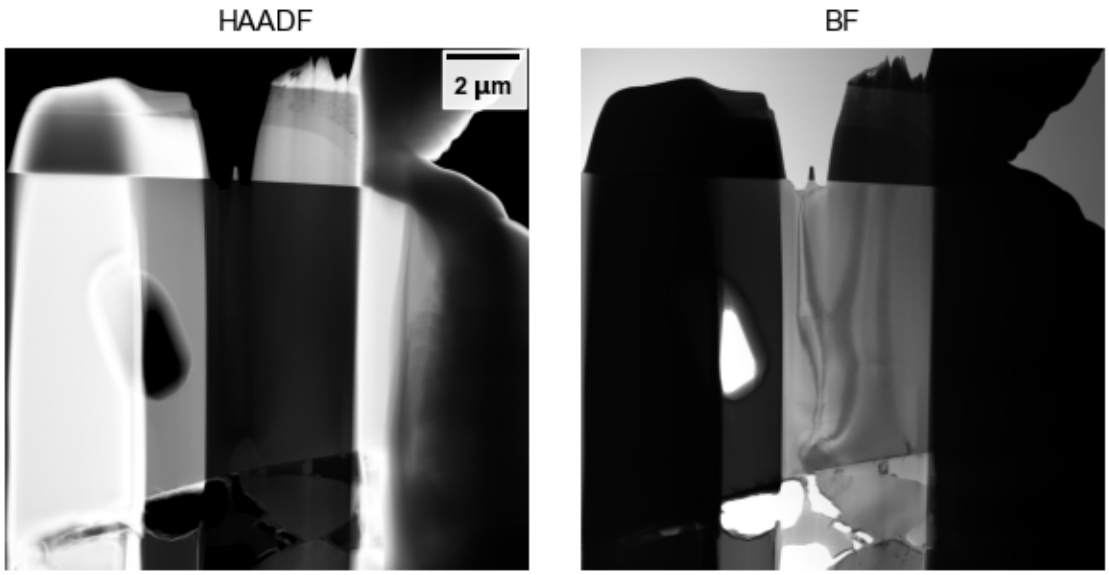


**Figure 81. Low-magnification STEM images of a FIB liftout from Irradiated Sample EPRI-4.**

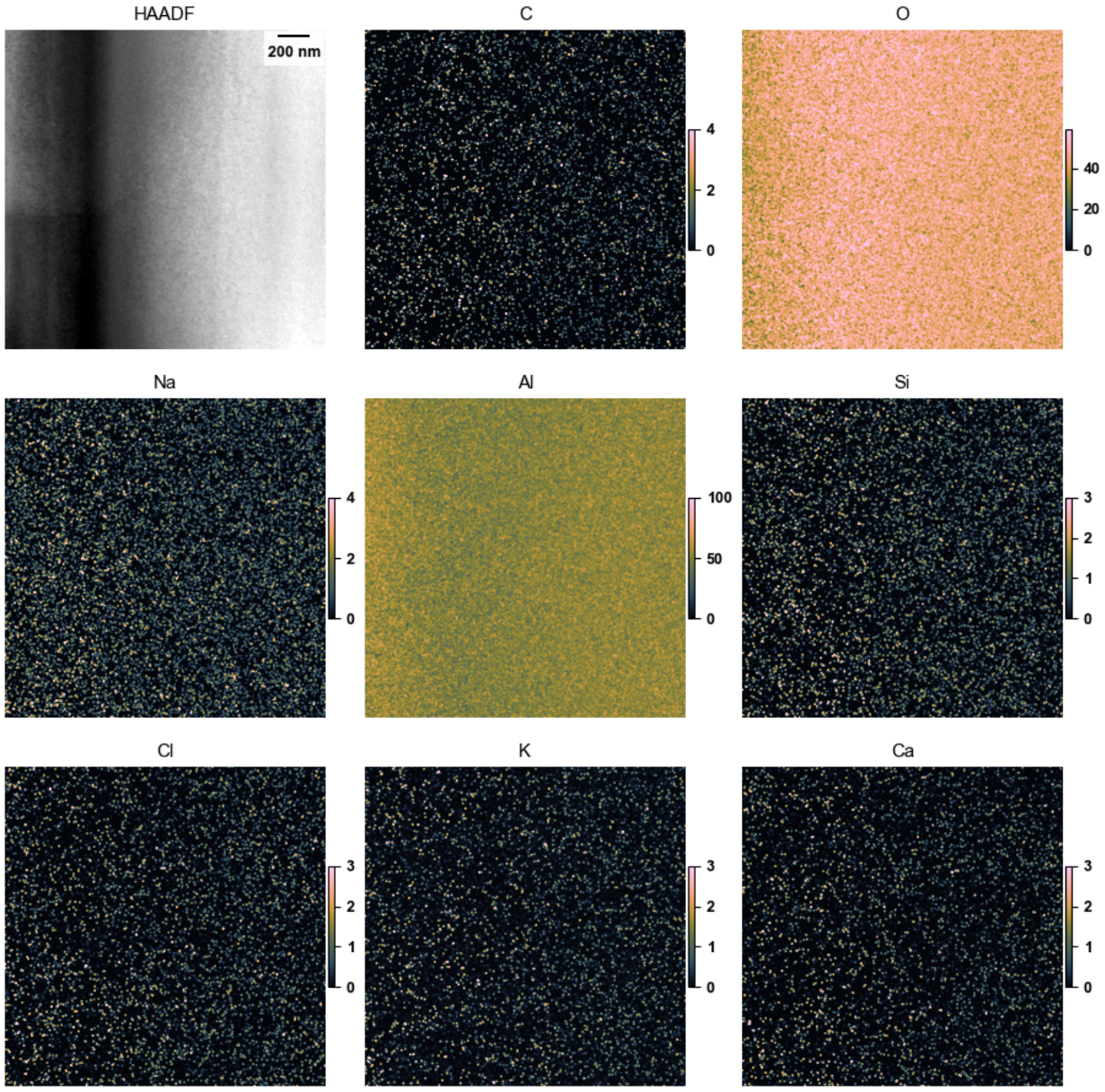


**Figure 82. X-ray maps, presented as estimated atom%, of a subregion of Figure 81. Speckle in the vacuum area is a quantification artifact and should be ignored.**

Towards the bottom of the right side, Figure 83, several of the ceramic grains and the binder layers are seen. The X-ray mapping is again consistent, Figure 84, in which Si-O glass is seen connecting the large and medium-sized grains, with small alumina grains intermixes, and the carbonaceous layer penetrating in from the right side.

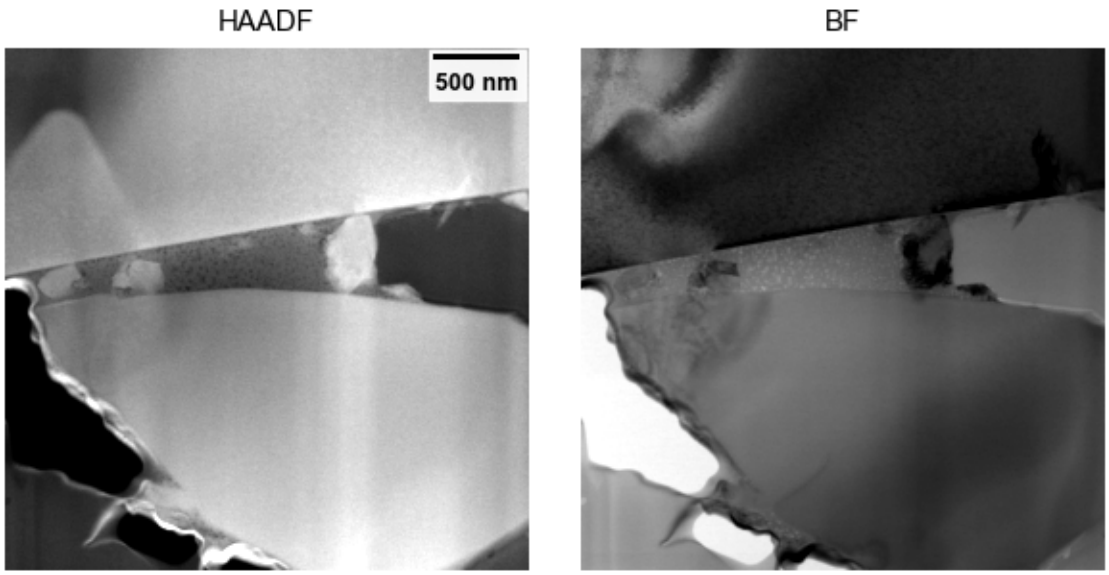


**Figure 83. High-magnification STEM images of a FIB liftout from Irradiated Sample EPRI-4.**

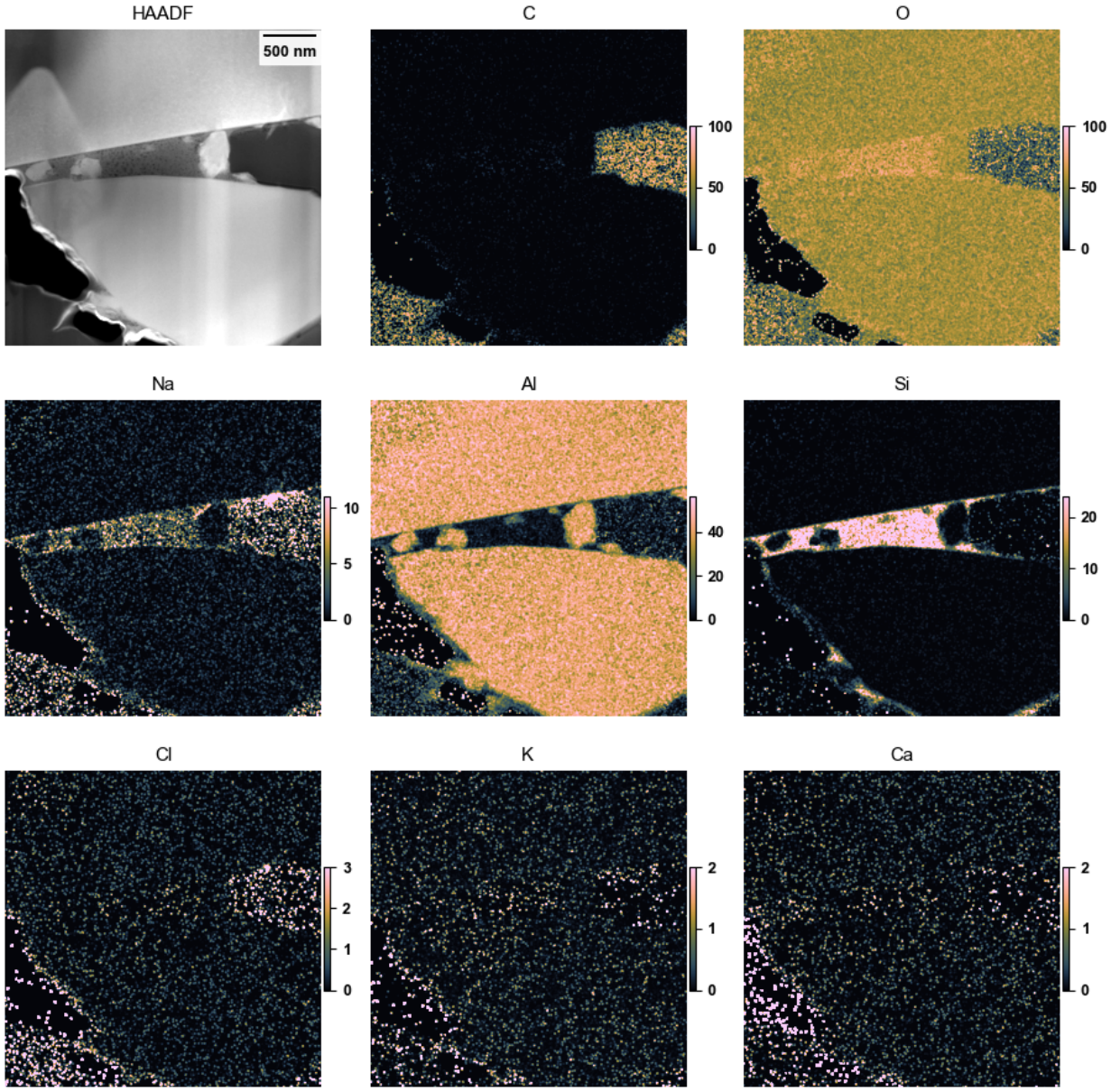


**Figure 84. X-ray maps, presented as estimated atom%, of the region of Figure 83. Speckle in the vacuum area is a quantification artifact and should be ignored.**

Overall, Irradiated Sample 4 is similar to Unirradiated Sample 5, and is consistent with an alumina based couplant layer containing Si-O binder with very small amounts of Na. Again, no major differences are apparent in the irradiated vs unirradiated state.

### 3.2.3 Sample EPRI-5: ZrO

Irradiated Sample 5 was another zirconia specimen, similar to Unirradied Sample 12. The prior work [1] found large, high-quality $ZrO_2$ particles in an Si-O matrix, along with a weak Ca signal.

The first FIB foil of Irradiated Sample 5 is shown in Figure 85. A large monolithic ceramic grain cuts across the top of the foil, and many more small grains cluster at the bottom. A detailed view of the small grains, Figure 86, shows a mixture of the ceramic grains with the surrounding binder matrix, and many cavities or low-atomic-number precipitates within the large grain. The X-ray mapping data, Figure 87, shows consistency with the unirradiated data for Unirradiated Sample 12. The consistencies are Zr-O grains with a few atom% Ca and ~1 atom% or less Hf, along with the scattered Al-rich precipitates in the Zr-O grains. Si-O rich glassy binder surrounds the grains, as well as ~~regoins~~regionsregio~~i~~ns of carbonaceous infiltration. Similarly to the unirradiated sample, a few blocky regions a few hundred nanometers in size and much richer in Ca than the surrounding areas are observed. At higher magnification, Figure 88 and Figure 89, the enveloping of the Zr-O grains by the Si-O is seen and the Ca-rich (reaching >10 atom%) regions are also seen in more detail, as well as a triangular Ca-Al-rich particle. Because the Ca-rich regions are clearly not the full thickness of the foil, and the "atom %" is integrated through the thickness of the foil, the contents are larger than this estimate.

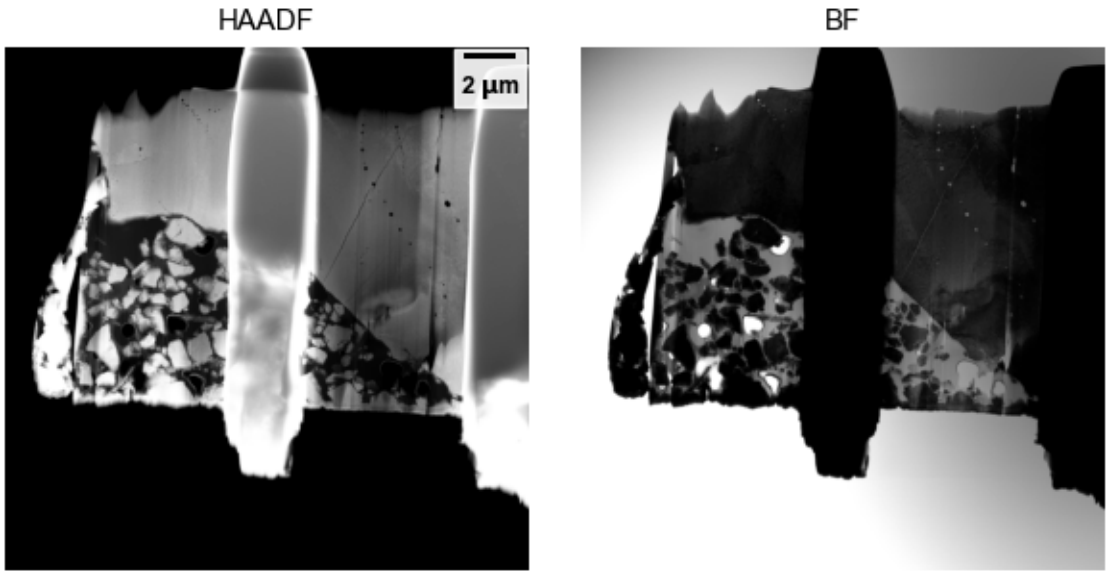


**Figure 85. Low-magnification STEM images of a FIB liftout from Irradiated Sample EPRI-5.**

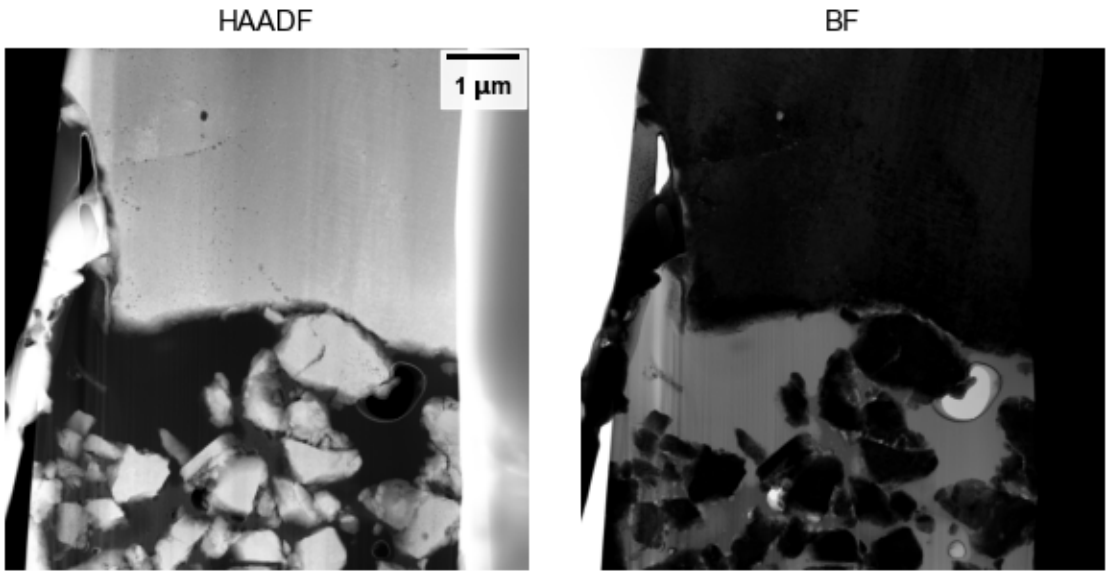


**Figure 86. Medium-magnification STEM images of a FIB liftout from Irradiated Sample EPRI-5.**

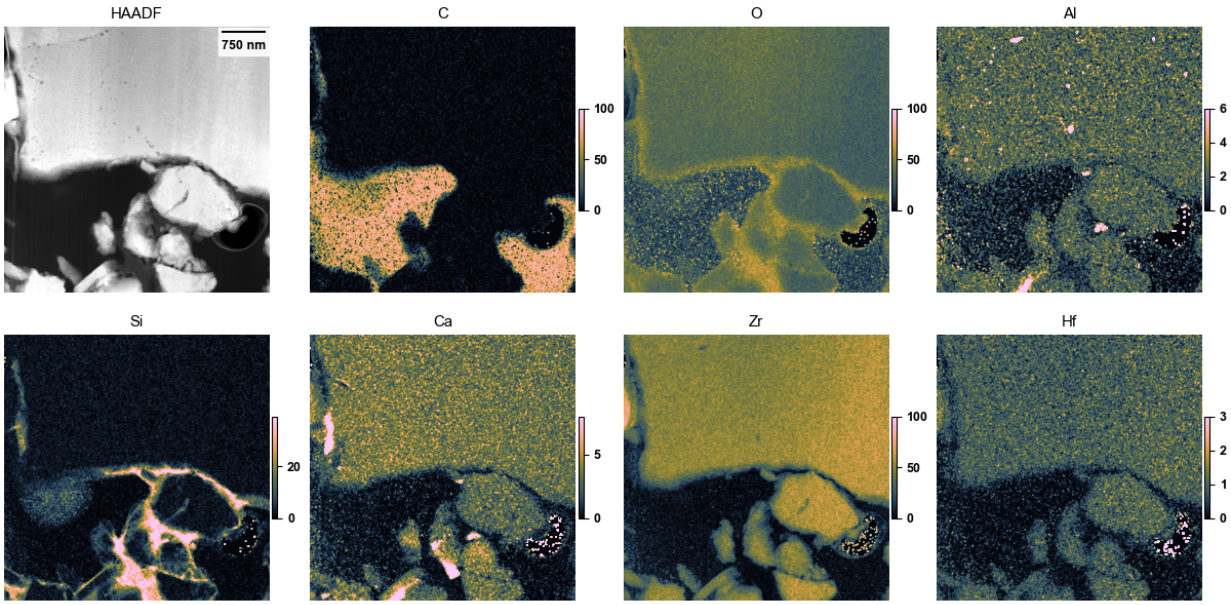


**Figure 87. X-ray maps, presented as estimated atom%, of the region of Figure 86. Speckle in the vacuum area is a quantification artifact and should be ignored.**

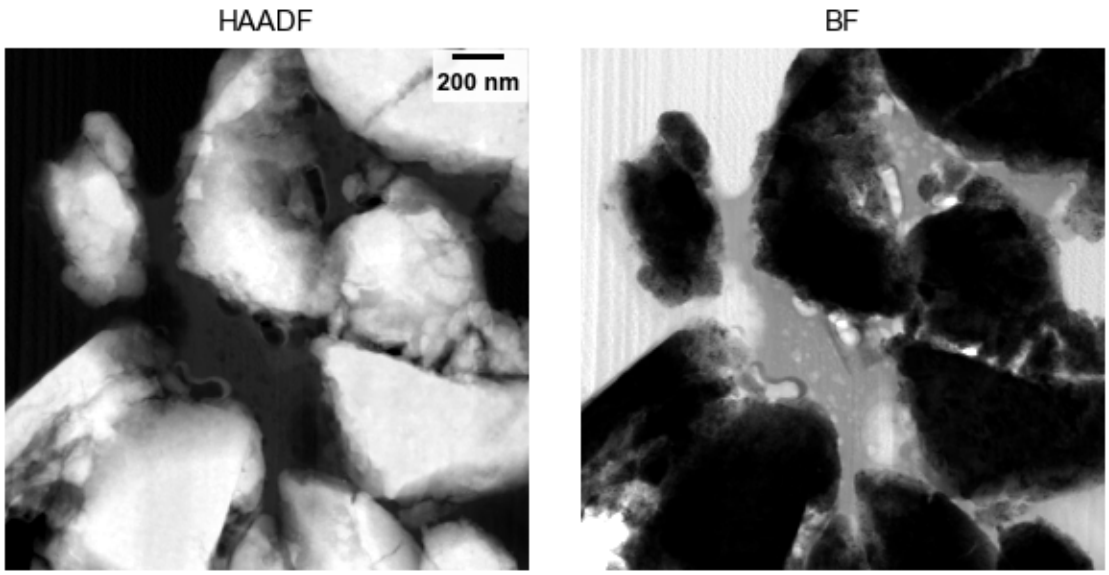


**Figure 88. High-magnification STEM images of a FIB liftout from Irradiated Sample EPRI-5.**

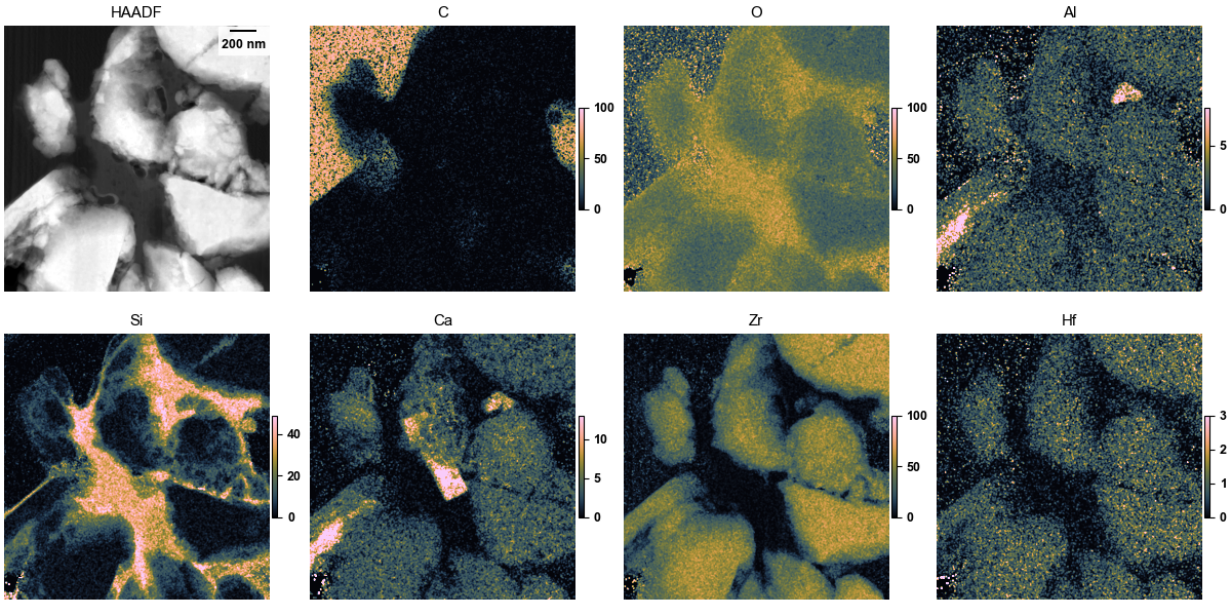


**Figure 89. X-ray maps, presented as estimated atom%, of the region of Figure 88. Speckle in the vacuum area is a quantification artifact and should be ignored.**

Shifting the view upward and right, a moderate-magnification view of the region where the small grains and the large grain meet is seen, Figure 90. Notably several large cracks are visible running through the large zirconia grains. The X-ray data indicates the Si-O layers are present along these cracks, Figure 91, which may be consistent with the cracks forming during processing, rather than irradiation, so that the Si-O could flow along the cracks.

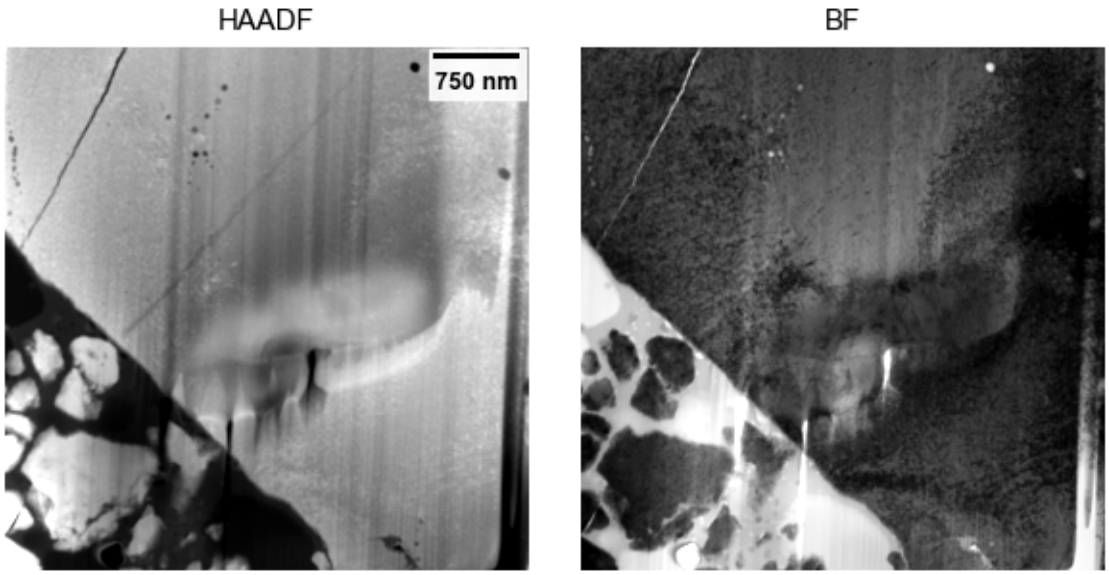


**Figure 90. Moderate-magnification STEM images of a FIB liftout from Irradiated Sample EPRI-5.**

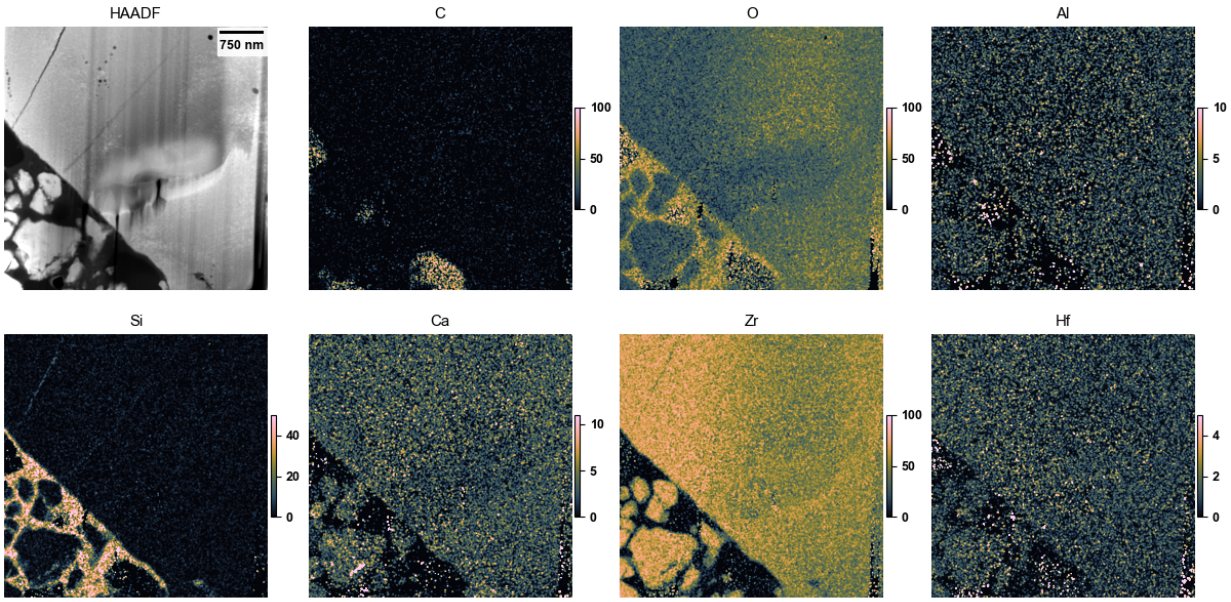


**Figure 91. X-ray maps, presented as estimated atom%, of the region of Figure 90. Speckle in the vacuum area is a quantification artifact and should be ignored.**

At high magnification, Figure 92, the structures are still consistent with the unirradiated case. The X-ray maps, Figure 93, similarly show Al-rich precipitate and alternating Ca-rich/Ca-poor domains within the zirconia structure, consistent with the partially-stabilized zirconia structure.

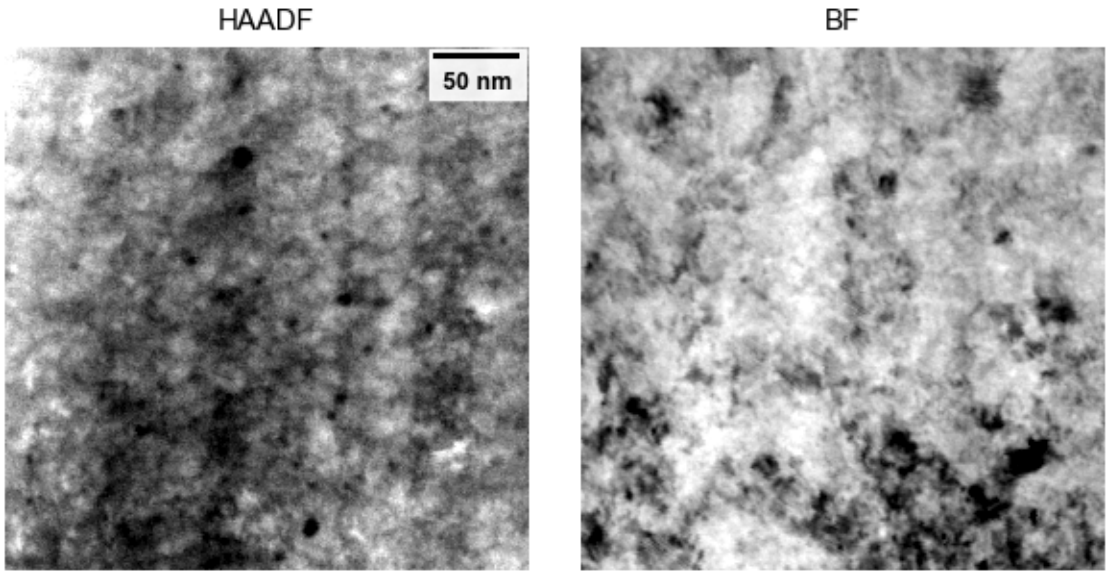


**Figure 92. High-magnification STEM images of a FIB liftout from Irradiated Sample EPRI-5.**

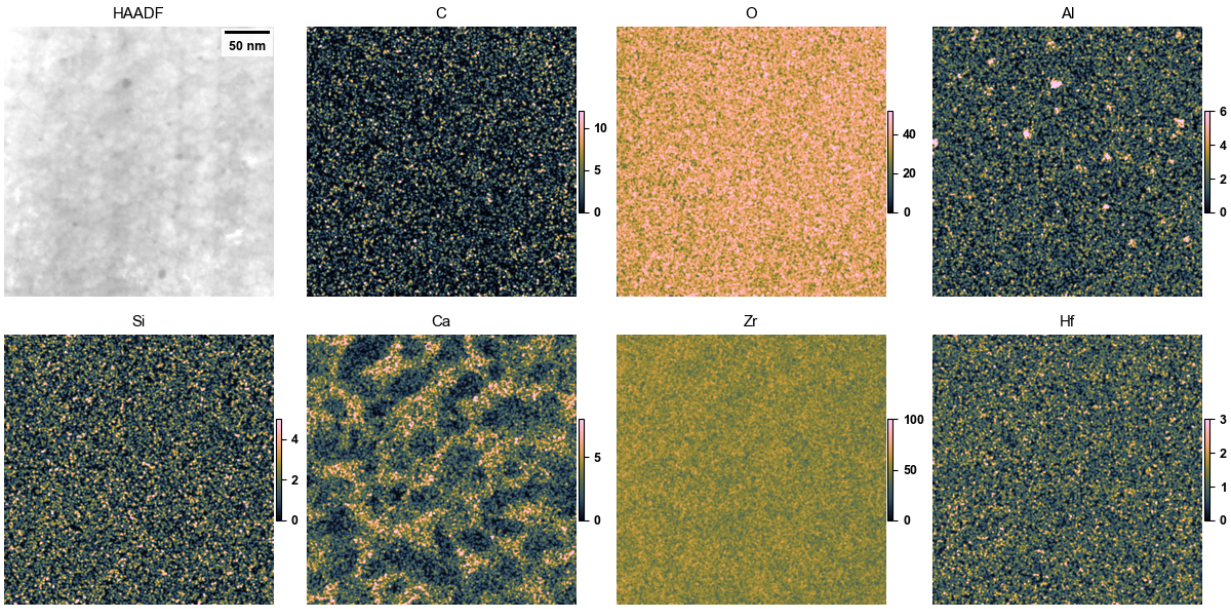


**Figure 93. X-ray maps, presented as estimated atom%, of the region of Figure 92. Speckle in the vacuum area is a quantification artifact and should be ignored.**

~~Examininaton~~Examinination of a crack crossing a cavity in the zirconia, Figure 94, and the associated X-ray mapping, Figure 95, the now-expected structures of Si-O along the crack surface, Al-rich precipaties, and the Ca-rich/poor alternating domains.

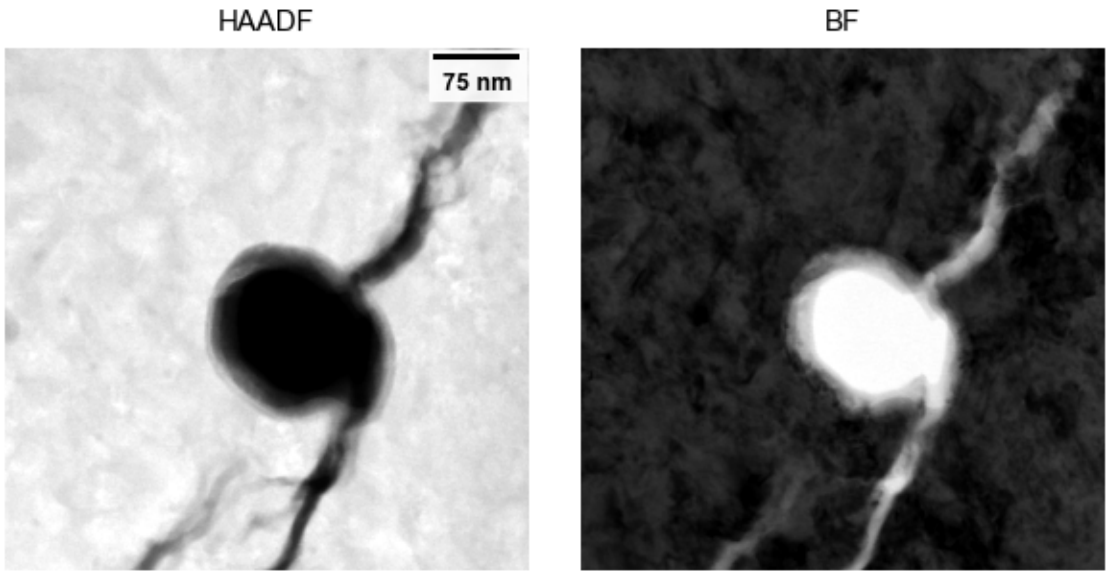


**Figure 94. Very high-magnification STEM images of a FIB liftout from Irradiated Sample EPRI-5.**

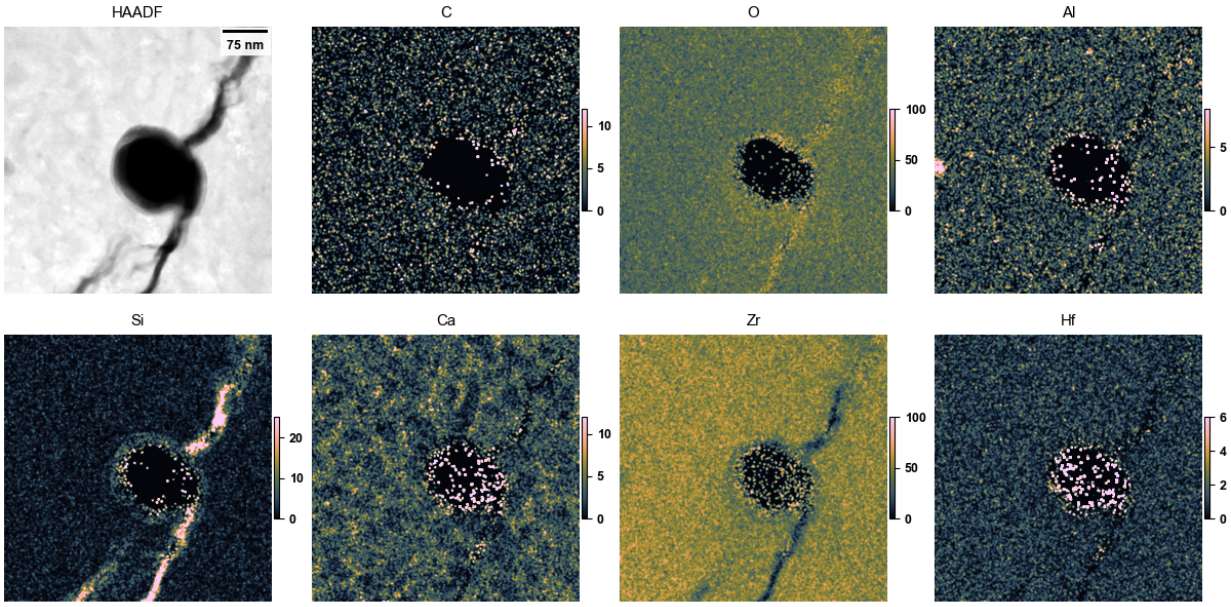


**Figure 95. X-ray maps, presented as estimated atom%, of the region of Figure 94. Speckle in the vacuum area is a quantification artifact and should be ignored.**

Another FIB foil is imaged in Figure 96. A large ceramic grain, containing small cavities or precipitates, along with a few small surrounding grains, are seen. Detailed examination of the area where the large and small grains meet, Figure 97, shows relatively sparse Si-O in X-ray mapping, Figure 98, but the Zr-O grains are clear and contain small amounts of Ca and Hf, as well as Al-rich ~~precipitates~~precipitates and a few regions of enhanced Ca content.

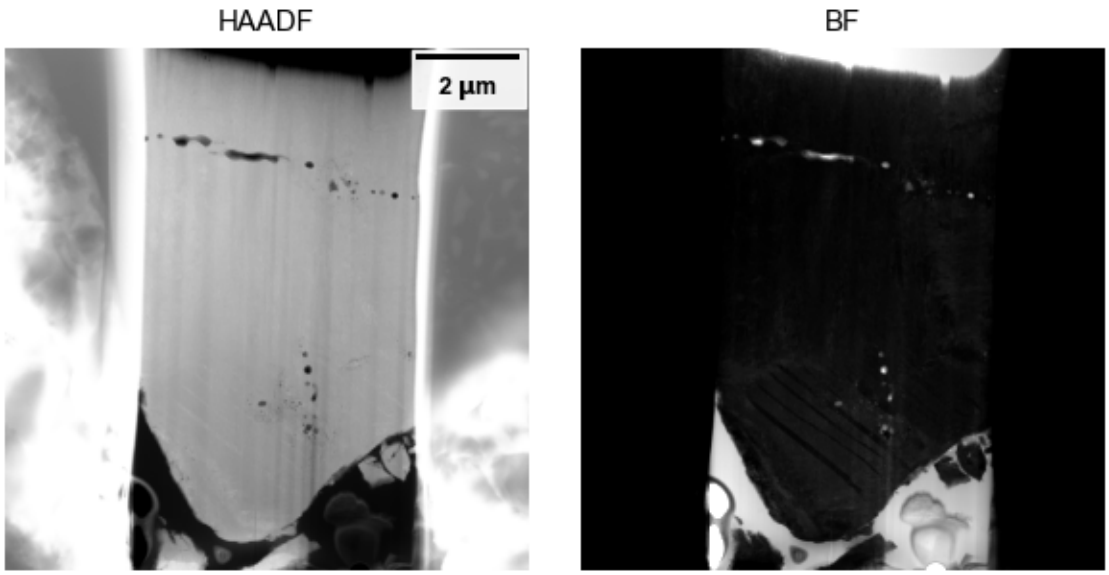


**Figure 96. Medium-magnification STEM images of a FIB liftout from Irradiated Sample EPRI-5.**

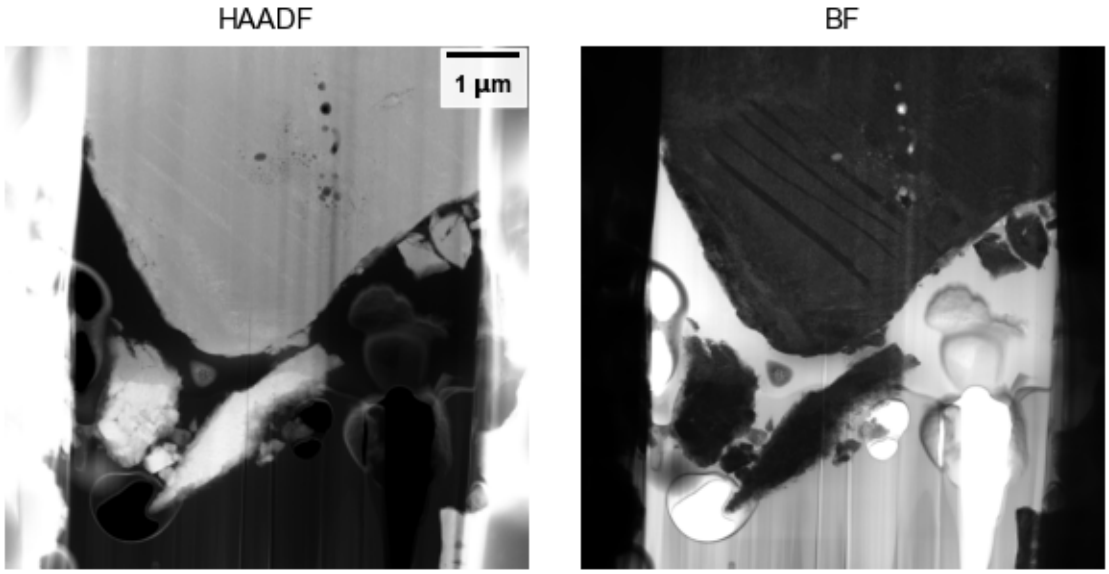


**Figure 97. High-magnification STEM images of a FIB liftout from Irradiated Sample EPRI-5.**

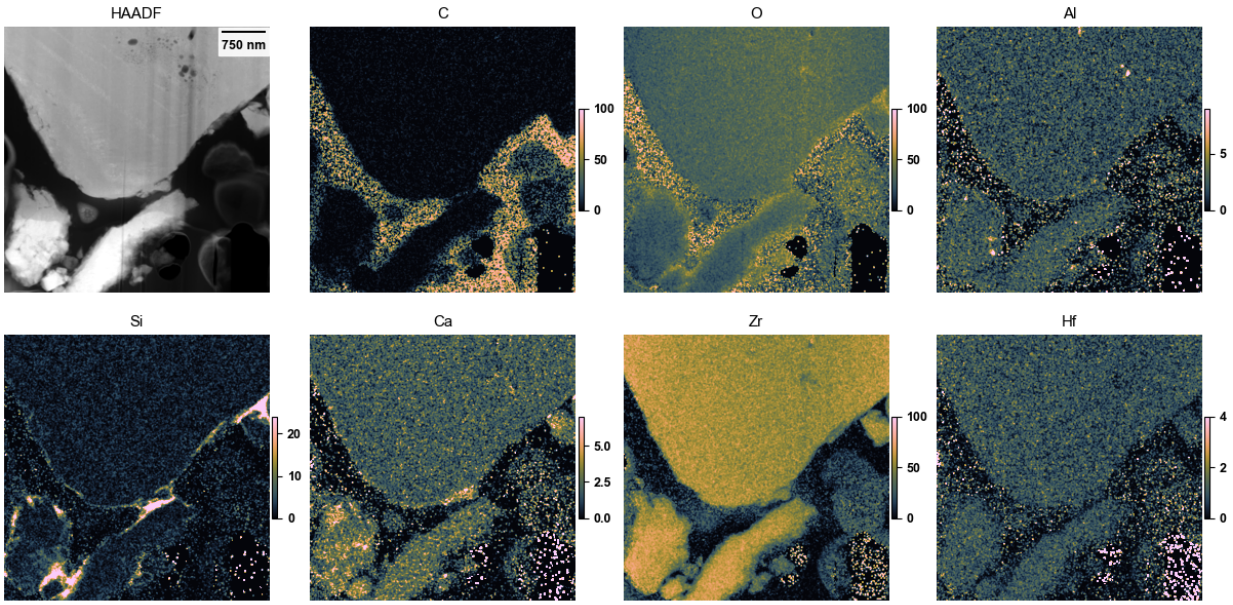


**Figure 98. X-ray maps, presented as estimated atom%, of the region of Figure 97. Speckle in the vacuum area is a quantification artifact and should be ignored.**

The U-shaped grain in Figure 97 is examined in more detail in Figure 99. A high density of small cavities are seen, along with Al-rich precipitates via X-ray mapping (Figure 100), and regions of enhanced and reduced Ca content. The larger cavities appear to be enhanced in O, but this is probably a quantification artifact from the effectively reduced foil thickness providing a slightly increased O signal due to reduced absorption of soft O-K X-rays. At higher magnification, of a very small field of view, no apparent features other than the Ca-rich regions is seen, Figure 101 to Figure 102.

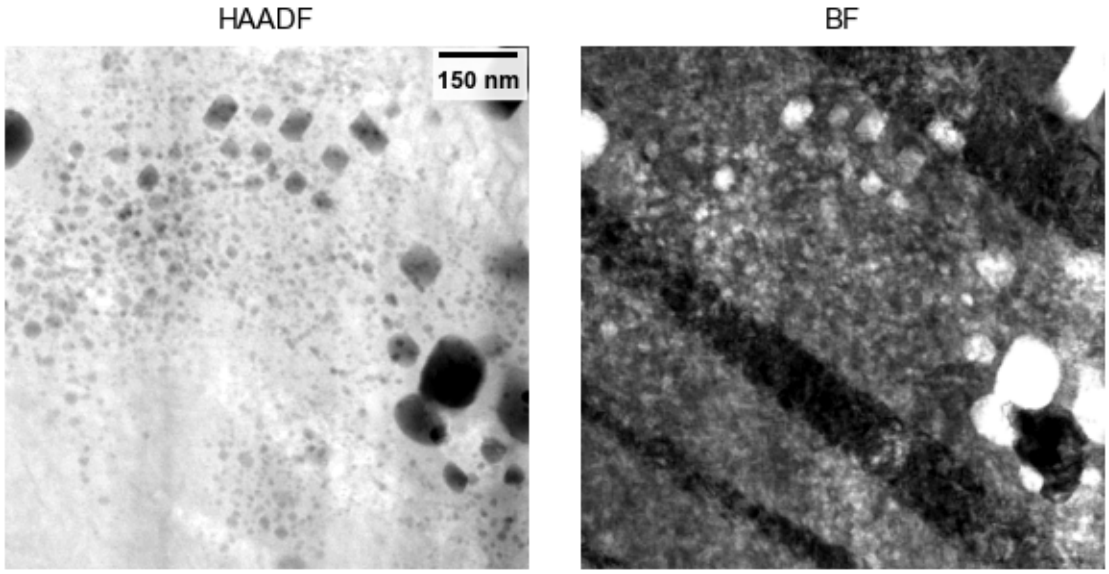


**Figure 99. High-magnification STEM images of a FIB liftout from Irradiated Sample EPRI-5.**

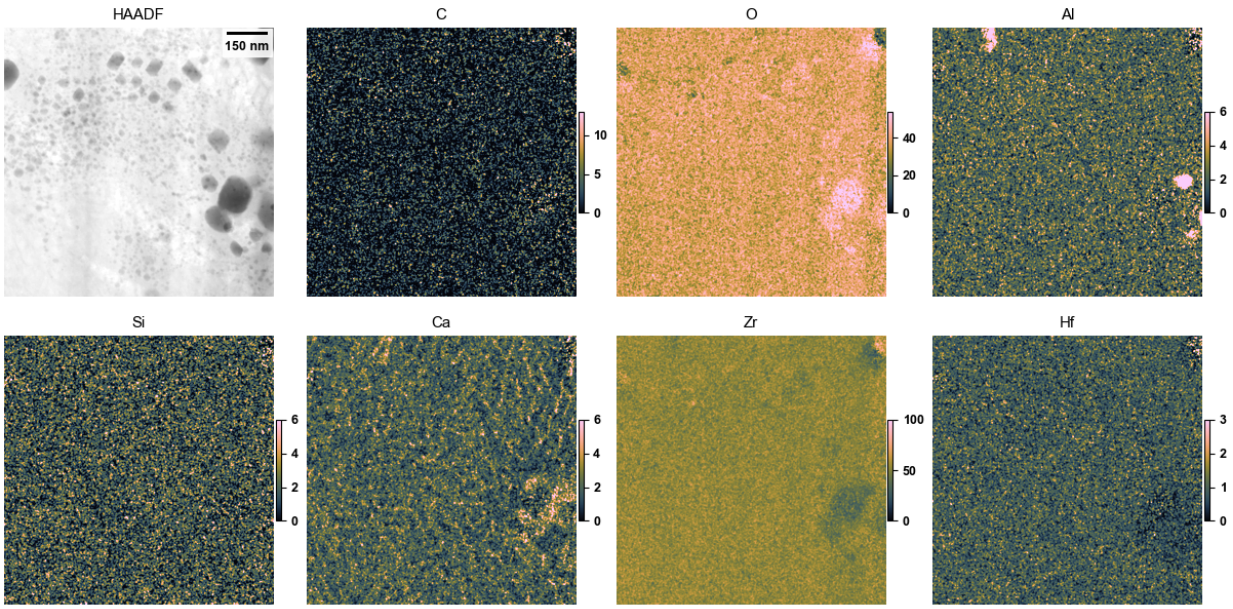


**Figure 100. X-ray maps, presented as estimated atom%, of the region of Figure 99. Speckle in the vacuum area is a quantification artifact and should be ignored.**

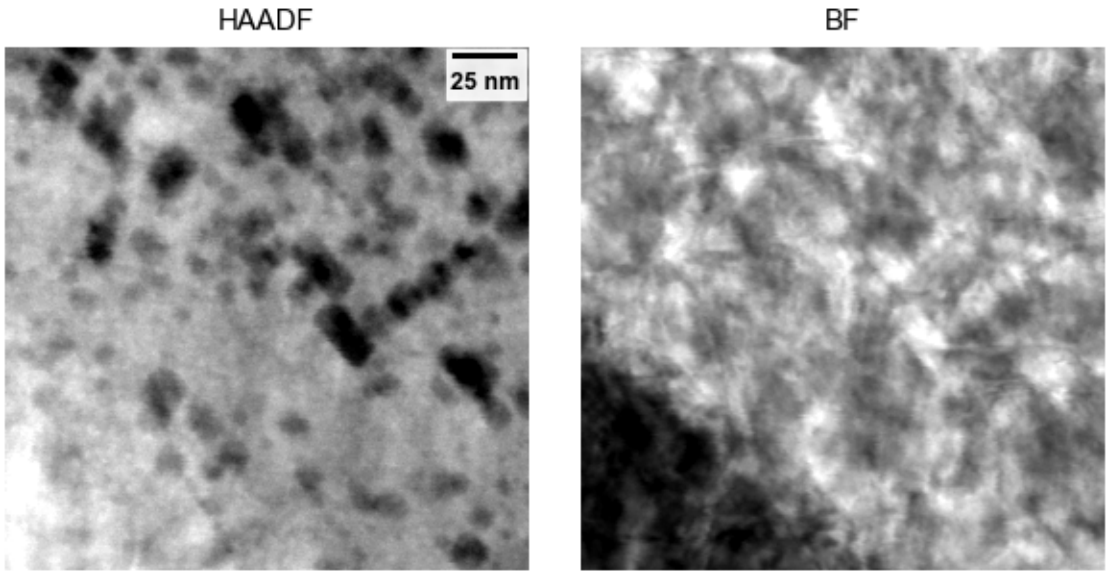


**Figure 101. Very high-magnification STEM images of a FIB liftout from Irradiated Sample EPRI-5.**

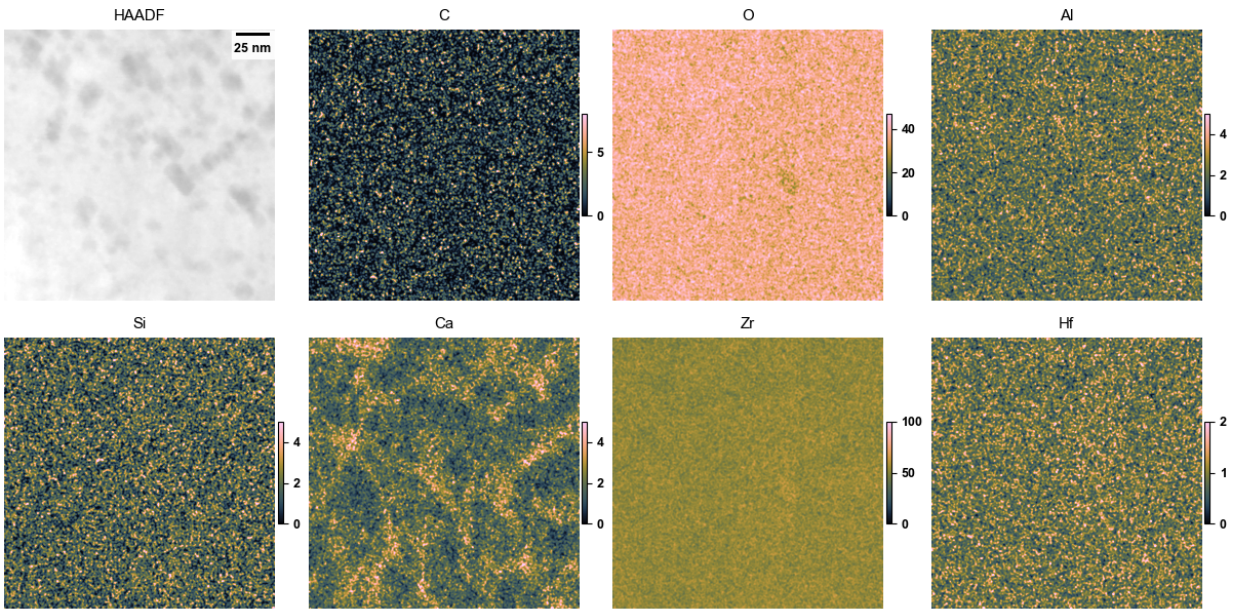


**Figure 102. X-ray maps, presented as estimated atom%, of the region of Figure 101. Speckle in the vacuum area is a quantification artifact and should be ignored.**

Irradiated Sample EPRI-5 is broadly similar to Unirradiated Sample 12, both being Zr-O based ceramics with small amounts of Ca, Hf, and Al in the ceramic grains, and Si-O binder matrix around them. The only apparent difference between the unirradiated and irradiated zirconia samples appears to be the high density of moderate sized (~10 nm) low-atomic-number features, possibly cavities, seen in, e.g., Figure 101. Although the irradiation temperatures ~~are~~ and doses were very low in these PULSTAR experiments, prior room- or cryogenic-temperature irradiations [e.g., 6, 7] showed evolution of smaller cavities; relating the present neutron + gamma dose levels to the ion-irradiation doses in the other experiments is unclear, however, and the ~~variet~~~~ies~~varieties of zirconia were also different: either fully-stabilized [6] or monoclinic [7] compared to what appeared to be partially-stabilized here.

## 4. CONCLUSIONS

In summary, four as-fabricated and three irradiated samples featuring alkali, alumina and zirconia based adhesive couplants were studied. The focus of the STEM work was to probe the microstructures of the adhesive couplants, thus FIB was used to create liftout samples analyzed in the SEM. The microstructures and chemical segregation in the couplants ~~was~~were determined. The epoxy bonded samples were not conducive to analysis using STEM so were omitted. The results presented show complex microstructures and interesting features but no obvious changes were directly attributed to the irradiation campaign. As presented in [2], two samples utilizing epoxy and one sample utilizing aluminosilicate to couple the sensors to the substrates generated usable ultrasonic data through the end of the irradiation campaign. Unfortunately, the aluminosilicate bonded sample that produced usable ultrasonic signals could not be examined using STEM due to shipping damage from NCSU PULSTAR to ORNL LAMDA. The unirradiated aluminosilicate bonded sample lift our sample showed large alumina grains encased in Si-O binder. The STEM results presented on both the unirradiated and irradiated adhesive couplants indicate that microstructural features present in the ceramic-based couplants may have affected their adhesion quality to the sensors and/or substrates, whereby making the ultrasonic data unusable.

## 5. ACKNOWLEDGEMENTS

This work was supported by the U.S. Department of Energy, Office of Nuclear Energy as part of Nuclear Science User Facilities award CINR RPA-20-19172.

## 6. REFERENCES

1. Parish, C., T. Dixon, and J. Wall, *Milestone Report on Microstructure of Irradiated Sensors and Coupling Adhesive Bonds*. 2023, Oak Ridge National Lab.(ORNL), Oak Ridge, TN (United States).
2. Wall, J.J., et al., *Irradiation of Ultrasonic Sensors and Adhesive Couplants for Application in Light Water Reactor Primary Loop Piping and Components.* Nuclear Engineering and Design, 2023. **414**: p. 112594.
3. Crameri, F., G.E. Shephard, and P.J. Heron, *The Misuse of Colour in Science Communication.* Nature Communications, 2020. **11**(1): p. 5444.
4. Badwal, S., *Zirconia-Based Solid Electrolytes: Microstructure, Stability and Ionic Conductivity.* Solid State Ionics, 1992. **52**(1-3): p. 23-32.
5. *Zirconium and Hafnium Statistics and Information*. [cited 2024; Available from: https://www.usgs.gov/centers/national-minerals-information-center/zirconium-and-hafnium-statistics-and-information.
6. Sickafus, K.E., et al., *Radiation Damage Effects in Zirconia.* Journal of Nuclear Materials, 1999. **274**(1-2): p. 66-77.
7. Liu, J., et al., *In-Situ Tem Study of Irradiation-Induced Damage Mechanisms in Monoclinic-Zro2.* Acta Materialia, 2020. **199**: p. 429-442.